

# Novel Molecular Architectures from Iptycene Polymers

by

Nicholas T. Tsui

B.S.E. in Materials Science and Engineering  
University of Pennsylvania, 2002

Submitted to the Department of Materials Science and Engineering in Partial  
Fulfillment of the Requirements for the Degree of

Doctor of Philosophy in Materials Science and Engineering

at the

MASSACHUSETTS INSTITUTE OF TECHNOLOGY

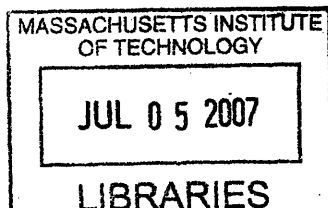
June 2007

© 2007 Massachusetts Institute of Technology  
All rights reserved

Author .....  
Department of Materials Science and Engineering  
May 7, 2007

Certified by .....  
Edwin L. Thomas  
Department Head and Morris Cohen Professor of  
Materials Science and Engineering  
Thesis Supervisor

Accepted by .....  
Samuel M. Allen  
POSCO Professor of Physical Metallurgy  
Chair, Department Committee on Graduate Students



ARCHIVES



# **Novel Molecular Architectures from Iptycene Polymers**

by

**Nicholas T. Tsui**

**B.S.E. in Materials Science and Engineering  
University of Pennsylvania, 2002**

Submitted to the Department of Materials Science and Engineering  
on May 7<sup>th</sup>, 2007, in Partial Fulfillment of the  
Requirements for the Degree of  
Doctor of Philosophy in Materials Science and Engineering.

## **Abstract**

This thesis explored the incorporation of iptycenes into polymers as a means to enhance the mechanical properties. Iptycene structures were targeted because they possess a unique structural property called internal molecular free volume. When these bulky pendant groups are incorporated into the backbone of a polymer chain, they produce a novel chain architecture called molecular barbed wire. This molecular barbed wire architecture not only influences individual polymer chain dynamics but also induces lateral interactions between polymer chains through the minimization of internal molecular free volume.

Work began by developing the concepts of internal molecular free volume and how to exploit its minimization. A formal definition for this property was created along with methods to identify and quantify its existence. Experimental results document the effects of introducing this property into polyesters and polycarbonates. Two specific novel inter-chain interactions were established: molecular threading and molecular interlocking. These steric interactions between polymers chains generate a non-bonded, network morphology and actively enhance the mechanical properties during deformation.

It was demonstrated that the stiffness, strength and ductility of polymers could be enhanced simultaneously through this method. Mechanical properties were observed in tension at quasistatic deformation rates and in compression at both quasistatic and ballistic deformation rates. Improved mechanical performances were related back to structural properties through x-ray scattering experiments. Concepts of internal molecular free volume were necessary to explain the structure-property relationships observed.

In addition, a prototype of enhanced polycarbonate was successfully developed for possible use in protective armor applications. This work provides a new pathway for the continued research and development in the field of ballistic protection.

Thesis Supervisor: Edwin L. Thomas.

Title: Department Head and Morris Cohen Professor of Materials Science and Engineering



## Acknowledgements

First and foremost, I would like to thank Prof. Ned Thomas for providing me with an incredible research environment. It is a scientist's dream to operate under almost unlimited resources, unwavering enthusiasm, intellectual freedom and a poignant mission statement. Still, it would be a euphemism to refer to MIT as an institution of "tough love." Throughout my journey, Ned has been the backboard, converting every close idea into a slam dunk and leaving only the air balls to be jeered by the crowd (of which I have had my fair share!). Not only has he shown me what it takes to be a great scientist, but also how to be an effective person. He has taught me many things that I will carry with me for the rest of my life.

I am forever indebted to a long list of professors, researchers, graduate students and undergraduate students. At the top of that list is Prof. Tim Swager. He and many members of his group have been integral in almost every step of my thesis work. Prof. David Roylance and Prof. Lorna Gibson both deserve praise for their invaluable contributions as committee members. I must also thank Dr. Alex Paraskos, Dr. Lokman Torun, Dr. Brian Pate, Dr. Jeff Baur, Dr. Tim Fornes, Dr. Alex Hsieh, Dr. Cathy Byrne, and Dr. Steve Kooi for their collaborations and assistance in the laboratory. I particularly want to acknowledge Joe Walish and Rafal Mickiewicz, who will both always feel like old war buddies to me. I hope that each of their "tours of duty" will be completed soon. I would also like to thank many members of the Thomas group, including Taras Gorishnyy, Rachel Pytel, Taeyi Choi and Chaitanya Ullal, for their friendship and camaraderie. Finally, I would like to thank my UROP Doug Fraser, who suffered almost two years of carrying out my research direction.

My family and friends have always been of paramount importance to me. They are the ones that I rely on for guidance, love and understanding. With their infinite patience, they have listened to me both complain tirelessly and brag endlessly. None of them will ever truly know exactly how grateful I am to have each of them in my life. I dedicate this Ph.D. to my parents and my sister, who have always showered me with immeasurable levels of encouragement. I am absolutely certain that I could not have finished this program without their support. Equally important to my time here has been my girlfriend, Shirley Tang, whom I treasure. She has stood by me through both the ups and the downs during this unique time in my life. My friends, Ben Larman, Brice Crawford, Drew Satorius, Nick Conway, Jeff Payne, David Nguyen and Neil Kumar have shared with me some of the most amazing memories that I will ever have (even some that we have vowed to never again mention!).

These past five years have been the most incredible of my life. I have had the most fun, worked the hardest, learned the most and experienced the most that I ever have. I would not trade these memories for anything.



# Contents

<b>1</b>	<b>Introduction</b>	<b>25</b>
1.1	Structure- Property Relationships .....	26
1.1.1	High Stiffness Approaches .....	27
1.1.2	High Ductility Approaches .....	31
1.1.3	Interlocking Networks .....	32
1.2	Applications .....	34
1.3	Iptycenes .....	35
1.3.1	Iptycenes for Low-k Dielectrics .....	37
1.3.2	Iptycenes for Sensing Applications .....	38
1.3.3	Iptycenes for Directive Ordering / Alignment .....	39
1.4	Objective .....	42
<b>2</b>	<b>Experimental Techniques</b>	<b>45</b>
2.1	Synthesis and Materials .....	45
2.1.1	Polyesters .....	46
2.1.2	Polycarbonates .....	48
2.2	Sample Preparation .....	51
2.2.1	Solvent Casting .....	51

2.2.2	Melt Pressing .....	52
2.2.3	Heat Treatments .....	54
2.2.4	Oriented Samples and Fiber Spinning .....	55
2.3	Characterization .....	56
2.3.1	Modeling .....	57
2.3.2	Molecular Weight .....	57
2.3.3	Structural Properties .....	57
2.3.4	Thermal Properties .....	58
2.3.5	Mechanical Properties .....	59
<b>3</b>	<b>Internal Molecular Free Volume (IMFV)</b>	<b>67</b>
3.1	Defining IMFV .....	67
3.1.1	Background .....	67
3.1.2	Experimental Methods .....	68
3.1.3	Results and Discussion .....	69
3.1.4	Conclusion .....	74
3.2	Using IMFV .....	74
<b>4</b>	<b>Random Segmented Polyesters</b>	<b>81</b>
4.1	Effects of Triptycene on the Structure and Tensile	
	Mechanical Properties of Polyesters .....	85
4.1.1	Background .....	85
4.1.2	Experimental Methods .....	86



4.1.3	Results and Discussion .....	86
4.1.4	Conclusion .....	101
4.2	Oriented Films and Fibers .....	102
4.2.1	Background .....	102
4.2.2	Experimental Methods .....	104
4.2.3	Results and Discussion .....	105
4.2.4	Conclusion .....	114
4.3	Varying Composition and Type of Iptycene Unit .....	115
4.3.1	Background .....	115
4.3.2	Experimental Methods .....	116
4.3.3	Results and Discussion .....	117
4.3.4	Conclusion .....	134
<b>5</b>	<b>Polycarbonates (PC) and PC Blends</b> .....	<b>139</b>
5.1	Low Molecular Weight PC Blends .....	143
5.1.1	Background .....	143
5.1.2	Experimental Methods .....	144
5.1.3	Results and Discussion .....	148
5.1.4	Conclusion .....	163
5.2	Low Molecular Weight Fire-Retardant PC Blends .....	165
5.2.1	Background .....	165
5.2.2	Experimental Methods .....	165
5.2.3	Results and Discussion .....	167

5.2.4	Conclusion	171
<b>6</b>	<b>Summary and Future Work</b>	<b>175</b>
6.1	Effective IMFV	177
6.2	Interlocking Index	179
6.3	Other Iptycene Incorporations	181
6.3.1	Blends	182
6.3.2	Alternate Covalent Tethering	182
6.4	Suppression of Novel Mechanisms / Blocking IMFV	183
6.4.1	Carbon Nanotubes (CNTs)	184
6.4.2	Closed Structures	188
6.5	High Molecular Weight PCs	189
6.6	Scratch Resistance	190
6.7	Fluorescent Tags	193
6.8	Other Polymer Systems	193
6.8.1	Polysulfones (PSU)	194
6.8.2	Polyurethanes (PU)	196
6.8.3	Highly Oriented Liquid Crystal (LC) Fibers	197
6.8.4	Non-Condensation Reaction Polymers	197
6.9	Other Applications	198
6.9.1	Auxetic Behavior	198
6.9.2	Phase Mixing / Dispersion of Additives	199
6.9.3	Drug Delivery and Medical Applications	200

6.10 Other Characterization Techniques .....	200
--	-----

<b>Bibliography</b>	<b>201</b>
---------------------	------------



# List of Figures

1-1	Hypothetical stress-strain ( $\sigma$ - $\epsilon$ ) curve for a ductile polymer showing the contributions of both stiffness and ductility to energy absorption.	27
1-2	Molecular representations of highly oriented fibers of polyethylene (PE), Kevlar® (PPTA), and M5 (PIPD) showing progressively increasing lateral interactions (adapted from [15]).	30
1-3	Energy absorption data (work) from quasistatic tensile mechanical tests (5 mm/min) of 12 $\mu\text{m}$ diameter Kevlar® PPTA fibers from DuPont and 50 $\mu\text{m}$ diameter Iupilon® PC fibers spun by Dr. Timothy Fornes (MIT DMSE, post-doctoral researcher). The gauge length is left out of the work calculation but was the same for both samples.	32
1-4	Representations of a) poly(ethylene glycol) based polyrotaxanes, b) the figure-of-eight covalent cross-link and c) cross-linked polyrotaxane gel from [35].	33
1-5	Structures of two iptycenes: triptycene and pentiptycene.	35
1-6	Schematic of two possible incorporations of triptycene into the backbone of a polymer: benzene (left) versus bridgehead (right).	36
1-7	Schematic of possible interlocking patterns of isolated triptycene units based off of x-ray data (adapted from [62]).	37
1-8	Depiction of analyte diffusion and binding from [47, 48]. The analyte particles occupy the cavities created by the iptycene units.	39
1-9	Internal free volume is illustrated (area inside of the arrows) along with representations of how surrounding molecules or polymer chains prefer minimize the total free volume of the system through the occupation of the triptycene cavities, modified from [53].	41

2-1	Basic route for random block copolymer synthesis of polyesters containing no ipitycene units [84, 85]. Concentrations of aromatic content versus aliphatic content can be controlled by changing the mixing ratios of A, B and C, which result in final x/y ratios for the polymer.	46
2-2	Basic route for random block copolymer synthesis of polyesters containing triptycene units [84, 85]. Using this template, any type of ipitycene unit or aromatic unit can be used as the A component. Concentrations of aromatic content versus aliphatic content can be controlled by changing the mixing ratios of A, B and C, which result in final x/y ratios for the polymer.	47
2-3	Set of random block copolyesters where $x/y = 1/5$ for a reference non-triptycene polyester (R), triptycene polyester (T), naphthalene-modified triptycene polyester (NpT), and tert-butyl-modified triptycene polyester (TbT). Appears in [86].	48
2-4	Basic outline of triptycene incorporation into bisphenol-A PC to form a Triptycene-PC (T-PC) copolymer.	49
2-5	Basic scheme of triptycene incorporation into Triton Systems, Inc.'s "FX" polymer to form Triptycene-FX (T-FX) copolymer.	50
2-6	Final chemical structures of polymers characterized in this thesis. All block copolymers were random polymerizations, and the chemical structures here are statistical representations that were "controlled" by molar concentrations and reactivity ratios (producing tailorable x and y values).	50
2-7	Diagram from which Teflon® boxes were manufactured by the MIT Central Machine Shop. Instructions also noted that all inside surfaces must be polished smooth and that it was critical that the bottom surface be perfectly level.	52
2-8	Ring mold setup for melt pressing polymers. In the case where the ring mold was not utilized, the rest of the setup remained identical.	53
2-9	Custom machined compression tool used to squeeze out bubbles in polymer disks. Entire assembly was placed between the hot press compression plates for operation.	54
2-10	Diagram of the essential parts of the melt spinning device used to produce oriented fibers. $\lambda$ = draw ratio.	56

2-11	Tensile test setups exhibiting the different grips utilized for the different sample sizes and geometries. Setup I was for thin films (~100 $\mu\text{m}$ ), II was for thick films (>1 mm) that usually contained notches or dogbones for stress concentration, and III was for very thin samples, such as single fibers.	61
2-12	Uniaxial compression tests using a Zwick/Roell mechanical testing machine with flat steel compression plates.	62
2-13	Schematic of the split-Hopkinson pressure bar (SHPB) test apparatus used for high strain rate uniaxial compression tests [94].	64
2-14	Characteristic data from parallel plate rheology graphically representing the identification of the plateau modulus ( $G_N^0$ ) from the $G'$ curve [95].	65
3-1	Depiction of internal free volume in triptycene (left) and pentiptycene (right).	68
3-2	The arrows mark the process of generating the three-dimensional space filling models. The example used here was triptycene. From left to right: constructing the triptycene, calculating the optimally stable conformation, and finally converting to the space-filling representation.	69
3-3	Face views of space-filling models of ethylene (left) and triptycene (right) showing the contrast in IMFV. The triptycene has significantly sized cavities; whereas, the ethylene does not.	70
3-4	Space-filling triptycene models showing (a) three-dimensional view, (b) width measurements along the triptycene axes, (c) method 1 where A is the cleft space, and (d) method 2 where S is the extra space outside of the triptycene unit when enclosed in a triangular prism.	71
3-5	Space-filling models of ethylene (E), triptycene (T), naphthalene-modified triptycene (NpT), tert-butyl-modified triptycene (TbT) along with calculations for the inherent IMFV of the isolated structures using method 1.	73
3-6	Schematics of (a) the typical “smooth” polymer chain contour and (b) “molecular barbed wire” generated by the incorporation of triptycene units (yellow).	75
3-7	A neighboring polymer chain can slide into the open triptycene cavity in order to minimize IMFV (and thus, the total FV of the system). Once occupied, the polymer chain can thread along the triptycene cavity during deformation.	76

3-8	Schematic of the new types of interactions (“threading” and “interlocking”) induced by the triptycene unit and the minimization of IMFV (bottom). The same polymer without triptycene relies on entanglements and will fail at early strains if there are poor lateral interactions (top).	77
3-9	Drawings of the (a) benzene substitution and (b) bridgehead substitution with space-filling schematics qualitatively showing the type of incorporation’s effect on the accessibility of the IMFV of triptycene.	78
4-1	Triptycene containing random segmented polyester. Nomenclature “x/y T” indicates the polyester’s composition and that it contains triptycene.	81
4-2	2-D x-ray diffraction patterns for the triptycene containing polyester set displaying semi-crystallinity and decreasing crystallinity with increasing triptycene content.	83
4-3	DSC of triptycene containing polyester set. Endotherm points down.	84
4-4	Chemical structures of the polyesters characterized here. 1/3 R: non-triptycene reference polyester. 1/3 T: 21 wt % triptycene containing polyester.	87
4-5	DMA of triptycene containing polyester (1/3 T) versus non-triptycene polyester (1/3 R) at 10 Hz (open circles) and 1 Hz (closed circles).	89
4-6	Shifted DSC curves for triptycene (1/3 T) and non-triptycene (1/3 R) polyesters with the endotherms up. Melting points ( $T_m$ ) are labeled but $T_g$ was not readily identifiable.	90
4-7	TGA curves for polyester samples in both air and nitrogen atmospheres.	91
4-8	Tensile properties of triptycene (1/3 T) and non-triptycene (1/3 R) polyester films at room temperature.	93
4-9	Representative optical microscope pictures at 5X magnification with cross-polarizers oriented at various degrees for film samples strained to failure: a) triptycene at 0°, b) triptycene at 90°, c) non-triptycene at 0° and d) non-triptycene at 90°.	94
4-10	-30°C tensile properties of non-triptycene films yield a modulus (E) of $1.61 \pm 0.10$ GPa, strength ( $\sigma_{UTS}$ ) of $24 \pm 8$ MPa, and strain to failure ( $\epsilon_b$ ) of $1.4 \pm 0.5$ % while triptycene polyester films exhibit a modulus (E) of $1.58 \pm 0.13$ GPa, strength ( $\sigma_{UTS}$ ) of $55 \pm 6$ MPa, and strain to failure ( $\epsilon_b$ ) of $47 \pm 9$ %.	96



4-11	WAXS of (a) non-triptycene polyester as-cast film, (b) triptycene polyester as-cast film, (c) triptycene polyester strained over 200% along the vertical axis. The bottom row displays the identical patterns but with the peaks labeled.	97
4-12	Integrated circularly averaged scans of the patterns in Fig. 4-11 a and b.	97
4-13	The in-situ deformation that shows how the WAXS evolves on the stress-strain curve for both triptycene and non-triptycene polyesters. The key point here is that observable structural change does not occur at relatively low deformations (<30%).	103
4-14	Room temperature tensile properties of THT triptycene polyester films.	106
4-15	Representative WAXS pictures of room temperature strained to failure (S) versus undeformed tension heated treated (THT) triptycene polyester films taken at ISN. The deformation axis is the y-direction.	108
4-16	(a) EQ: Equatorial, (b) ME: meridional, and (c) 60° sector scans in WAXS of strained and THT triptycene polyester films with the peaks of interest labeled in accordance with section 4.1. Part (d) shows the angular definitions of each scan.	109
4-17	Single fiber tensile tests for non-triptycene polyester (1/3 R) and triptycene polyester (1/3 T) melt spun fibers. The bottom plot shows a superposition of representative samples compared to 1/3 T THT film.	111
4-18	WAXS of fiber bundles oriented in the y-direction.	113
4-19	Chemical structures of the reference non-iptycene polyester (R), triptycene polyester (T), naphthalene-modified triptycene polyester (NpT), and tert-butyl-modified triptycene polyester (TbT).	117
4-20	Triptycene (T), naphthalene-modified triptycene (NpT), and tert-butyl-modified triptycene (TbT) along with inherent IMFV calculations from Chapter 3. Also shown is a schematic of the steric interactions induced by the minimization of IMFV.	118
4-21	WAXS of 1/5 solvent cast (SC) films of reference (R), triptycene (T), naphthalene-modified triptycene (NpT), and tert-butyl-modified triptycene (T) polyesters.	120
4-22	Circular integrations of WAXS of solvent cast (SC) films with crystalline peaks numbered in red.	121
4-23	DSC of solvent cast (SC) and melt pressed (MP) 1/5 polyester films.	122

4-24	Tensile stress-strain curves of melt pressed 1/5 polyester films. Two deformation regimes are specified in the ductile films (D = drawing; WH = work hardening).	125
4-25	2D WAXS patterns of unstretched (U) and strained to failure (S) 1/5 melt pressed films. R(S) was not taken due to the low failure strains. The stretching direction is vertical.	127
4-26	WAXS circular integrations of unstretched (U) 1/5 films and equatorial integrations with a width of 10 azimuthal degrees after strain to failure (S). X-ray patterns of R(S) were not taken due to the low failure strains in the non-triptycene polymer.	128
4-27	Hypothetical curves for the concentration dependence of modulus and strain to failure based on experimental observations for the polyesters studied.	136
5-1	DMA spectra for Lexan® 9034 PC, adapted from Mulliken [103], showing the storage modulus ( $G'$ - solid line) and loss modulus ( $G''$ - dashed line).	140
5-2	Lexan® data, adapted from Mulliken [103], for uniaxial compression tests at various true strain rates. Plots of characteristic stress-strain curves (a) and rate-dependence of yield strength (b).	141
5-3	Linear dependence of the $\beta$ -transition with deformation frequency, adapted from Mulliken [103], along with linear extrapolation of peak position at high strain rates (ballistic projectile impact rates $\geq 10^4 \text{ s}^{-1}$ ).	142
5-4	Chemical Structures of IUP, PC-1, and T-PC monomers.	145
5-5	2 <sup>nd</sup> heat cycle DSC scans of powders of IUP, PC-1, and T-PC along with the 1 <sup>st</sup> heat cycle scans of the blends after compression molding. 1 <sup>st</sup> heat cycle scan of compression molded IUP (not shown) was identical to the powder's 2 <sup>nd</sup> heat cycle scan (shown) only without the small endotherm just after the $T_g$ . $T_g$ 's are labeled next to the curves.	149
5-6	PC and T-PC Blends display the same level of optical transparency as IUP. Specimens shown are approximately 6 mm in diameter and 2 mm in height.	149
5-7	Uniaxial compression curves at various engineering strain rates of IUP (black), PC Blend (blue) and T-PC Blend (red).	151
5-8	Engineering strain rate dependence of the yield strengths of IUP (black), PC Blend (blue) and T-PC Blend (red).	152

5-9	DMA of IUP (black), PC Blend (blue) and T-PC Blend (red). Curves are at 1 Hz unless labeled otherwise.	154
5-10	Representative stress-strain curves from uniaxial tensile tests of dogbone samples.	156
5-11	Representative data from parallel plate rheometry of IUP (black), PC Blend (blue) and T-PC Blend (red). The storage modulus curves are accented by bold lines.	157
5-12	Chemical structures of Iupilon® PC (IUP), phosphorus containing polymer (FX), and phosphorus containing polymer with triptycene (T-FX). As indicated in the diagram, the weight percent of triptycene in T-FX is ~14.4 wt %.	166
5-13	2 <sup>nd</sup> heat cycle DSC scans of powders of IUP, PC-1, and T-PC along with the 1 <sup>st</sup> heat cycle scans of the blends after compression molding. 1 <sup>st</sup> heat cycle scan of compression molded IUP (not shown) was nearly identical to the powder's 2 <sup>nd</sup> heat cycle scan (shown). T <sub>g</sub> 's are labeled next to the curves.	168
5-14	Uniaxial compression stress-strain data at various engineering strain rates (marked at the bottom right of each plot) for IUP (black), FX Blend (blue) and T-FX Blend (red). Data for IUP at 0.001 s <sup>-1</sup> , 0.01 s <sup>-1</sup> , and 0.1 s <sup>-1</sup> are from the experiments presented in section 5.1.	169
5-15	Top: Average values for true yield strengths versus engineering strain rates for uniaxial compression tests of IUP (black squares), FX Blend (blue squares), and T-FX Blend (red squares). Previous IUP data (open circles) is superimposed to demonstrate consistency of testing across different dates. Bottom: Range of values slightly offset following the same color scheme as the top.	171
6-1	Space-filling models of a) T, b) NpT, and c) TbT with the interlocking volume highlighted with dotted lines. Volumes calculated were 275 Å <sup>3</sup> , 394 Å <sup>3</sup> , and 736 Å <sup>3</sup> for T, NpT, and TbT, respectively. Widths (not shown) were determined using methods from Chapter 3.	181
6-2	Schematic of triptycene tethered to a polymer backbone through different benzene units.	183
6-3	Schematic of triptycene threaded by high aspect ratio cylindrical units.	184
6-4	Functionalization and blending of single-walled carbon nanotubes (SWCNTs) with 1/5 R and 1/5 T polyester samples in THF.	185

6-5	Representative curves from tensile mechanical tests of strips of solvent cast films of 1/5 polyesters with and without SWCNTs.	186
6-6	DMA of solvent cast films of 1/5 R (LEFT) and 1/5 T (RIGHT) with varying amounts of CNTs colored and labeled accordingly.	187
6-7	Schematic of triptycene with one cavity closed off by hypothetical modifications made to the periphery of the benzenes.	188
6-8	Depth vs. lateral distance of scratch for IUP (black), PC Blend (blue) and T-PC Blend (red).	191
6-9	Optical microscope pictures of scratches made through nanoindentation.	192
6-10	Integration of triptycene into the PSU backbone through copolymerization with commercially available Udel® P-1700.	194
6-11	DSC of PSU samples with varying triptycene content according to the molar ratios “n-m” defined in Fig. 6-10.	196
6-12	Illustration of contrasting responses of a positive versus negative Poisson’s Ratio ( $\nu$ ) material during impact, adapted from Evans [159].	198

# List of Tables

1.1	Compilation of mechanical properties of steel [9], Spectra® 1000 (PE) [9], Kevlar® 149 (PPTA) [10], Zylon® (PBO) [11, 12], M5 (PIPD) [13], EPP Ertalon® Nylon 6,6 (PA) [9] and Lexan® 223R (PC) [9]. $E$ = Young's modulus, $\sigma_{UTS}$ = ultimate tensile strength, and $\epsilon_b$ = strain to failure.	29
4.1	Triptycene containing polyesters synthesized by Dr. Paraskos. Data measured and provided by Dr. Paraskos. $M_n$ from GPC.	82
4.2	Number average molecular weight ( $M_n$ ), weight average molecular weight ( $M_w$ ), and polydispersity ( $PDI = M_w/M_n$ ) data on polyesters from GPC. Number of monomer repeats calculated from $M_n$ values.	87
4.3	Summary of the thermal properties as assessed by DMA, DSC, and TGA.	92
4.4	Summary of film tensile tests 1/3 R films of $80 \pm 3 \mu\text{m}$ thickness and 1/3 T films of $87 \pm 13 \mu\text{m}$ thickness. HIR = Highest Individual Result (not plotted in Fig. 4-8 to avoid clutter), $\rho$ = density, $E$ = Young's modulus, $\sigma_y$ = yield strength, $\sigma_{UTS}$ = ultimate tensile strength, and value given in parenthesis is for one standard deviation.	93
4.5	WAXS d-spacings of the polymers of as-cast films, except where indicated otherwise by an (S). The strained sample (S) was elongated over 200% before failure.	98
4.6	Summary of film tensile tests. HIR = highest individual result, $t$ = thickness, and the values in parentheses report standard deviations.	107
4.7	WAXS results from equatorial ( $-5^\circ$ to $5^\circ$ ), meridional ( $85^\circ$ to $95^\circ$ ), and $60^\circ$ azimuthal angle ( $55^\circ$ to $65^\circ$ ) scans.	109
4.8	Single fiber tensile properties. HIR = highest individual result, $d$ = fiber diameter, and the values in parentheses report standard deviations.	112

4.9	Measured molecular weights of polyesters along with the calculated number of monomer repeat units and polymer contour length (C.L.) based on number average molecular weight ( $M_n$ ).	119
4.10	Crystalline peak d-spacings measured from circular integrations of WAXS of solvent cast films.	121
4.11	Thermal properties of polyesters. <sup>a</sup> Taken by researchers at DuPont ( $\pm 0.01$ ). <sup>b</sup> 1 Hz tan delta curve of DMA. <sup>c</sup> DSC – U: unstretched isotropic films; S: films that were strained to failure; N/A: data not taken. <sup>d</sup> TGA of powders in air and assumed to be independent of processing conditions. * Solvent cast films from section 4.1. The rest of the films were melt pressed.	123
4.12	Tensile properties of polyester films. <sup>a</sup> $m_{WH}$ = slope of stress-strain curve in the work hardening regime. <sup>b</sup> Standard deviations for these values were all around $\pm 0.005$ . * Solvent cast films from section 4.1. The rest of the films were melt pressed.	124
4.13	WAXS d-spacings of melt pressed 1/5 polyester films. <sup>a</sup> Measured from circular integrations in Fig. 4-26. <sup>b</sup> Could be a superposition of peaks 3 and 4.	126
5.1	Average molecular weight values ( $M_n$ and $M_w$ ) and polydispersity index (PDI) determined via gel permeation chromatography (GPC) with THF eluent by Yong Yang (MIT Chemistry, graduate student).	144
5.2	Compressive yield strengths at various engineering strain rates. Standard deviations for low strain rates were less than 1 MPa. Standard deviations for high strain rates were about 1 MPa. Data for Lexan® 9034 PC by Mulliken [103].	152
5.3	Tensile mechanical properties: $\rho$ – density at room temperature, standard deviations $\approx 0.01$ g/cc; E - Young's modulus from DMA (1Hz at 25 °C), standard deviations $\approx 0.02$ GPa; $\sigma_y$ - tensile yield strength, standard deviations $\approx 1$ MPa; $\epsilon_b$ - strain to break, highest value observed.	156
5.4	Measured plateau modulus ( $G_N^0$ ) and calculated entanglement molecular weight ( $M_e$ ) values with standard deviations.	157
5.5	Molecular weights of the polymer materials used in this study.	166
5.6	True yield strengths at various engineering strain rates. * represents data from section 5.1, which was taken on a separate occasion from the rest of the data in this section. $\rho$ – density, standard deviations $\approx 0.01$ g/cc.	169

6.1	Composition and molecular weights of triptycene polycarbonates, following x/y notation for T-PC chemical structures shown in Fig. 2-6.	190
6.2	Molecular weights and other characteristics of PSUs synthesized containing various amounts of triptycene.	195





# Chapter 1

## Introduction

The subject of this thesis is the investigation of novel inter-chain interactions and their effects on the mechanical properties of polymers. Polymers (or plastics) can be found in just about every form imaginable. They have always existed naturally in the very building blocks of life, including proteins and DNA. But in 1839, Charles Goodyear created an elastomeric rubber by cross-linking natural rubber through a process called vulcanization. This sparked a flurry of industrial activity followed by the creation of the field of polymer science. Today, over 160 years later, the polymer industry produces over 100 billion pounds of raw plastics each year.

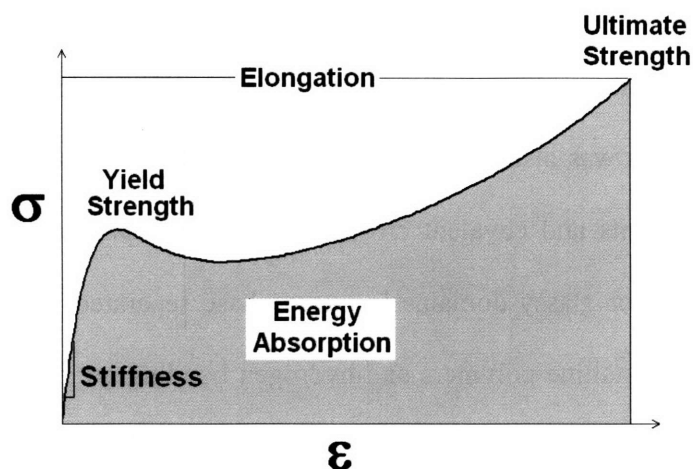
Polymers are the most versatile materials known to exist. They can be as soft as cooked spaghetti or as stiff as steel. They can also stretch thousands of percent or be as brittle as chalk. Due to such a wide range of accessible mechanical properties, polymers find applications in automobiles, sports equipment, medical devices, packaging and even armor. The mechanical characteristics of a particular polymer depend greatly on its structure, which can be a result of synthetic chemistry or processing. Thus, it is fitting

that one of the most dominant fields in polymer science is the study of structure-property relationships.

In this introductory chapter, different types of polymer structures will be surveyed and a number of known structure-property relations will be outlined. While changing the structure of a polymer can alter many of its properties (including optical, electrical, rheological, etc.), the main focus of this thesis was on the solid-state mechanical properties. The purpose of this work was to examine novel molecular architectures in polymers with a particular interest in producing high energy absorption characteristics in solid materials through enhanced inter-chain interactions. Therefore, the discussion of known polymer structures and their mechanical properties will be followed by sections detailing the applications for solid materials with high energy absorption, the approach to designing a new structure, and the final creation of this new polymer architecture.

## 1.1 Structure-Property Relationships

Energy absorption has two main contributing components measurable on a stress-strain curve: stiffness and ductility. Stiffness is a material's initial resistance to deformation and is typically reported as the elastic modulus or Young's modulus. Ductility is a material's yield behavior and post-yield plasticity, as reflected in elongation or strain to break. Yield strength and ultimate strength are also relevant values and are linked to the stiffness and ductility of a material. Energy absorption is the integration of the stress-strain response, and Figure 1-1 illustrates how a sample's stiffness and ductility both play important roles.



**Figure 1-1:** Hypothetical stress-strain ( $\sigma$ - $\epsilon$ ) curve for a ductile polymer showing the contributions of both stiffness and ductility to energy absorption.

The approaches used to achieve polymer systems with high stiffness often conflict with those used to obtain high ductilities. Therefore, it is frequently seen that there is a stiffness/ductility tradeoff. There are rare circumstances where this tradeoff is averted, and these examples will be highlighted in the following sections.

### 1.1.1 High Stiffness Approaches

The evolution of the random walk model for the conformation of polymer chains was described by Flory [1] and concluded that entropy favored random coil chain orientations. Rubber elasticity theories [2-5] and experiments [6-8] have shown that in amorphous polymers, the resistance to deformation is principally governed by the energy penalty of forcing polymer chain conformations to deviate from the random coil. Therefore, higher chain orientations yield higher stresses (assuming no strain-induced crystallinity). Additionally, as polymer chains are stretched significantly and approach full extension, the rigidity of the system increases rapidly because deformation begins to require deviation from the desired covalent bond rotational potentials, bond angles and

bond lengths along the backbone of the polymer chains. This is one major motivation for anisotropy in polymer samples. As for isotropic samples, it was known early on that the stiffness of polymers was also dependent on the “network” nature of the system. This includes entanglements and covalent cross-linking in amorphous polymers, as well as physical cross-links or glassy domains in micro phase separated polymers. Crystalline domains in semi-crystalline polymers and hydrogen bonding are also common forms of interconnectivity. The most successful approaches to enhancing the stiffness of polymers have typically combined these concepts. For example, highly oriented polymer systems also crystallize readily, thereby producing anisotropic samples with a large degree of interconnectivity (hydrogen bonding is often additionally employed to enhance lateral interactions).

The most effective method of achieving high orientation of polymer chains is through fiber spinning. This process uses high extensional forces on either a polymer solution or polymer melt to draw (or “spin”) small diameter fibers ( $\approx 10 \mu\text{m}$ ). Fibers produced in this way contain polymer chains that can be highly elongated. Because of the high aspect ratio of elongated chains, these fibers can often achieve very high levels of crystallinity ( $> 90\%$ ) with stereo-regular chains. Polymers oriented in this way have been observed to display modulus values on the order of and sometimes even greater than that of steel (see Table 1.1).

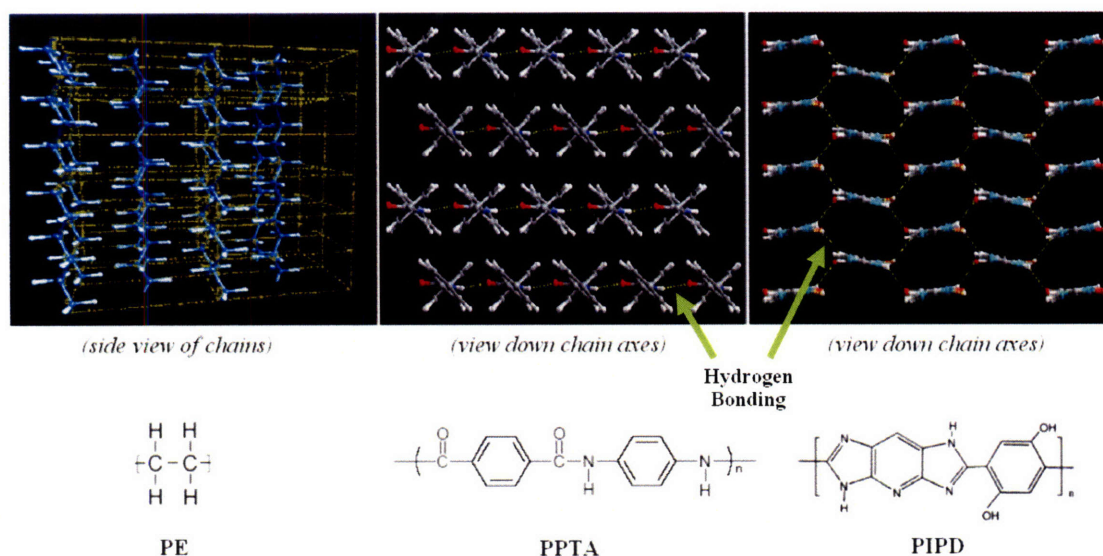
Material	E (GPa)	$\sigma_{UTS}$ (MPa)	$\epsilon_b$ (%)
1010 Steel	205	365	20
Spectra® 1000 (PE)	101	3100	3.3
Kevlar® 149 (PPTA)	138	2150	1.5
Zylon® (PBO)	352	5600	3.5
M5 (PIPD)	320	4000	1.5
Nylon 6,6 (PA)	1.45	50	100
Lexan® (PC)	2.35	65	100

**Table 1.1:** Compilation of mechanical properties of steel [9], Spectra® 1000 (PE) [9], Kevlar® 149 (PPTA) [10], Zylon® (PBO) [11, 12], M5 (PIPD) [13], EPP Ertalon® Nylon 6,6 (PA) [9] and Lexan® 223R (PC) [9]. E = Young's modulus,  $\sigma_{UTS}$  = ultimate tensile strength, and  $\epsilon_b$  = strain to failure.

Theoretically, any polymer can be oriented using this method, but a well entangled system can complicate the process. For example, polyethylene (PE) can be drawn into a well aligned fiber, but requires dilute gel spinning [14] in order to achieve the alignment required for very high levels of crystallinity (>90%) because of the steric hindrance from entanglements. To remedy this, a special class of polymers was created called rigid-rod polymers. They were named for having very large persistence lengths, which behave like rigid rods instead of the traditional random coil and induce the system to form a nematic liquid crystalline (LC) phase. The naturally highly extended chain conformations, low levels of entanglements and LC phases combine to make these polymers the dominant materials for manufacturing the most highly oriented fibers. Commercially available rigid-rod fibers include Kevlar® (poly(p-phenylene terephthalamide) or PPTA) and Zylon® (poly(p-phenylene benzobisoxazole) or PBO).

The fiber spinning process and invention of rigid-rod polymers were aimed at achieving high axial orientation and stiffness. However, it was observed in Kevlar® that additional lateral interactions could also influence axial stiffness. The amide linkages

along the backbone of Kevlar® create two-dimensional sheets through hydrogen bonding [15] (see Figure 1-2). This morphology results in about a 40% increase in stiffness over PE fiber Spectra® 1000 [10] (see Table 1.1). The M5 fiber (chemical formula abbreviated as “PIPD”) was invented [15-17] to extend this concept into three-dimensions. Although M5 has stiffness slightly less than that of the chemically similar Zylon®, it is still in its beginning stages and is expected to increase as optimization improves.



**Figure 1-2:** Molecular representations of highly oriented fibers of polyethylene (PE), Kevlar® (PPTA), and M5 (PIPD) showing progressively increasing lateral interactions (adapted from [15]).

In addition to using hydrogen bonding to induce lateral inter-chain interactions, heavy covalent cross-linking is also a viable strategy to increase a polymer’s stiffness. The cross-link density controls the effects on the mechanical properties, and the cross-links function like “permanent” entanglements. While this produces a stiff system, it also results in a brittle, insoluble thermoset [18, 19]. Additionally, attempts to combine cross-

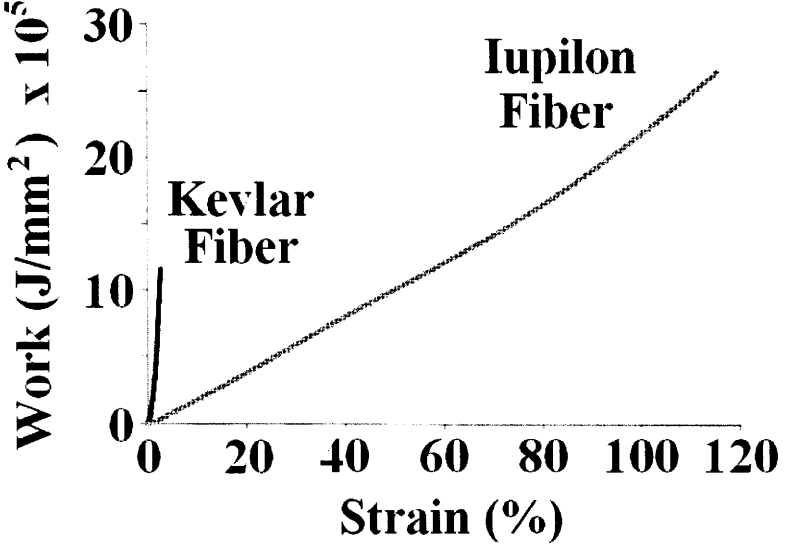
linkable groups into LC systems failed because the added groups disrupted the alignment and crystallinity of the polymer chains, ultimately resulting in a lower stiffness [20-22].

Enhancements to the stiffness of polymers can also be achieved by the addition of fillers. Some of the most popular modern techniques involve blending in highly anisotropic stiff nanoparticles, such as carbon nanotubes [23-25] or clay sheets [26, 27]. But in either case, it is typically seen that enhancements to stiffness result in sacrifices to ductility. There are rare cases where this trade off can be avoided. If deformation mechanisms are altered, such as eliminating craze behavior [28] or enhanced stress transfer from molecular reinforcements [29], it is possible to enhance the stiffness and ductility simultaneously, but these cases are unusual and there is no general method for achieving such improvements.

### 1.1.2 *High Ductility Approaches*

As seen in Fig. 1-1, high ductility also contributes to the total energy absorbed during deformation. Common techniques for increasing the ductilities of polymers include the reverse of those described in the previous section [30], *lightly* cross-linking or increasing the number of entanglements above the entanglement density [15], and incorporation of a rubbery phase [31] either through blending or copolymerization. Introducing additional [28, 29] or length-scale dependent [32] deformation mechanisms can also increase ductility. One in-depth study has correlated the existence of sub- $T_g$  thermally activated mechanical relaxations with the ductility of polymers [33]. This work is of particular importance when the sub- $T_g$  transition occurs at a temperature that corresponds to the high frequencies that may arise during ballistic impact events. As will be discussed in

greater detail in Chapter 5, such unique deformation mechanisms in ductile polymers can produce energy absorption levels comparable to highly oriented systems. Fig. 1-3 shows the energy absorption characteristics of Iupilon® polycarbonate (PC) compared to Kevlar® PPTA. It can be seen that due to PC's high ductility, very high levels of energy can be absorbed.



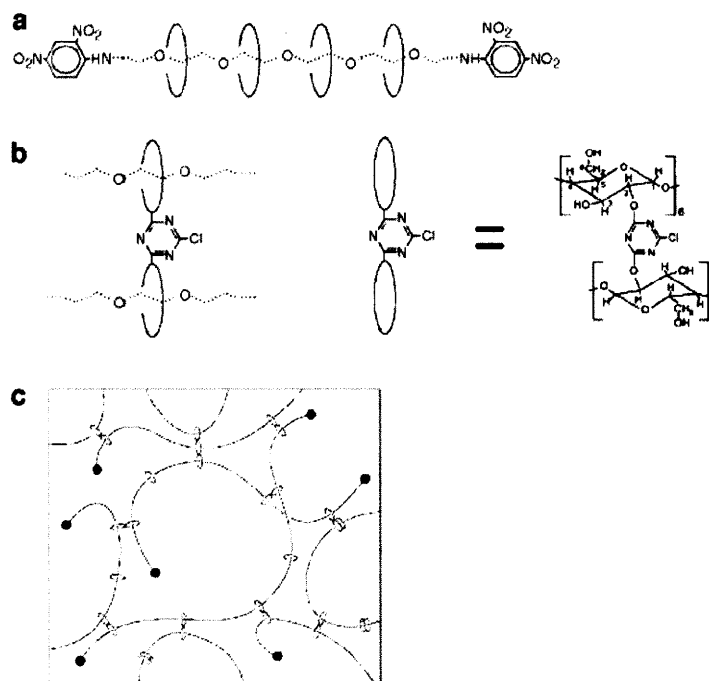
**Figure 1-3:** Energy absorption data (work) from quasistatic tensile mechanical tests (5 mm/min) of 12 μm diameter Kevlar® PPTA fibers from DuPont and 50 μm diameter Iupilon® PC fibers spun by Dr. Timothy Fornes (MIT DMSE, post-doctoral researcher). The gauge length is left out of the work calculation but was the same for both samples.

*1.1.3 Interlocking Networks*

Network morphology in polymers can be created from entanglements, hydrogen bonding, and covalent cross-linking. They can also be created from unique structural morphologies, as in the case of segmented polyurethanes or the double gyroid [34] in PS/PI/PS systems. But there are very few studies aimed at utilizing steric interlocking to



create novel morphologies, despite the fact that entanglements may be the most common type of inter-chain interaction in polymers. One particular study involves the threading of polymer chains through ring-like constructions, called rotaxanes [35, 36] to create “sliding gels.” The concept of sliding gels was first suggested by de Gennes [37], and a number of studies have focused on the unique strain hardening observed [38-40], which is uncommon in typical polymer gels. In these systems, polymer chains are able to thread through the rotaxane rings, promoting ductility in an interlocked but flexible network. However, in order to create this network, the rotaxane rings must be synthesized around the polymer chains. And without end caps, the polymer chains will slide out of the rings. Fig. 1-4 illustrates these “figure-of-eight cross-links.” This notion of threading and the short comings of this particular design will be addressed later.



**Figure 1-4:** Representations of a) poly(ethylene glycol) based polyrotaxanes, b) the figure-of-eight covalent cross-link and c) cross-linked polyrotaxane gel from [35].

## 1.2 Applications

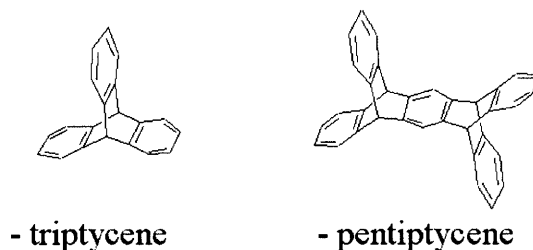
This work was funded by the U.S. Army Research Office (under Contract DAAD-19-02-0002) and was conducted at the Institute for Soldier Nanotechnologies. The mission was to investigate novel polymer architectures for enhanced energy absorption characteristics for use by soldiers and other first responders. Polymers are used in many applications over alternative materials, such as metals or ceramics, because of relative cost, ease of processing and weight. Also, a number of desirable properties are only accessible by polymers, such as flexibility, solubility, and multifunctionality from tunable properties. Transparency for polymers also comes at a much lower cost than for ceramics. Therefore, high strength polymers have many military and non-military uses.

The primary use by military (and other first responders) for high strength polymers is in protective clothing. PPTA, for example, is used to weave bullet-proof vests. As a bendable fiber with high tensile modulus, it can be also be used in woven mats and fiber-reinforced composites like helmets. Ductile polymers, such as PC and polyurethanes (PU), are used in non-flexible shielding applications. Both PC and PU are often used in bullet-proof windows, eye and face protection, and blast shields. Additionally, there are non-military related applications for high strength polymers. High strength fibers are used in tire cord, motor cycle jackets and helmets, boat frames, and gloves. Ductile, transparent polymers are used in automobile parts, sport visors, and packaging.

As the applications for high strength polymers are wide spread, significant advances in the field would therefore generate much military, commercial and public interest.

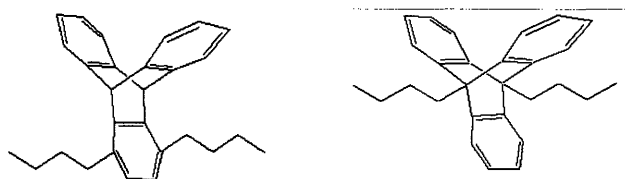
## 1.3 Iptycenes

Relatively little attention has been given to nanoscopic, shape persistent, three-dimensional structures and their interactions with polymer chains. One family of such structures is called iptycenes (Fig. 1-5). Iptycenes are fused aromatic structures with unique, rigid molecular geometries that create internal local cavities accessible by adjacent molecules in their surroundings. This is in contrast to most molecular units that function as essentially spherical or cylindrical particles. Adamantyl groups, for instance, have been found to decrease inter-chain interactions [41, 42] when introduced into polymer systems. Cage-like structures, such as polyhedral oligosilsesquioxane (POSS), also do not promote interactions between polymer chains. Although as pendant units, they have been seen to aggregate amongst themselves and therefore effectively create inter-chain interactions. But this is because of the substituents added to the edge of the POSS cage and not from the physical structure of the POSS itself [43-46]. Iptycenes are distinctive in their ability to induce steric-driven interactions without requiring controlled syntheses as in the case with rotaxanes.



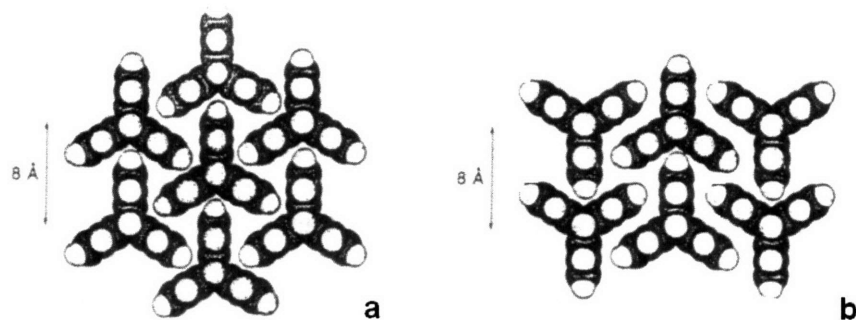
**Figure 1-5:** Structures of two iptycenes: triptycene and pentiptycene.

While pentiptycenes [47-52] and other particular types of iptycenes [53, 54] have been studied in various systems, the most popular iptycene has been the triptycene. Triptycene was originally synthesized into polymer systems as far back as 1969, when DuPont incorporated units into polyesters, polyamides, and polyurethanes using a “bridgehead” substitution [55] shown in Fig. 1-6. The goal of this study was to produce colorless, thermally stable polymers. Solvent cast films were reported to be highly crystalline and brittle. Of the fifteen polymers synthesized with triptycene, only the mechanical properties of two films were stated. The modulus values were 2-3 GPa and elongation was 5% for both polymers.



**Figure 1-6:** Schematic of two possible incorporations of triptycene into the backbone of a polymer: benzene (left) versus bridgehead (right).

Triptycene units were then envisioned as “paddle-wheel” structures capable of interlocking and creating molecular devices, such as ratchets [56], gears [57, 58] or propellers [59]. It was shown numerous times through both modeling and x-rays that isolated iptycenes could interlock with one another as illustrated in Fig. 1-7 [60-63]. However, none of these studies had produced any applications until work done by the Swager group in the Department of Chemistry at MIT was finally able to utilize the unique structure of not only triptycene, but many other iptycenes as well.



**Figure 1-7:** Schematic of possible interlocking patterns of isolated triptycene units based off of x-ray data (adapted from [62]).

### 1.3.1 Iptycenes for Low- $\kappa$ Dielectrics

The local cavities of iptycene units can be viewed in some senses as internal porosity. If these cavities remain unoccupied, then the free volume of the system increases. This was the goal of studies aimed at the molecular design of low- $\kappa$  dielectric materials. Low- $\kappa$  dielectrics are of important commercial interest due to the direct relationship between the dielectric constant of the inter- and intralayer insulators and the interconnect delay times caused by resistive-capacitance crosstalk [64]. The dielectric constant becomes critical as the semiconductor industry drives feature sizes smaller and smaller [65, 66]. The Intel Pentium 4 processors are based on 0.18  $\mu\text{m}$  feature sizes [67], and currently, leading organic dielectric materials have a  $\epsilon = 2.65$  [68]. Recently, porosity has been the focus of generating low- $\kappa$  materials [69-71], and future projections indicate that short term industrial targets are  $\epsilon = 2.0 - 2.5$  and long term targets are  $\epsilon < 2.0$  [72-76] in order to meet feature size estimates.

The use of iptycenes to introduce molecular-level porosity into polymer samples was a novel approach by Swager to designing materials with low dielectric constants. Long and Swager [77] synthesized many different types of iptycene-containing polymers with

very short monomer lengths (often only a few carbon atoms). Certain types of incorporations were more successful than others, but they found that the samples with iptycenes consistently had lower dielectric constants than the analogous polymers without iptycenes. They were able to achieve dielectric constants as low as  $\epsilon = 2.41$  (10 kHz). In addition, it was found that the presence of iptycene units also enhanced the thermal stability of these polymers by as much as 200 °C.

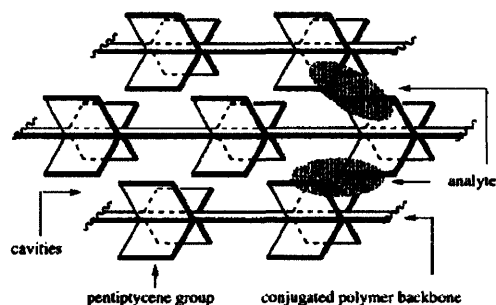
Other groups have tried to extend this approach to different types of units, such as adamantyls [78], but those materials exhibited higher dielectric constants than the iptycene polymers with  $\epsilon = 2.92$  (1 MHz). These studies further supported that iptycene units did more than simply disrupt chain packing (as any bulky substituent may be expected to do). The iptycene cavities created a unique porosity for which the applications were just beginning to unfold.

### *1.3.2 Iptycenes in Sensing Applications*

Conjugated polymer-based fluorescence has utilized energy migration along the polymer backbone to create chemosensory devices [79, 80]. It has been shown that local analyte binding creates traps for the excitations and quenches the fluorescence of the system. The Swager group has been using pentiptycenes in poly(phenyleneethynylenes) to create molecular sites for local analyte binding [48, 81, 82]. In particular, they were investigating methods for the detection of trace vapors of 2,4,6-trinitrotoluene (TNT) and 2,4-dinitrotoluene (DNT), both of which are highly explosive and the primary constituents of land mines [83]. They showed that the signal attenuation was extraordinarily fast. For a 25 Å film, the fluorescence quenching for TNT at 10 ppb was

75% in 60 seconds. For DNT at 10 ppb, the same film exhibited 91% fluorescence quenching in 30 seconds.

The mechanism through which this chemical detection occurs is schematically shown in Fig. 1-8. The cavities of the pentiptycenes create a porous polymer system conducive towards the diffusion of analyte particles. The analytes fill the cavity spaces of the pentiptycenes, modifying the energy landscape that controls the mobility of energy and charge carriers. This results in the fluorescence quenching observed. It was also shown that larger cavities promoted more analyte binding which resulted in higher levels of fluorescence quenching.



**Figure 1-8:** Depiction of analyte diffusion and binding from [47, 48]. The analyte particles occupy the cavities created by the iptycene units.

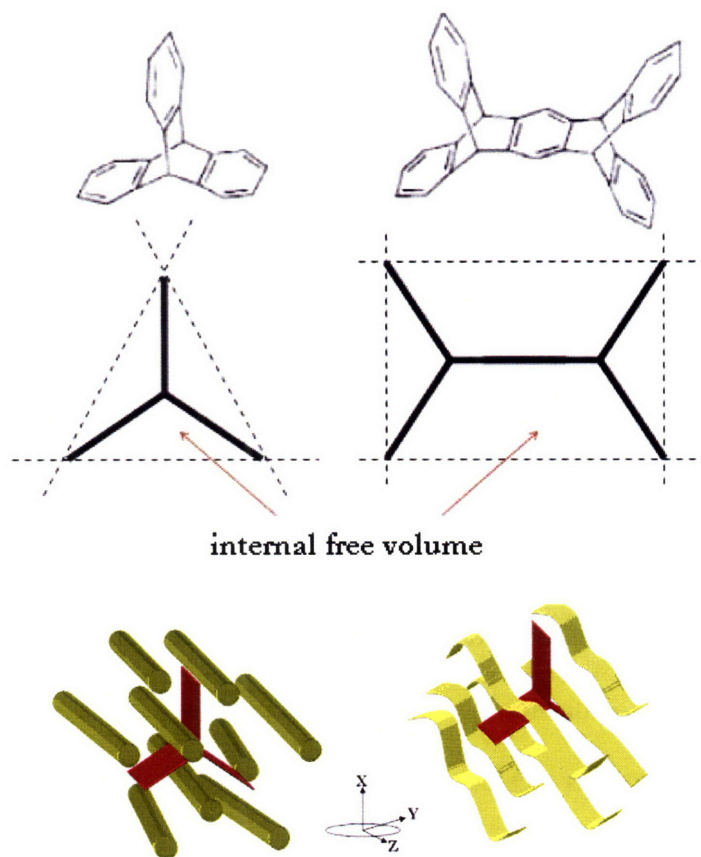
This was the first case of successful utilization of the occupation of iptycene cavities, and it sparked additional work focusing on the possible applications of this behavior.

### 1.3.3 *Iptycenes for Directive Ordering / Alignment*

As shown in Fig. 1-7, it had been noted in the past that isolated triptycene units would interlock with one another in order to minimize free volume. This tendency to fill the

cavity spaces created by the iptycene structure was seen again in the previous section with analyte particles. In 2001, Long and Swager [53] qualitatively defined the unique structural characteristic of iptycenes as “internal free volume.” Internal free volume described the local cavities created by the shape-persistent aromatic structures (Fig. 1-9). Long and Swager found that iptycene units blended into nematic liquid crystals (LC) and stretched polymers would align perpendicular to what their longest aspect ratios would dictate. Iptycene units oriented themselves such that their *empty cavity spaces* (rather than the space-filling structure itself) coincided with the direction of the surrounding moieties allowing for the maximum occupation of space with the minimum disruption to order. This indicated a strong preference to pack or fill these cavities with neighboring LC molecules or polymer chains (Fig. 1-9).





**Figure 1-9:** Internal free volume is illustrated (area inside of the arrows) along with representations of how surrounding molecules or polymer chains prefer to minimize the total free volume of the system through the occupation of the triptycene cavities, modified from [53].

This was shown using dichroic measurements. Although Swager had actually already been using this concept in the detection of small molecules for chemosensor applications [47, 48], this was the first time that the unique structural characteristic of iptycenes had been given a name.

The minimization of internal free volume directs the mutual alignment of surrounding molecules through packing or “threading” along iptycene cavities. This was used to enhance chromophore alignment [50, 54] and was the first usage of iptycenes to *guide*

interactions. Whereas other systems with very short monomer units increased the free volume of the system, here, in these 1 wt % blends, just the opposite occurred. Aside from concentration dependence, another key difference in the work by Swager's group was the replacement of the bridgehead substitution used by DuPont with a benzene substitution. This architecture places less hindrance to the occupation of the cavities, which will be discussed in greater detail in Chapter 3.

## 1.4 Objective

The purpose of this thesis was to exploit the minimization of free volume in iptycene containing polymers to enhance the mechanical properties. In particular, the presence of these types of unique units creates a novel molecular architecture, and this work focused on the ability for iptycenes to enhance inter-chain interactions and the effects on the mechanical properties of polymers. First, the need for a quantitative and qualitative definition of the structural property introduced by Swager as "internal free volume" was addressed. Then, we examined a number of polymer systems containing various iptycene units incorporated into the backbone through a benzene unit (Fig. 1-6). We investigated polymers with long monomer units (polyesters) as well as those with short monomer units (polycarbonate). At many points in the thesis, the packing of surrounding moieties into the cavities of iptycene units is referred to as "threading." This is a slightly different type of threading than the conventional notion of passing a long, thin object (e.g., a needle) through a ring (e.g., a thread). Threading through a ring is a highly improbable event unless synthesized as such, which is why the interlocking gels in Fig. 1-4 must be synthesized with the rotaxanes around the polymer backbone and held in place by

endcaps. Here, the term “threading” is used because of the similarities in the concept of space-filling and sliding along that space. But in this case, the accessibility of these open cavities makes this type of threading much more probable and involves easier chemistry to synthesize. This thesis concludes with suggestions for future work based on the discoveries made here.



## Chapter 2

# Experimental Techniques

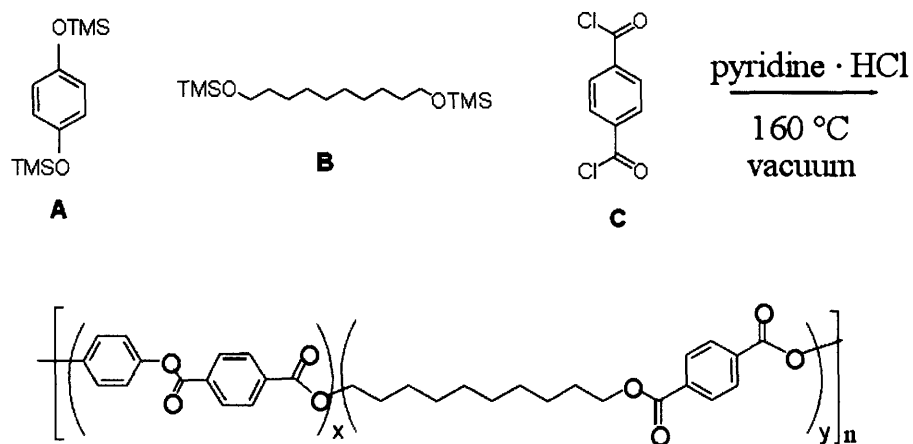
This chapter describes sample preparation as well as the experimental techniques used to characterize the polymer samples. A number of experimental details will be revisited as they become relevant in later chapters, but many equipment particulars are noted only here. Chapter 2 is divided into three main sections: polymer synthesis, sample preparation and characterization.

### 2.1 Synthesis and Materials

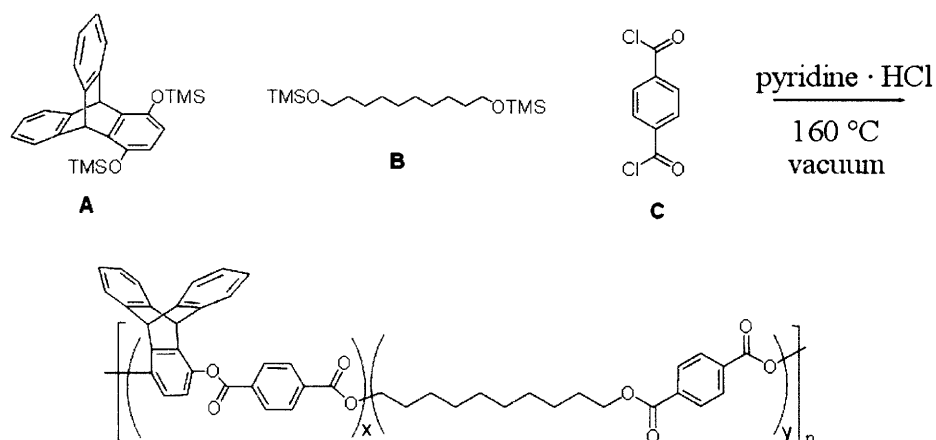
The polymers used in this study were synthesized by a variety of sources, some internal to MIT and some external. The bulk of polymer material was synthesized by members of Prof. Timothy M. Swager's group at MIT's Department of Chemistry to whom I am greatly indebted. The specific contributors will be acknowledged by name in this chapter where appropriate. Additionally, material suppliers external to MIT will be recognized in relevant discussions.

### 2.1.1 Polyesters

Polyesters containing both aromatic and aliphatic components with varying concentrations of triptycene units were synthesized by Dr. Alexander J. Paraskos (MIT Chemistry, Ph.D. '04, in Prof. Swager's group) in Chapter 6 of his dissertation [84]. The condensation reactions utilized are covered in great detail in his thesis. The basic polyesters (shown in Fig. 2-1) synthesized from random copolymerization of three components (**A**: di(trimethylsiloxy) benzene, **B**: 1,10-bis(trimethylsiloxy) decane and **C**: terephthaloyl chloride) served as a baseline reference polymer for comparison of thermal, structural and mechanical properties. The triptycene-containing polyester followed a similar synthetic scheme replacing di(trimethylsiloxy) benzene as the **A** component with a triptycene monomer in Fig. 2-2.



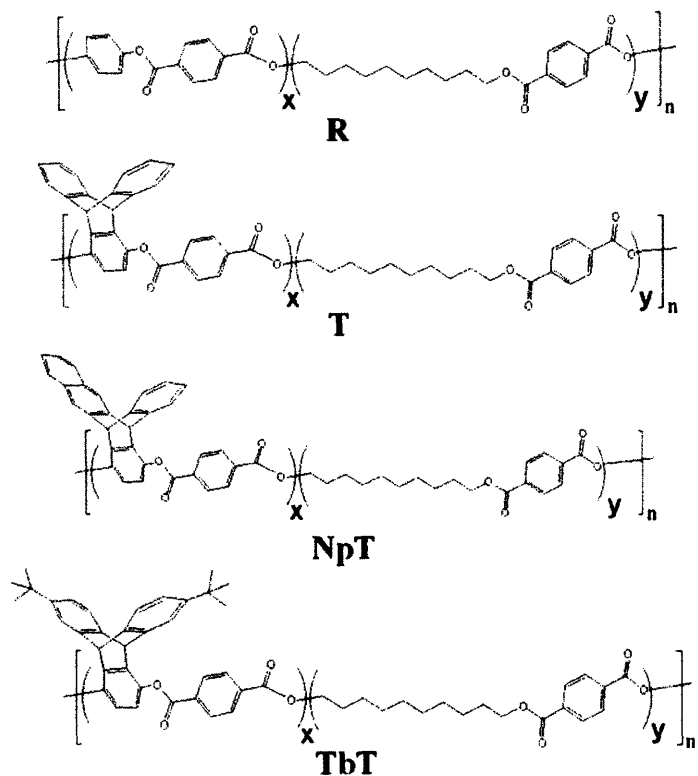
**Figure 2-1:** Basic route for random block copolymer synthesis of polyesters containing no triptycene units [84, 85]. Concentrations of aromatic content versus aliphatic content can be controlled by changing the mixing ratios of **A**, **B** and **C**, which result in final  $x/y$  ratios for the polymer.



**Figure 2-2:** Basic route for random block copolymer synthesis of polyesters containing triptycene units [84, 85]. Using this template, any type of triptycene unit or aromatic unit can be used as the **A** component. Concentrations of aromatic content versus aliphatic content can be controlled by changing the mixing ratios of **A**, **B** and **C**, which result in final x/y ratios for the polymer.

Dr. Paraskos produced a range of low molecular weight polymers with small x/y ratios for initial screening of mechanical and structural properties. After this initial screening, ratios of 1/3 and 1/5 were chosen for “scale-up” of molecular weight.

As a follow up, Dr. Lokman Torun (a post-doctoral researcher in the Swager group) utilized Dr. Paraskos’ synthesis methods to produce another set of random block copolyesters. He generated four different polyesters by varying the **A** component as: di(trimethylsilyloxy) benzene, di(trimethylsilyloxy) triptycene, di(trimethylsilyloxy) naphthalene-modified triptycene, and di(trimethylsilyloxy) tert-butyl-modified triptycene. The resultant set of polyesters is displayed in Fig. 2-3.



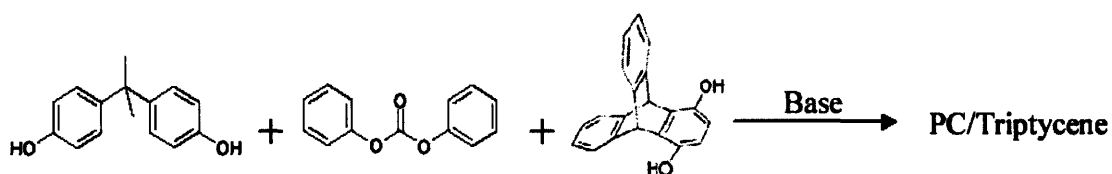
**Figure 2-3:** Set of random block copolyesters where  $x/y = 1/5$  for a reference non-triptycene polyester (R), triptycene polyester (T), naphthalene-modified triptycene polyester (NpT), and tert-butyl-modified triptycene polyester (TbT). Appears in [86].

### 2.1.2 Polycarbonates

Polycarbonates (PC) with and without triptycene that were studied here were synthesized by a variety of sources. A commercial grade bisphenol-A PC provided by Mitsubishi Engineering Plastics under the trade name Iupilon® E2000 was used as a baseline standard for all thermal and mechanical characterization. Under the direction of the principal investigators of ISN Project 1.1, Triton Systems, Inc. (TSI) manufactured copolymers of PC containing triptycene in various concentrations using melt condensation reactions detailed in their quarterly reports [87-90]. The basic scheme is



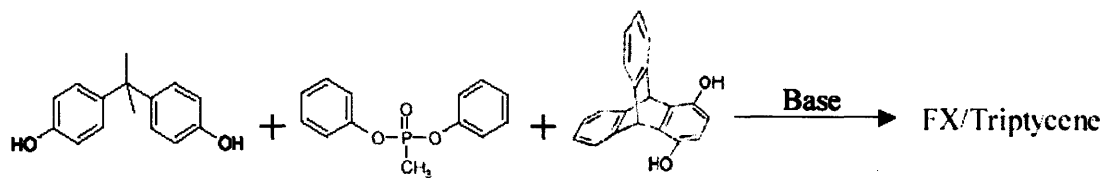
shown in Fig. 2-4. Additionally, TSI synthesized a bisphenol-A PC with a chemical structure identical to that of Mitsubishi's commercial available Iupilon® brand using the same scheme as in Fig. 2-4 excluding the triptycene hydroquinone. TSI was only able to produce low molecular weight ( $M_n \sim 6,000 - 13,000$  g/mol) samples that were not comparable to commercial grade PCs ( $M_n \sim 30,000$  g/mol).



**Figure 2-4:** Basic outline of triptycene incorporation into bisphenol-A PC to form a Triptycene-PC (T-PC) copolymer.

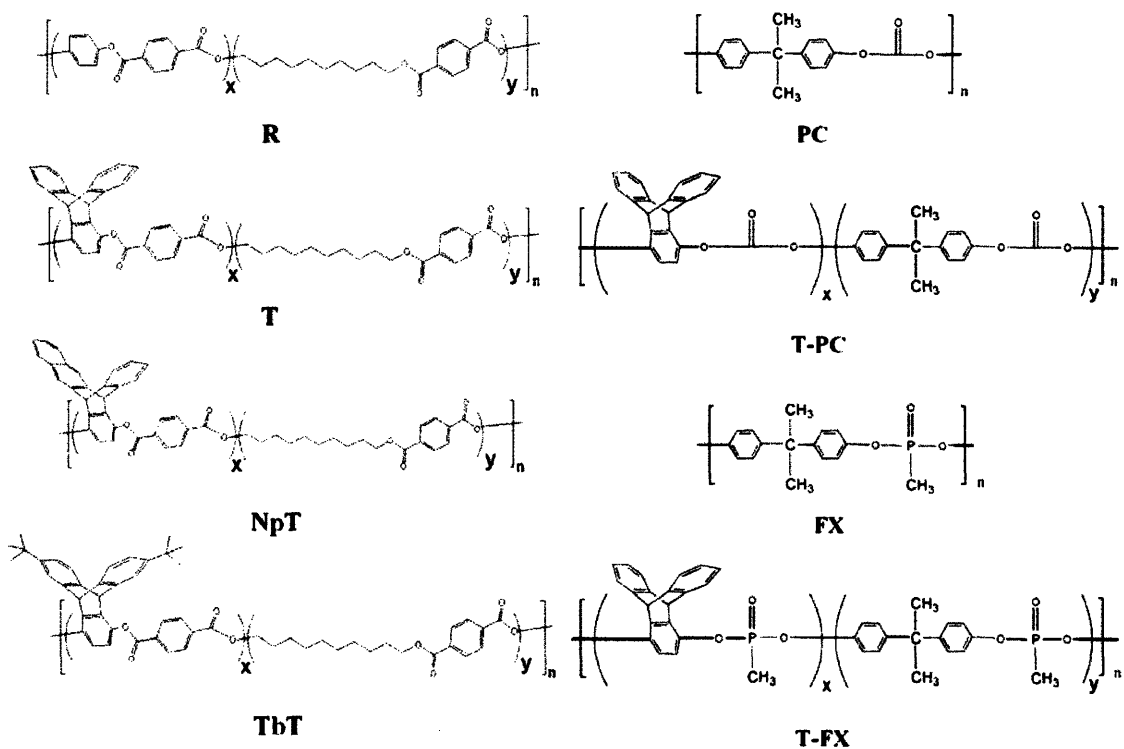
Utilizing a similar process, Yong Yang (a chemistry graduate student in Prof. Swager's group) synthesized more triptycene containing polycarbonates (T-PC), providing a range of triptycene concentrations at much higher molecular weights. Employing an additional catalyst not used by TSI, he was able to achieve molecular weights comparable to those of commercial grade PCs.

TSI also prepared phosphorus-containing copolymers ("FX") for usage in fire retardancy applications. Both the chemical structure and synthesis route are based on the approach used for the PC and T-PC samples. Triptycene-FX copolymers (T-FX) were prepared, and the synthetic scheme is displayed in Fig. 2-5. As in the case with the PC synthesis, the pure FX synthesis was identical to that shown in Fig. 2-5 excluding the triptycene hydroquinone. Molecular weights ( $M_n \sim 3,000 - 4,000$  g/mol) were again much lower than commercial grade.



**Figure 2-5:** Basic scheme of triptycene incorporation into Triton Systems, Inc.’s “FX” polymer to form Triptycene-FX (T-FX) copolymer.

Fig. 2-6 summarizes all of the polymers synthesized for characterization in this thesis.



**Figure 2-6:** Final chemical structures of polymers characterized in this thesis. All block copolymers were random polymerizations, and the chemical structures here are statistical representations that were “controlled” by molar concentrations and reactivity ratios (producing tailorable x and y values).

## 2.2 Sample Preparation

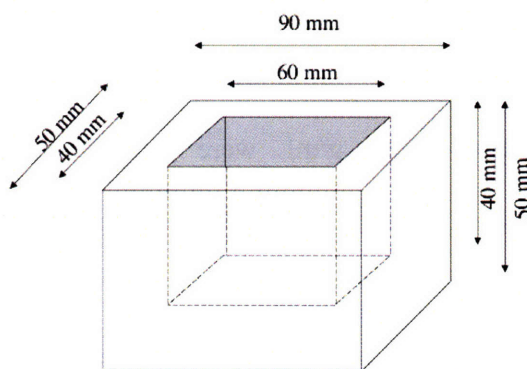
Post-synthesis, polymer samples were in the form of powders that had to be processed for many of the thermal and mechanical characterizations used. Most of these procedures will be revisited in greater detail in the later chapters that pertain to them.

### 2.2.1 *Solvent Casting*

Solvent casting was utilized during the processing of both polyester and polycarbonate samples. Both polyesters and polycarbonates are soluble in dichloromethane (a.k.a., CH<sub>2</sub>Cl<sub>2</sub> or methylene chloride) at room temperature. However, a hot plate was usually employed to accelerate the process. At moderate temperatures (~60 °C), solutions with concentrations of about 0.01-0.03 g/mL were stirred by Teflon®-coated magnetic spinners in closed glass vials. Polymers were completely dissolved within 24 hours forming colorless solutions.

Solutions contained varying levels of cloudiness due to unknown impurities in the chemistry. Polymers that had been processed carefully during synthesis formed clear solutions, while others had sometimes significant levels of insoluble impurities. As the NMR and GPC used to characterize these materials used solutions that had been passed through a 0.2 µm Teflon® filter, it was fitting to use the same filtration for thermal and mechanical testing. In most cases, syringe filtering was manageable for quantities not exceeding 100 mL at a time. In situations where the amounts of impurities were visibly significant (from extreme cloudiness), centrifuging the insoluble particles to the bottom of the vials helped immensely with the filtration process.

Filtered solutions were allowed to evaporate slowly in custom machined Teflon® boxes. These boxes were machined by the MIT Central Machine Shop from the diagram instructions in Fig. 2-7. It was found that this was the best way to cast consistent, even-thickness films from solution. Once these boxes were filled with polymer solution, glass bowls were used to cover the boxes to promote a slow and constant rate of evaporation in a fume hood while simultaneously protecting the solution from contamination. Typical solutions of dichloromethane ranged from about 40-80 mL and would routinely take 2-3 days to evaporate completely at room temperature in a hood.

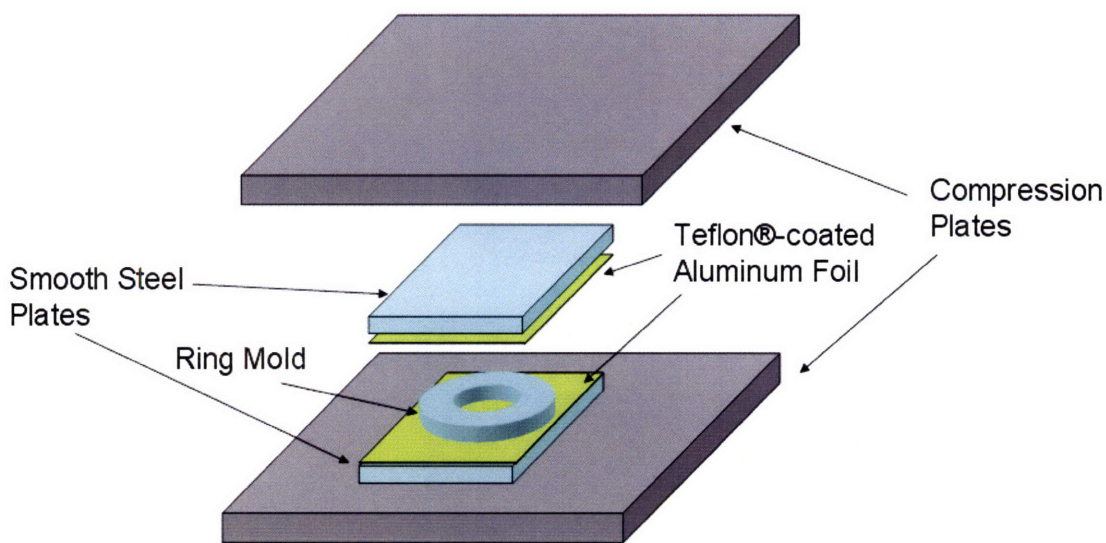


**Figure 2-7:** Diagram from which Teflon® boxes were manufactured by the MIT Central Machine Shop. Instructions also noted that all inside surfaces must be polished smooth and that it was critical that the bottom surface be perfectly level.

### 2.2.2 Melt Pressing

A Carver hydraulic hot press was used to prepare samples out of the melt state. Polymer films prepared by solvent casting were placed between two smooth metal plates with thin sheets of Teflon®-coated aluminum foil to separate the polymer from the metal. This process was suitable for melting thin films (~0.1-0.3 mm thick) using almost no pressure when touching the heating plates. When thicker samples were needed (~2-3 mm thick), a

ring mold (with a Teflon® surface coating deposited by chemical vapor deposition) was used to confine the molten polymer (shown in Fig. 2-8). With the ring mold, pressures of 7,500 psi were used.



**Figure 2-8:** Ring mold setup for melt pressing polymers. In the case where the ring mold was not utilized, the rest of the setup remained identical.

Whether using the ring mold or not (and thus, using pressure or not), melted samples were cooled back down to room temperature using water cooling coils. Samples could then be removed from the mold and/or plates easily. In some cases, there were bubbles in the compression molded disks from trapped air unable to escape the melt. If the bubbles were significant, a custom machined compression tool was used in the hot press to squeeze out the bubbles. The custom machined pressing tool, shown in Fig. 2-9, was built to allow a compression molded disk to be reheated to temperatures high enough to allow for flow but not a low viscosity melt state. Therefore, with tight tolerances, only

the air bubbles could escape during pressing at 15,000 psi. After 15,000 psi was reached, cooling was immediately initiated. Disks removed were found to have the bubbles successfully pressed out.



**Figure 2-9:** Custom machined compression tool used to squeeze out bubbles in polymer disks. Entire assembly was placed between the hot press compression plates for operation.

### 2.2.3 Heat Treatments

In all cases, after solvent casting, samples were dried in a vacuum oven at 65 °C for at least 12 hours to ensure the removal of all solvent. Before melt processing, the samples had to be dried again to remove all water. In the case of polyesters, 65 °C in a vacuum oven the night before processing was sufficient. For polycarbonates, samples were stored

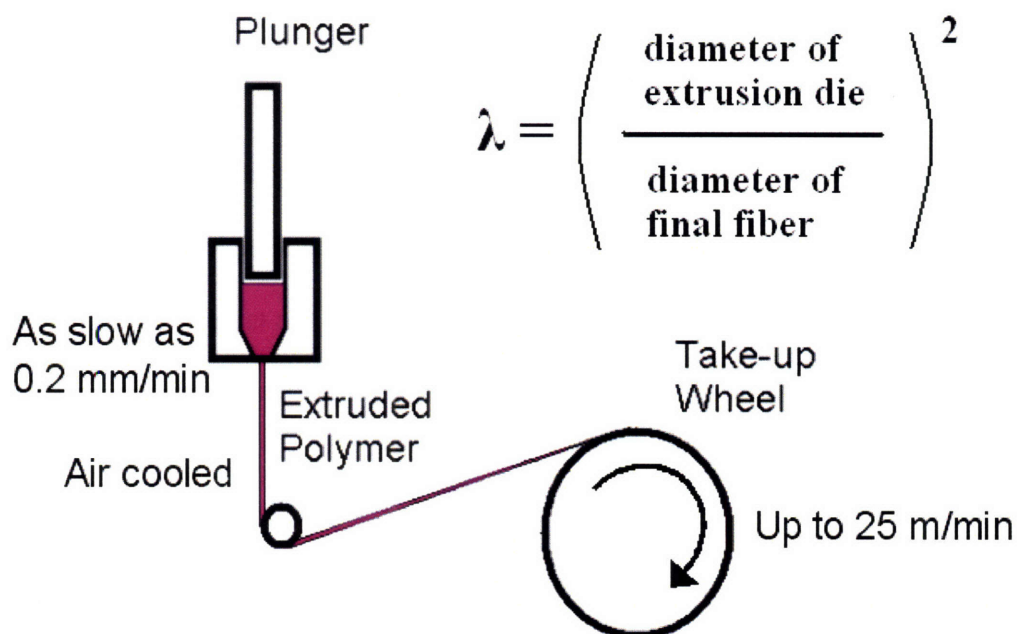
at 120 °C in vacuum overnight. There was often a time lag between sample processing and testing. Therefore, before testing, the samples must be dried again to eliminate water content. This process involved a 55 °C vacuum for a minimum of one week. The only time this was not employed was if the samples were immediately stored in a desiccator after processing and were not exposed to air/moisture until testing.

#### *2.2.4 Oriented Samples and Fiber Spinning*

The Zwick mechanical testing apparatus (which will be discussed further in section 2.3.5) included a temperature controlled chamber inside of which samples could be heated or cooled. Film samples could be heated, stretched inside of the temperature chamber, and then held in tension while the chamber cooled down to preserve orientation imparted to the samples.

A second method of preparing oriented samples was to melt spin fibers. A donated DuPont melt press spinner was custom modified to process polymer batch sizes of 1-2 grams (much lower than the ~100 gram quantities it was made for). A wide range of spinnerets were available for use, including monofilament and multifilament. The diagram in Fig. 2-10 illustrates the essential functional parts of the apparatus. Polymer is melted inside of a chamber (under vacuum) that is enclosed in a digital temperature control heat band. A plunger, which could run at multiple speeds, drives the polymer through the spinneret hole where it is immediately cooled by the surrounding air. The extruded polymer is then redirected to a variable speed take-up wheel. The difference in the speed of the take-up wheel versus the speed at which the polymer exits the die generates extensional forces on the extruded molten polymer as it is cooling that result in

orientation of the microstructure. Therefore, the minimum plunger speed coupled with the maximum take-up speed that the molten polymer can sustain should produce optimally oriented fibers. Using this method, some polymers observed in this study could be readily drawn down to fibers with 30-50 micron diameters.



**Figure 2-10:** Diagram of the essential parts of the melt spinning device used to produce oriented fibers.  $\lambda$  = draw ratio.

## 2.3 Characterization

Polymers were characterized thoroughly for structural, thermal and mechanical properties. This section details specific techniques utilized to analyze the properties of interest to this work. As with the previous section, additional experimental details that pertain to specific samples will be revisited as they become relevant in later chapters. However, many experimental particulars are mentioned only here.



### 2.3.1 *Modeling*

Accelrys Materials Studio software was used to construct molecular models of iptycene units. Discover Dynamics Smart Minimizer<sup>TM</sup> with medium convergence for 5000 steps was used to determine the most energetically stable conformation for a structure. This software was also used to calculate the volume occupied by a particular molecular unit using a van der Waals isosurface.

### 2.3.2 *Molecular Weight*

Molecular weights for polymer samples were obtained using a Waters gel permeation chromatograph (size exclusion chromatograph) at 35 °C. Four columns were employed with THF eluent to measure values for number average molecular weight ( $M_n$ ) and weight average molecular weight ( $M_w$ ) relative to polystyrene standards. Polydispersity (PDI) was calculated from the relative values measured.

### 2.3.3 *Structural Properties*

Nuclear magnetic resonance (NMR) was used to confirm the chemical structure of the polymers synthesized. This was performed by the various members responsible for the synthesis in Prof. Swager's group in the Chemistry Department at MIT. Individual credit for each polymer synthesized and characterized by NMR is given in section 2.1.

Crystallinity and orientation of processed samples (both undeformed and deformed) were probed using X-ray analysis. Wide-angle X-ray scattering (WAXS) patterns were taken at the X27C beamline at the Brookhaven National Synchrotron Light Source. Typical exposure times for films of about 100  $\mu\text{m}$  in thickness were 300 seconds. WAXS

patterns were also taken using a Molecular Metrology small-angle X-ray scattering device with a custom-machined attachment that allowed WAXS  $d$ -spacings to be observed. Typical exposure times for films of about 100  $\mu\text{m}$  in thickness were 3600 seconds. All images were normalized for sample thickness, exposure time, and beam flux. The  $d$ -spacings were calibrated using  $\text{Al}_2\text{O}_3$  with Polar software (licensed to ISN) and Fit2D (freeware).

Optical microscopy was also utilized to characterize molecular orientation for some film samples using a Zeiss Axioskop 2 with cross-polarizers.

Density measurements were taken using a Micromeritics AccuPyc 1330 He pycnometer through a collaboration with DuPont. The pycnometer fills an enclosed chamber containing the sample of known mass with Helium gas to measure the volume occupied by the sample. Density is calculated by dividing the mass and volume measurements. All samples were stored in vacuum for at least a week prior to testing.

#### 2.3.4 *Thermal Properties*

A TA Instruments Q1000 differential scanning calorimeter (DSC) was used to examine a number of thermal properties of polymer samples. DSC measures how much heat it takes to raise the temperature of a sealed aluminum pan containing about 4-6 mg of sample compared to any empty pan. Melting endotherms provide data for the analysis of sample crystallinity, melting points and thermal history. Additionally, this technique often detects glass transition temperatures ( $T_g$ ) and can give an indication of phase mixing or phase separation if multiple  $T_g$ 's are present. The Q1000 has a temperature range of -170 to 550  $^\circ\text{C}$  with heating rates of 0.1 to 200  $^\circ\text{C}/\text{min}$  and a maximum cooling rate of

140 °C/min. ASTM D3418-03 covers extensively the proper methods to analyze DSC data and extract the aforementioned information.

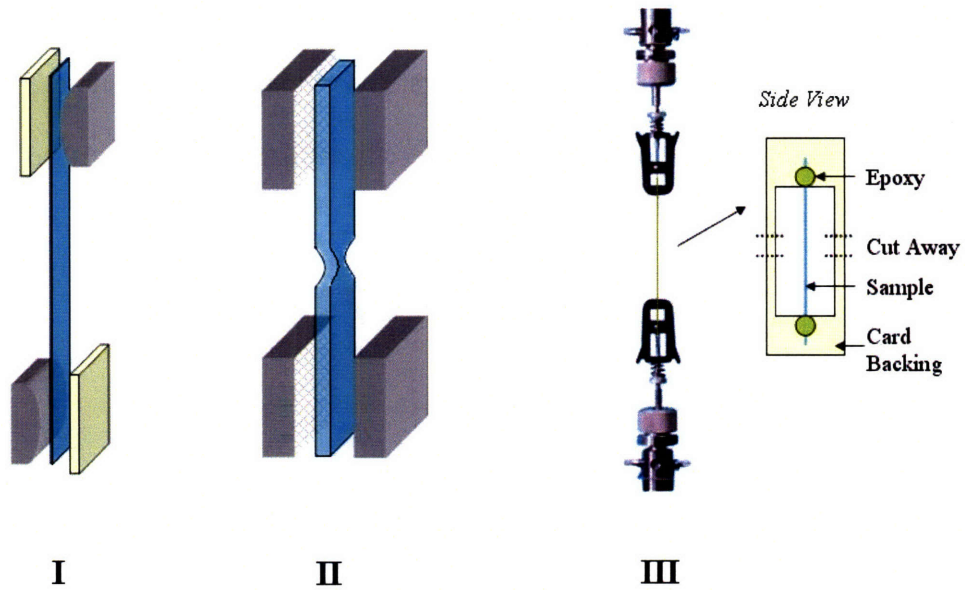
A TA Instruments Q50 thermal gravimetric analyzer (TGA) was used to determine degradation temperatures in air and in nitrogen up to 1000 °C. 10-20 mg of polymer sample are loaded onto a suspended platinum pan and then sealed in a chamber of either nitrogen gas or air delivered from a tank of compressed gas. TGA measures the mass as a function of temperature, which can be set to rise from 0.1 to 100 °C/min. The inflection point of the mass versus temperature curve is often reported as the degradation point ( $T_d$ ) and can be measured with computer software or by the peak of the derivative of the mass percent curve. Another temperature often measured is that for which 10% of the mass has degraded. It is critical to note that this experiment measures “degradation” as actual mass lost (material vaporized). Therefore, it is possible for a polymer to have degraded into monomer or other basic constituents without TGA registering a mass change.

### 2.3.5 *Mechanical Properties*

Dynamic mechanical analysis (DMA) was used to probe the thermal-mechanical relaxation spectra of materials in tensile mode. A TA Instruments Q800 imposes a fixed oscillatory strain on rectangular film or bar specimens and records the force as temperature is ramped at a fixed rate. The TA software uses the measurements recorded to calculate storage modulus ( $G'$ ), loss modulus ( $G''$ ), and tan delta ( $\delta$ ). The instrument is capable of conducting experiments in the temperature range of -150 to 600 °C although it was found that data was inaccurate once the material had passed through its  $T_g$  unless the

sample contained a very large amount of crystallinity. Frequency can be varied as well from 0.01 to 200 Hz.

A Zwick/Roell Z010 servo-hydraulic mechanical testing device was utilized to conduct quasistatic-rate deformation tests in both tensile and compressive modes. Different load cells and grips were used to accommodate different sample sizes and geometries. The load cells available were 10 kN, 500 N, and 10 N. For tensile tests of thin film ( $\sim 100\ \mu\text{m}$ ) samples, the 500 N load cell was employed with PN8133 grips. The PN8133 grips consisted of a flat “soft” polyurethane face and a convex “hard” aluminum face between which the sample was loaded and held in place by a tightened screw as shown in Fig. 2-11, setup I. Samples can then be deformed in tension at a constant engineering strain rate. This was the only mode used in this work although the apparatus is capable of more complicated modes, such as cyclical deformation or increasing rates of deformation, but not constant true strain rate.

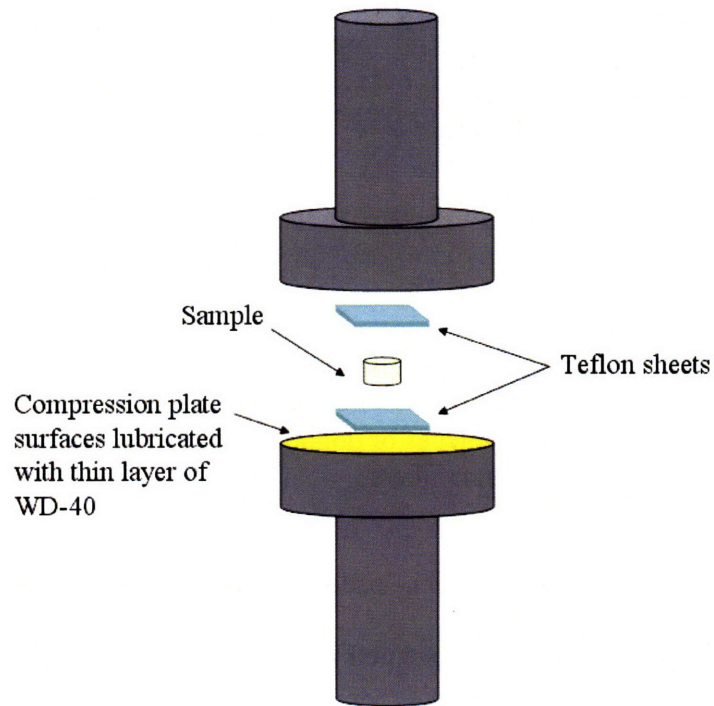


**Figure 2-11:** Tensile test setups exhibiting the different grips utilized for the different sample sizes and geometries. Setup **I** was for thin films ( $\sim 100 \mu\text{m}$ ), **II** was for thick films ( $> 1 \text{ mm}$ ) that usually contained notches or dogbones for stress concentration, and **III** was for very thin samples, such as single fibers.

For thicker films ( $> 1 \text{ mm}$ ), 8302 spring-loaded clamps with hashed steel faces were used to grip the samples, and the 10 kN load cell was used to record the forces. For very thin samples ( $< 100 \mu\text{m}$ ), such as single fibers, samples were first mounted by Loctite® Poxy Pak™ epoxy to cardboard backings for support and allowed to cure for 12 - 24 hrs. Instron #2711-006 spring-loaded rubber-faced fiber grips (modified to interface with the Zwick/Roell) were then used to grip the cardboard. Once properly aligned and secure in the grips, the cardboard was cut such that only the sample remained in tension. The 10 N load cell was used in this setup. Both of these tensile arrangements are also displayed in Fig. 2-11 as **II** and **III**.

The Zwick/Roell mechanical testing apparatus was also used to conduct compression tests. A 10 kN load cell was used with circular, parallel compression grips. Samples of cylindrical geometry were loaded between the grips, and barreling was prevented by two

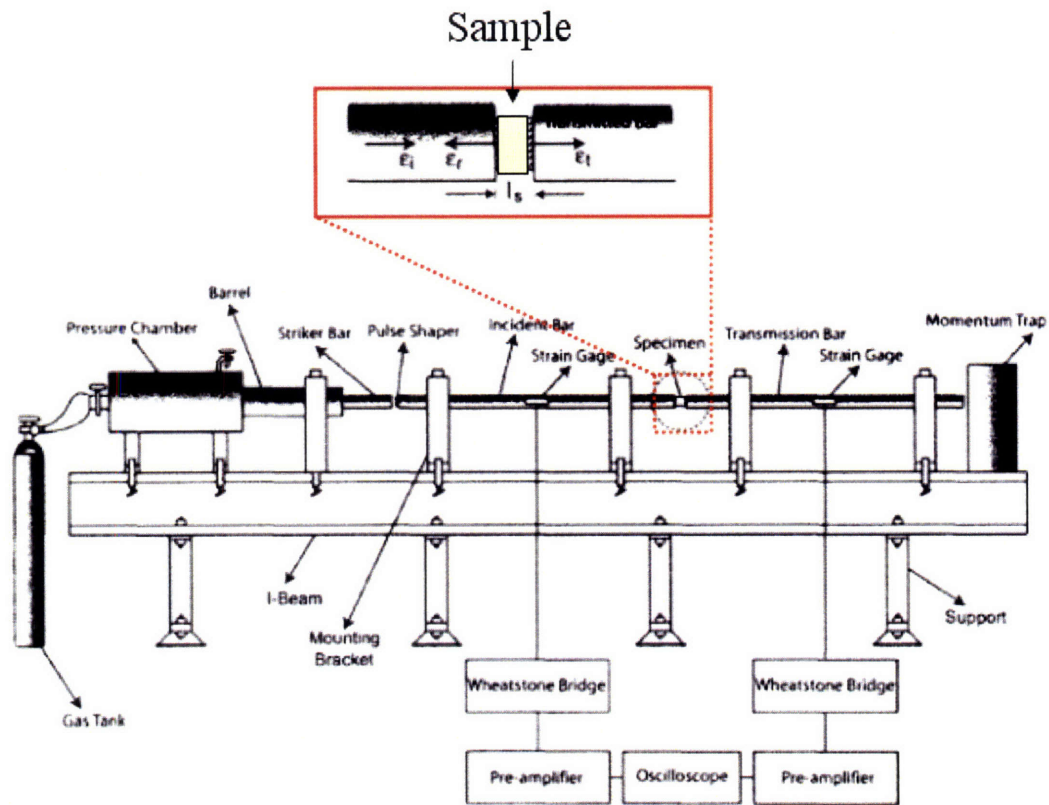
layers of lubrication: thin Teflon® sheets and WD-40 (between the Teflon® and metal). The setup shown in Fig. 2-12 was calibrated for compliance within the system before samples were tested. Test control and speeds available are identical to that in tensile mode.



**Figure 2-12:** Uniaxial compression tests using a Zwick/Roell mechanical testing machine with flat steel compression plates.

High strain rate uniaxial compression tests were performed on a split-Hopkinson pressure bar (SHPB) test apparatus designed and built in collaboration with Physics Applications, Inc. of Dayton, Ohio. This apparatus employs solid aluminum pressure bars with a length of approximately 2.3 meters and a diameter of 19.05 millimeters. A cylindrical polymer sample (typically, height ~ 2.5 mm and diameter ~ 5 mm) is placed between the two bars, and compression is initiated by a striker bar. The striker bar is

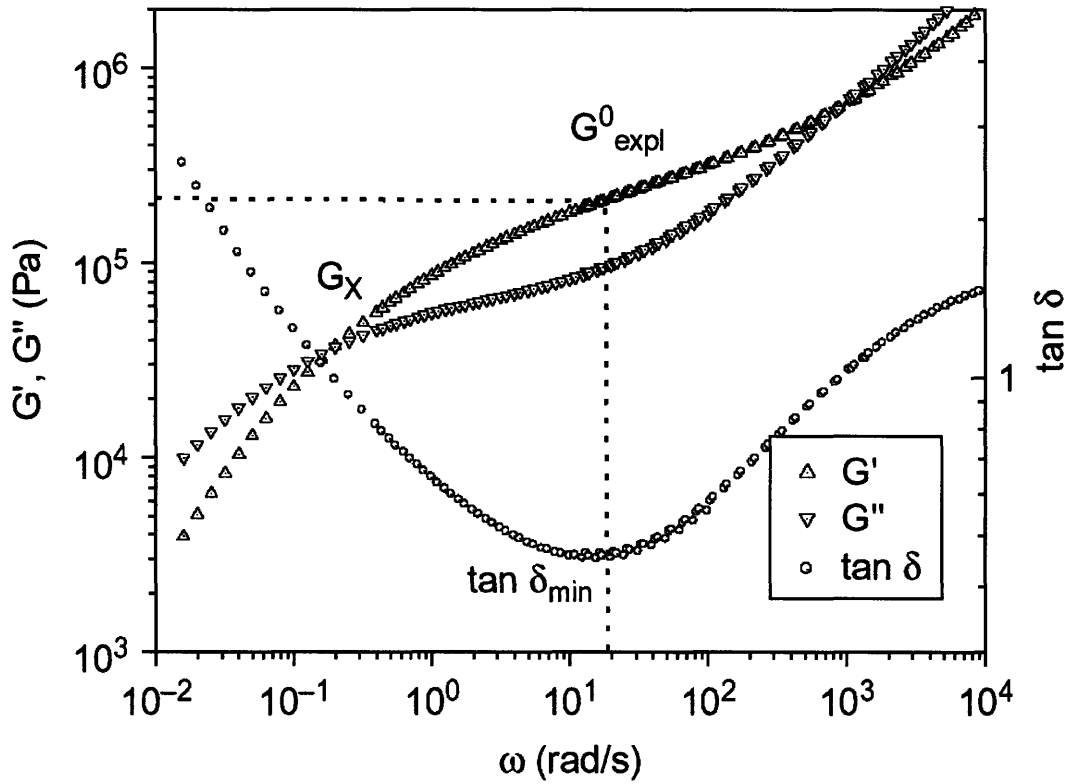
launched by pressurized gas. By controlling the gas pressure released, the user can dictate the strain rate and the amount of strain induced. A schematic of the device is exhibited in Fig. 2-13. It has been shown that an aspect ratio of 1:2 (height:diameter) of the samples to be tested is optimal in negating the effects of longitudinal and radial inertia in the specimen [91] while also minimizing wave attenuation in the strain gage signals [92, 93]. All high-rate specimens were lubricated with a thin layer of petroleum jelly on both faces to eliminate barreling. Due to the nature of the SHPB test, the amount of strain achieved is directly coupled to the speed at which the compression takes place. Therefore, “slower” rates will have lower total strains than “faster” rates. But the end of the stress-strain curve is not due to sample failure. There is also a time delay associated with the ability to calculate accurately the stress on the sample from the gauges. It takes a few microseconds for the strain gauges to produce reliable data as the incoming compressive strain wave reaches steady-state. This prevents the SHPB technique from providing the initial elastic stress-strain data necessary to calculate a Young’s modulus. SHPB can achieve strain rates of  $10^3$  to  $10^4$   $s^{-1}$  and is intended to simulate results from a ballistic impact (which typically occurs at  $\geq 10^4$   $s^{-1}$ ). While it is not explicitly proven in this work, the assumption is that materials that perform favorably in the SHPB should express commensurate behavior in other ballistic tests.



**Figure 2-13:** Schematic of the split-Hopkinson pressure bar (SHPB) test apparatus used for high strain rate uniaxial compression tests [94].

A TA Instruments Advanced Rheometer 2000 was used to measure shear stress data on molten polymer samples with disk geometries (height  $\sim 2$  mm, diameter up to 25 mm). Storage modulus versus frequency measurements were then used to calculate entanglement densities. Fig. 2-14 shows hypothetical data from which the plateau modulus ( $G_N^0$ ) can be calculated. While the figure shows one method of using the tan delta minimum, other approaches can also be used [95].





**Figure 2-14:** Characteristic data from parallel plate rheology graphically representing the identification of the plateau modulus ( $G_N^0$ ) from the  $G'$  curve [95].

Using the formula,

$$G_N^0 = \frac{4}{5} \frac{\rho RT}{M_e}$$

the entanglement molecular weight ( $M_e$ ) can then be calculated. The AR2000 parallel plate rheometer is capable of shearing rates of 0.01 to 600 rad/sec and temperatures over 300 °C in air.

## Summary

The experiments described in the following chapters follow the procedures outlined here.

In each of the later chapters, the relevant experiments reference the procedures specified here, often reiterate the important details, and provide further specifics where appropriate.

# Chapter 3

## Internal Molecular Free Volume (IMFV)

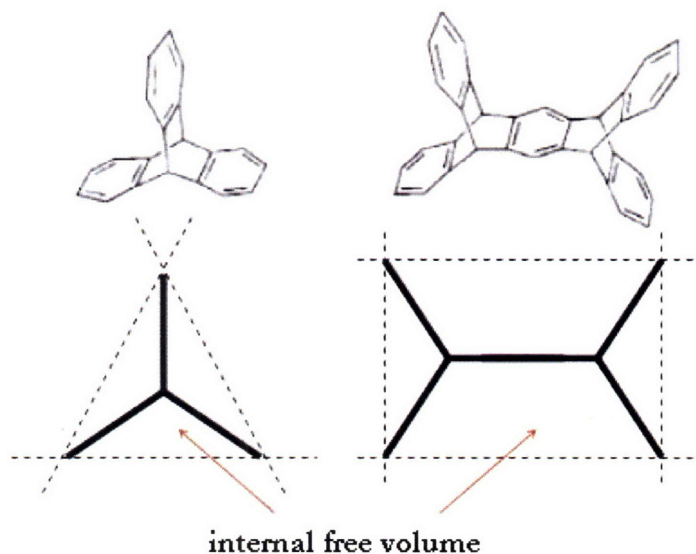
Chapter 1 contains a survey of past work that has been done regarding iptycenes. While many studies have observed intriguing properties associated with the structure of iptycene units, few have gone very far towards quantifying these effects. This chapter begins by addressing this need and defining a new structural characteristic: internal molecular free volume (IMFV). The second half of this chapter relates to the application of this newly defined characteristic.

### 3.1 Defining IMFV

#### 3.1.1 *Background*

The shape persistent, three-dimensional nature of iptycene units creates a distinctive geometry characterized by significant empty spaces within the boundaries of the structures. These empty spaces or cavities are easily accessible, in contrast to other porous cage-like structures such as polyhedral oligosilsesquioxane (POSS) or zeolites.

This characteristic has been called “internal porosity” or “internal free volume” in various works from the Swager group at MIT (revisited in Fig. 3-1).



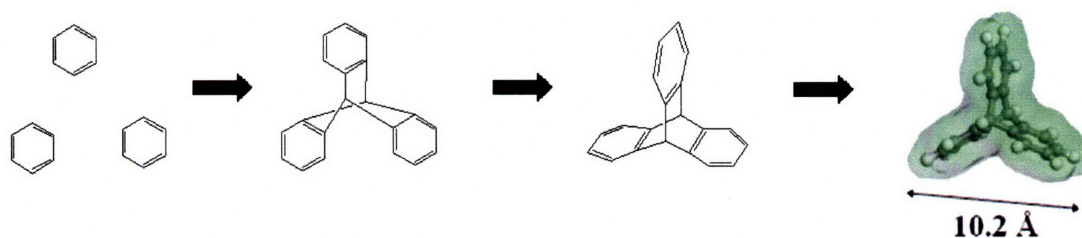
**Figure 3-1:** Depiction of internal free volume in triptycene (left) and pentiptycene (right).

While these studies were pioneering in their identifications and utilizations of iptycene structures, they did not provide a formal qualitative definition of this characteristic. There also exists no formulaic method to identify or quantify of this property. This first section of thesis work addresses these needs and begins by re-labeling this characteristic as “internal molecular free volume” or IMFV.

### 3.1.2 *Experimental Methods*

Both sections of this chapter utilized the molecular modeling program, Materials Studio™ by Accelrys. Iptycenes were not listed amongst the default structures, so they had to be built up from benzenes. When the appropriate iptycenes were constructed, the

Discover Dynamics Smart Minimizer™ with medium convergence setting for 5000 steps was used to determine the most energetically stable conformation. The software generated a three-dimensional space-filling model and could calculate the volume of structures with a van der Waals isosurface. This process is shown for triptycene in Fig. 3-2.



**Figure 3-2:** The arrows mark the process of generating the three-dimensional space filling models. The example used here was triptycene. From left to right: constructing the triptycene, calculating the optimally stable conformation, and finally converting to the space-filling representation.

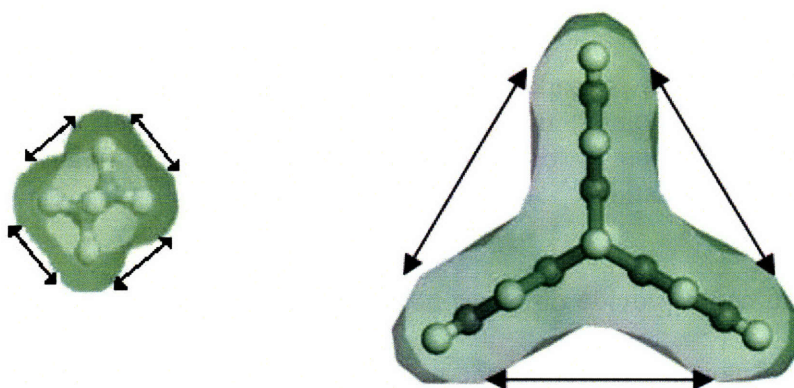
The software could provide distances between specific molecules but not between any chosen spatial points. Therefore, the molecule-molecule distance function was used to provide a scale-bar. Images were then printed out with the scale-bars allowing for the calculations of any desired distance.

### 3.1.3 Results and Discussion

First, the structural characteristic that had been previously referred to as *internal free volume* was renamed *internal molecular free volume* in order to provide a more descriptive title and to distinguish it further from the traditional concept of total free volume of an amorphous system used with regards to the glass transition of the material. IMFV was then given the formal definition of “the difference in volume between that

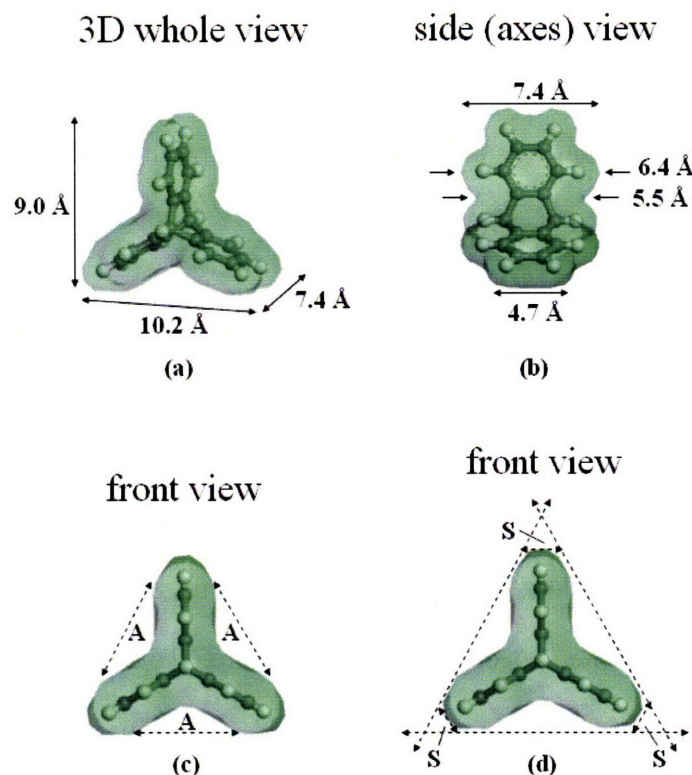
which is generated by the geometry of a structure and that which is occupied by the structure itself.” By the accumulation of local free volume effects, IMFV contributes to the total free volume of a system.

IMFV can be seen conceptually in Fig. 3-3. Here, a triptycene unit is compared to an ethylene molecule in space-filling dimensions. It can be seen that the triptycene unit contains noticeable amounts of IMFV. Comparatively, the ethylene contains almost zero amounts of IMFV. But beyond pictorial comparisons, there is a need to calculate exactly how much IMFV exists in a structure.



**Figure 3-3:** Face views of space-filling models of ethylene (left) and triptycene (right) showing the contrast in IMFV. The triptycene has significantly sized cavities; whereas, the ethylene does not.

There are multiple ways to calculate a value for the IMFV of a structure given the definition presented, and two methods will be described here. Most of these triptycene structures are actually more complex than a cursory glance would suggest, especially along the width of the axes (see Fig. 3-4b). Fig. 3-4 displays multiple views of a space-filling model triptycene unit with its dimensions labeled.



**Figure 3-4:** Space-filling triptycene models showing (a) three-dimensional view, (b) width measurements along the triptycene axes, (c) method 1 where A is the cleft space, and (d) method 2 where S is the extra space outside of the triptycene unit when enclosed in a triangular prism.


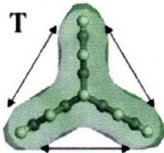
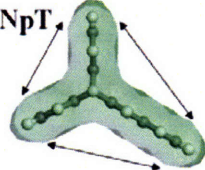
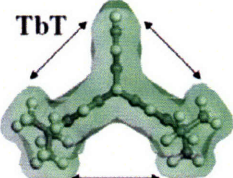
Also shown in Fig. 3-4 are the two proposed methods of calculating IMFV. The first method (Fig. 3-4c) is a direct geometric calculation of the internal cavities created by the structure. This method does not require the measurement of the volume that the structure itself occupies or the proper assignment of a volume swept out. The different spaces defined in Fig. 3-4c represent the portions used to calculate the total IMFV of the triptycene unit. These volumes can be measured in a number of ways. One approach is to use the symmetrical cavities labeled A, which are approximated as triangles defined by the van der Waals surfaces of the phenyls. As seen from Fig. 3-4b, the maximum width

of the cavities (defined by the para-hydrogens of the phenyls) is 7.4 Å. The maximum width is appropriate for a calculation because this is the distance over which the triptycene cavity will influence its local environment. The IMFV by this model for an individual triptycene is  $3 \times A \times 7.4 \text{ \AA} \approx 90 \text{ \AA}^3$ .

For simple triptycene structures, cavities can be approximated by an appropriate polygon. This method should be applicable in almost every case. However, in more complex structures, there could be complications with identifying which spaces *should* contribute to IMFV. Therefore a more general formula was constructed for the second method. The basic procedure is to determine the volume swept out by the geometry and then subtract off the volume occupied by the structure. To determine the volume swept out by the geometry of the structure, simply identify the smallest convex polyhedron that fully encloses the structure. A triangular prism is the most efficient polyhedron for the case of triptycene. Subtracting off the volume of the triptycene unit itself (calculated by the van der Waals isosurface), this method estimates IMFV at  $220 \text{ \AA}^3$ , a significantly larger value than the first method. This happens for two reasons. First, this simple polyhedron overestimates the total volume swept out by a triptycene unit because it doesn't properly account for the rounded shape of the isosurface near the corners. To correct for this, the small triangular prisms labeled S need to be subtracted. Still, this only brings the IMFV estimate down to about  $200 \text{ \AA}^3$ , again much higher than the estimate from the first method. The second and perhaps more significant reason is the varying width of the triptycene structure (Fig. 3-4b). Using the extremity of 7.4 Å as the width of the enclosing polyhedron assigns the spaces created by the contour along the triptycene axes as IMFV. The ability of these irregular spaces to contribute to IMFV will



depend on the polymer conformations, and presently, it is not possible to determine the fractional occupancy. For this reason, these spaces were neglected in the first method. Therefore, this second method will always deliver a higher estimation of IMFV. The types of width variations that cause this higher estimation will be specific to the particular structure of interest, and therefore, this second determination will not necessarily overestimate IMFV by the same amount from unit to unit. Because of these reasons, the first method is the preferred method of calculating IMFV. This method sufficed for all the units surveyed in this thesis and results of calculations are shown in Fig. 3-5.

<u>Structure</u>	<u>Inherent IMFV</u>
E 	$\sim 0 \text{ \AA}^3$
T 	$\sim 90 \text{ \AA}^3$
NpT 	$\sim 160 \text{ \AA}^3$
TbT 	$\sim 290 \text{ \AA}^3$

**Figure 3-5:** Space-filling models of ethylene (E), triptycene (T), naphthalene-modified triptycene (NpT), tert-butyl-modified triptycene (TbT) along with calculations for the inherent IMFV of the isolated structures using method 1.

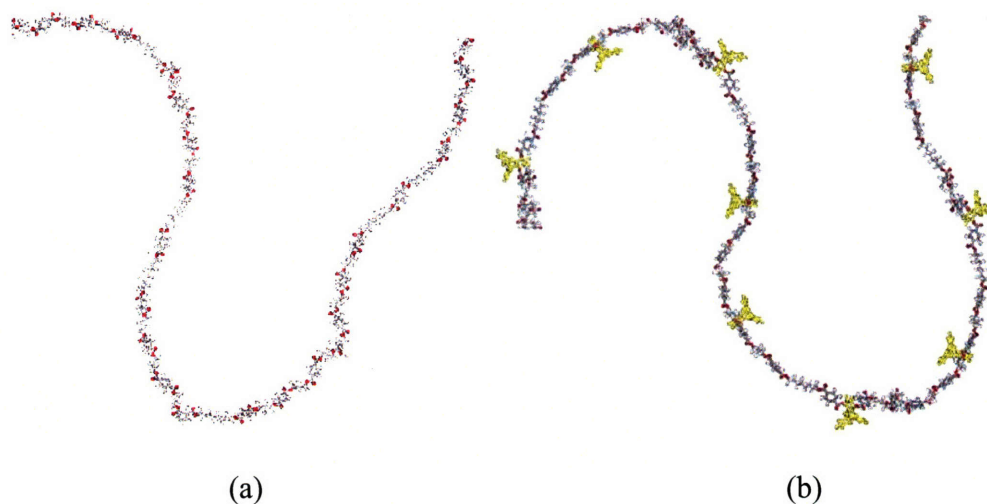
### 3.1.4 Conclusion

This section of thesis work has provided a formal definition for a new structural characteristic known as internal molecular free volume (IMFV). Additionally, the work outlined two methods for the identification and quantification of this property. It is important to note that these methods for the calculation of IMFV only apply to isolated units, but the intent of this work is to introduce these units into *polymer* systems. A complete understanding of systems would require consideration of complex synergisms between components, distributions of conformations, and allowances for the inherent chemical irregularities of a random copolymer. Therefore, calculations for isolated structures, as in Fig. 3-5, represent what will be referred to as “inherent” IMFV. Once structures with IMFV are introduced into systems, there will be an “effective” IMFV that takes into account how these local cavities affect the system around them. This is the topic of the next section.

## 3.2 Using IMFV

The purpose of this thesis was to exploit the minimization of IMFV in polymer systems for the enhancement of the solid-state mechanical properties. The manner in which iptycene units were incorporated into polymers was detailed in Chapter 2 and involved the copolymerization of units into the backbones of polymers. This type of incorporation creates a novel molecular architecture with regards to the polymer chain contour. Fig. 3-6a illustrates the typical polymer chain usually regarded as having a “smooth” surface contour. The addition of periodic pedant groups (e.g., the phenyls in PS) serves only to thicken the polymer chain locally while largely retaining the surface smoothness.

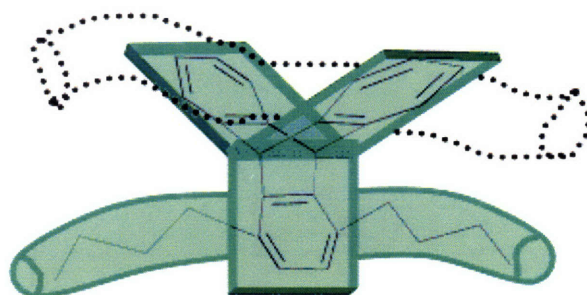
However, the presence of bulky, iptycene groups spaced relatively far apart from one another produces a polymer chain that resembles “molecular barbed wire.” Fig. 3-6b shows a representation of this molecular architecture using triptycene as an example.



**Figure 3-6:** Schematics of (a) the typical “smooth” polymer chain contour and (b) “molecular barbed wire” generated by the incorporation of triptycene units (yellow).

The purpose of adding iptycene units into polymer chains extends beyond merely altering the surface contour. The objective was to utilize the systems desire to minimize the IMFV about a triptycene to induce novel steric interactions between chains. It was asserted in previous work [53] that polymer chains could thread through the iptycene cavities (in blends) in order to achieve this minimization. With the incorporation of triptycenes into the backbone of a polymer, the occupation of the triptycene cavity by a polymer chain satisfies the minimization of IMFV (see Fig. 3-7) and creates a threaded network morphology. This type of threading is distinct from colloquial uses of threading the eye of a needle. Because the IMFV is not enclosed by the structure that created it, it

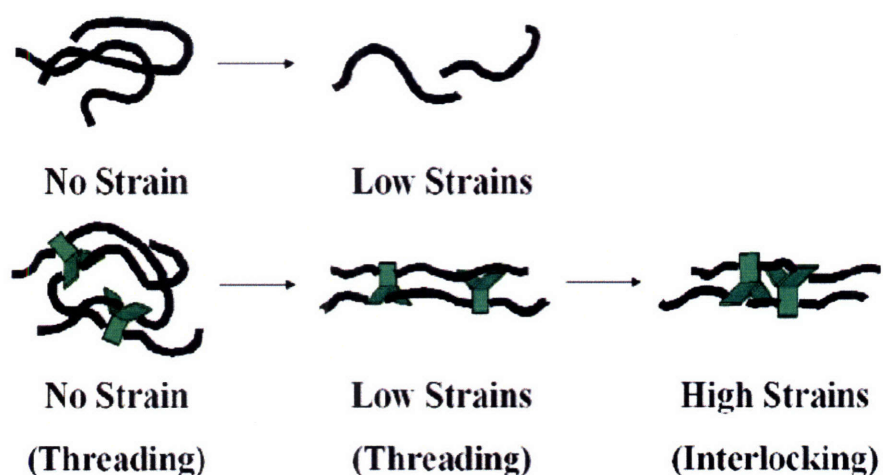
is easily accessible and the threaded state is maintained by the energy optimization associated with it.



**Figure 3-7:** A neighboring polymer chain can slide into the open triptycene cavity in order to minimize IMFV (and thus, the total FV of the system). Once occupied, the polymer chain can thread along the triptycene cavity during deformation.

This polymer system should now exhibit enhanced stiffness over systems without triptycene (all else being the same) because of two factors. First, the bulky triptycene (or any other iptycene) groups should serve to stiffen the backbone of the polymer. And second, the threaded network morphology reduces the molecular mobility of the system. However, one novel aspect of this arrangement is that the enhancement to stiffness should not necessitate embrittlement (as most stiffness enhancements do). This is because the triptycene-polymer chain threading represents a steric interaction, not chemical bonding. Importantly, during deformation, chains can slide along the triptycene cavities while maintaining the threaded state. The enhanced lateral chain interactions allow for efficient transfer of stress across polymer chains resulting in high ductility. At very high strains, there could be situations where iptycene units mutually threading along one another's chains come in contact with each another. This would prompt the steric

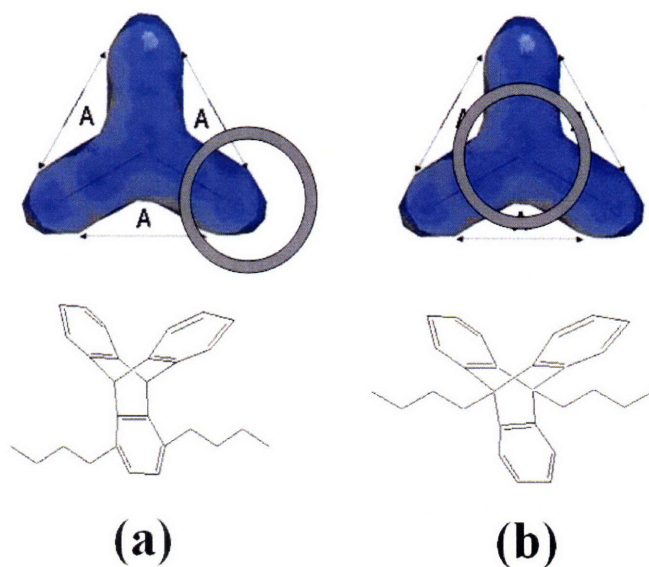
interlocking of these bulky units and create a new work hardening mechanism increasing the ultimate strengths of these polymers. This last effect is called “molecular interlocking.” Therefore, the incorporation of iptycene units into polymers could result in an overall simultaneous enhancement of stiffness, strength and ductility through these processes summarized in Fig. 3-8.



**Figure 3-8:** Schematic of the new types of interactions (“threading” and “interlocking”) induced by the triptycene unit and the minimization of IMFV (bottom). The same polymer without triptycene relies on entanglements and will fail at early strains if there are poor lateral interactions (top).

It was mentioned at the end of section 3.1 that there is a difference between the inherent IMFV of an isolated unit and the effective IMFV associated with that unit’s incorporation into a polymer system. Fig. 3-7 draws a polymer chain threading only one triptycene cavity, but it is possible that the other cavities are occupied by chains as well. It is also likely that a polymer chain occupying an iptycene cavity will have a persistence length that will be influenced by the interaction even outside of the threaded portion of

the chain. The precise chemical nature of the triptycene incorporation into the polymer backbone can play a significant role. For example, attaching the polymer backbone to a benzene group of a triptycene (as was done in this work) can affect the accessibility of two of the three triptycene cavities. But it can also be seen that one cavity is left completely unobstructed (Fig. 3-9). On the other hand, attaching to the polymer backbone through the bridgehead position significantly blocks access to all three of the cavities of the triptycene unit.



**Figure 3-9:** Drawings of the (a) benzene substitution and (b) bridgehead substitution with space-filling schematics qualitatively showing the type of incorporation's effect on the accessibility of the IMFV of triptycene.

Therefore, despite having virtually the same chemical structure and the same inherent IMFV, the two polymer systems shown in Fig. 3-9 would have very different values for effective IMFV. In fact, the earlier DuPont study discussed in Chapter 1 [55] employed bridgehead substitution for incorporating triptycene into their polymers. Because of this,

none of the advantageous outcomes predicted here would apply to the triptycene polymers synthesized by DuPont. And, in accordance, the mechanical properties reported with that incorporation did not display any significantly positive results.

Unfortunately, quantifying the effective IMFV of a system is a much more daunting task than calculating the inherent IMFV. Such an analysis would have to account for the accessibility of IMFV, persistence lengths of backbone chains, and fractional occupancy of local IMFV sites. It should be noted that it is possible for the effective IMFV to be greater than the inherent IMFV because a particular type of incorporation may enhance the spatial influence of an individual structure. However, at this point, this thesis work shifts into the thermal and mechanical characterization of polymers containing iptycene units in order to determine experimentally the effects of IMFV in polymer systems. Computer modeling and/or will not be discussed again until sections regarding future work.

## Summary

With the newly defined characteristic, IMFV, and ways to compare quantitatively the various amounts of inherent IMFV in iptycene units, the next few chapters proceed to investigate the thermal and mechanical effects of these units on polyesters and polycarbonates. The methods and models described in this chapter were used to analyze and explain the data observed. Conversely, the forthcoming experimental data was also applied to test the validity of the models created here.

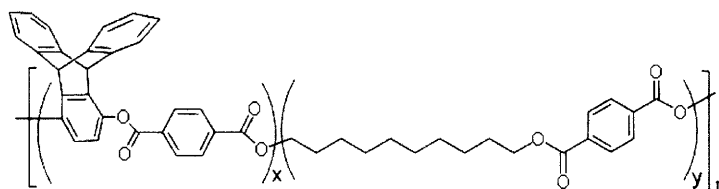




## Chapter 4

# Random Segmented Polyesters

This chapter begins the characterization of the structure-property relationships of polymers containing triptycene units in their backbone. Triptycenes were incorporated into polyesters according to the syntheses described in Chapter 2. Dr. Paraskos synthesized a set of relatively low molecular weight random segmented polyesters of the form shown in Fig. 4-1. Triptycene content was varied by controlling the molar ratios of the mixing components to achieve a final desired x/y ratio.



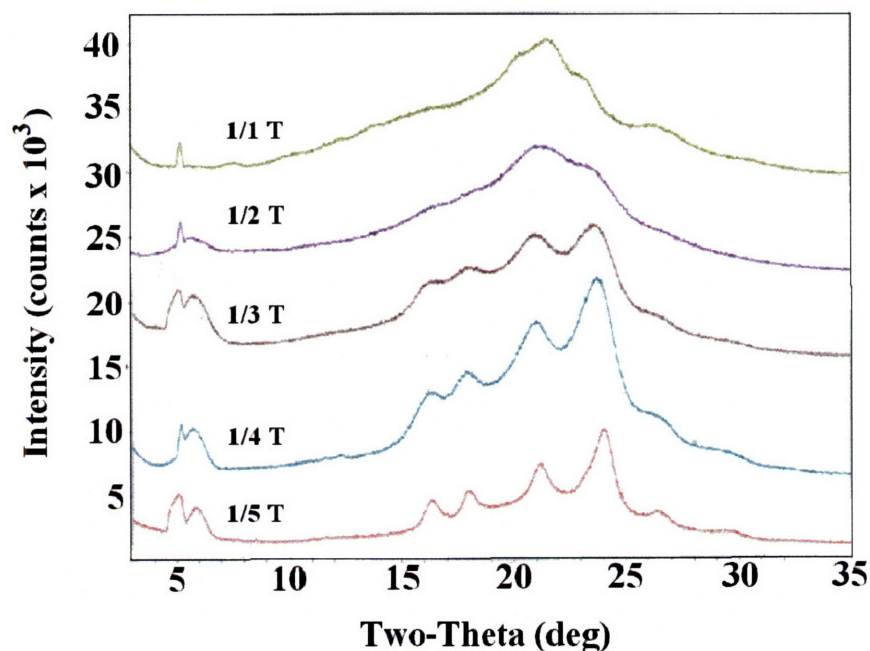
**Figure 4-1:** Triptycene containing random segmented polyester. Nomenclature “x/y T” indicates the polyester’s composition and that it contains triptycene.

The initial set (listed in Table 4.1) was surveyed for sample processibility. All were soluble in common polar solvents, such as dichloromethane or tetrahydrofuran at ambient temperatures.

<b>Polymer</b>	<b>% Triptycene</b>	<b>M<sub>n</sub> (g/mol)</b>	<b>Length per repeat</b>	<b>No. repeats</b>
1/1 T	39 wt %	21,200	33 Å	29
1/2 T	28 wt %	22,100	53 Å	21
1/3 T	21 wt %	22,900	76 Å	17
1/4 T	17 wt %	23,000	94 Å	14
1/5 T	15 wt %	23,200	114 Å	12

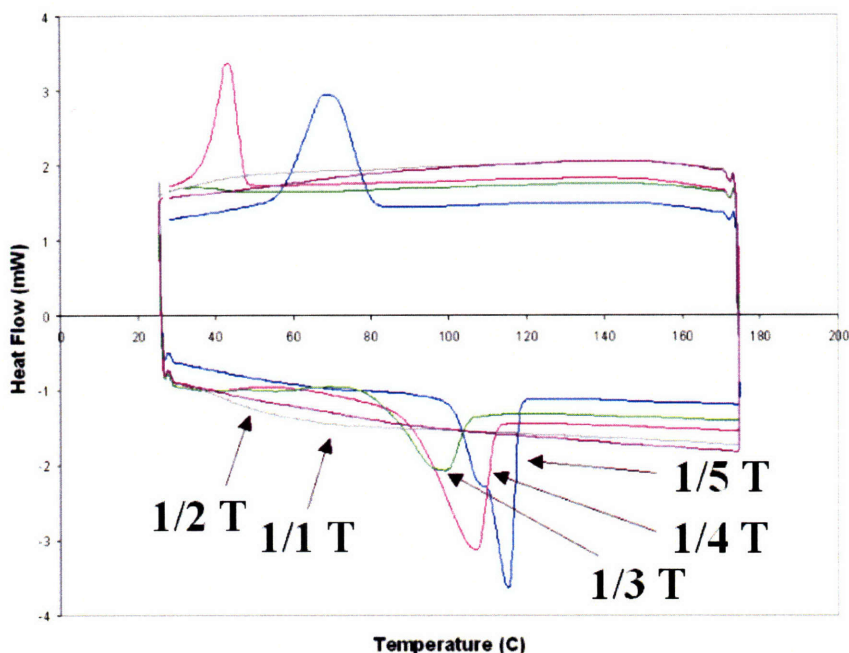
**Table 4.1:** Triptycene containing polyesters synthesized by Dr. Paraskos. Data measured and provided by Dr. Paraskos. M<sub>n</sub> from GPC.

Preliminary observations noted that the solubility increased with triptycene content. Films were solvent cast in thimbles for characterization. X-ray analysis indicated that films were semi-crystalline and that crystallinity decreased with triptycene content, as displayed in Fig. 4-2. Differential scanning calorimetry (DSC) in Fig. 4-3 confirmed these trends.



**Figure 4-2:** 2-D x-ray diffraction patterns for the triptycene containing polyester set displaying semi-crystallinity and decreasing crystallinity with increasing triptycene content.

Other cursory experimental observations included toughness of solvent cast films (as measured by simple hand deformation) and viscosity (as measured by hand drawing fibers on a hot plate). Based on the high ductility of samples with less than 25 wt % triptycene, concentrations were picked for “scale-up” of both molecular weight and amount of material. In addition, it was concluded that an analogue polyester must be used as a basis of comparison for thermal, mechanical and structural properties.



**Figure 4-3:** DSC of triptycene containing polyester set. Endotherm points down.

This chapter describes the complete characterization of the “scaled-up” iptycene containing random segmented polyesters with a focus on the effects of IMFV on the mechanical properties of solid-state films. Section 4.1 will discuss the effects of triptycene on one particular composition of polyester. Section 4.2 will re-examine the same system for the influence of orientation on the structural and mechanical properties. And section 4.3 will explore changing the composition, type of iptycene unit, and processing conditions. This chapter constitutes the main basis for two publications by Tsui, et al.: “Minimization of Internal Molecular Free Volume: A Mechanism for the Simultaneous Enhancement of Polymer Stiffness, Strength and Ductility” (2006) [85] and “Molecular Barbed Wire: Threading and Interlocking for the Mechanical Reinforcement of Polymers” (2007) [86].

## 4.1 Effects of Triptycene on the Structure and Tensile Mechanical Properties of Polyesters

### 4.1.1 *Background*

While covalent bonding and hydrogen bonding have been studied in great detail as mechanisms to enhance inter-chain interactions, it was proposed in Chapter 3 that interlocking steric interactions between adjacent chains during the deformation of polymers may produce dramatic enhancements in the mechanical properties. These steric interactions are generated by the presence of units with IMFV (e.g. iptycenes) and the system's desire to minimize that IMFV. The results serve to influence ongoing efforts to understand how to design molecular level changes to achieve high stiffness and/or high ductility and toughness.

This section reports the thorough comparative studies conducted on a pair of polymers: a polyester containing triptycene and an analogue polyester without triptycene. Triptycene was presented in Chapter 3 as one basic example of a unit from the iptycene family that possesses IMFV. Triptycenes, when properly substituted, direct the organization of polymer chains via the minimization of IMFV or, specifically, the “threading” of polymer chains through triptycene cavities (shown schematically in Fig. 3-7). The profound effects of triptycene substitution on the mechanical properties of a polyester are demonstrated here.

#### 4.1.2 *Experimental Methods*

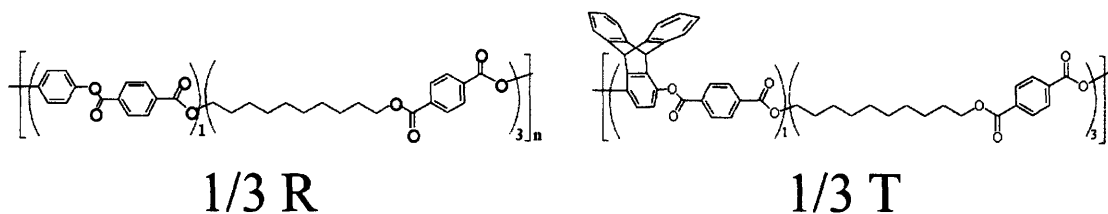
The materials used in this section were provided by Dr. Alex Paraskos (MIT Chemistry, Ph.D. 2004) and are outlined in detail in Chapter 2. For this section, isotropic films were prepared by the slow evaporation of filtered solutions in Teflon® dishes using a process described in detail in section 2.2.1. Films of about 80-90  $\mu\text{m}$  thickness were stored in a vacuum oven at 65 °C to eliminate all residual solvent. These films were then cut into strips for various structural, thermal, and mechanical analyses.

DSC was conducted on samples of 4-6 mg at a heating rate of 10 °C/min. TGA was performed on samples of about 15 mg at 5 °C/min. DMA scanned tensile properties of films (cut to 20 mm x 5 mm) at oscillatory strains of 0.15% for frequencies of 1 and 10 Hz while the temperature was raised at 2 °C/min. Films (cut to 50 mm x 5 mm) were evaluated by tensile mechanical testing using Setup I from Fig. 2-10. The gauge length used was 40 mm, and the strain rate was 40 mm/min. WAXS patterns were taken at the ISN on a Molecular Metrology x-ray apparatus. All other details about characterization followed the descriptions in section 2.3.

#### 4.1.3 *Results and Discussion*

Triptycene units were incorporated into a polyester at 21 wt. % and compared to the homologous polyester without triptycene (Fig. 4-4). From the notation established in Chapter 2, the triptycene polyester is labeled “1/3 T” and the non-triptycene reference polyester is labeled “1/3 R.” However, for this section where only this one particular chemical composition is discussed, the polyesters will mostly be referred to as either

tritycene or non-tritycene. The notation will become more critical in later sections when multiple concentrations (various x/y ratios) are introduced.



**Figure 4-4:** Chemical structures of the polyesters characterized here. 1/3 R: non-tritycene reference polyester. 1/3 T: 21 wt % triptycene containing polyester.

The molecular weights are displayed in Table 4.2. Although the molecular weight of the triptycene polyester is slightly higher than that of the non-tritycene polyester, the two polymers synthesized here have approximately equal chain contour lengths due to the additional molecular weight associated with the triptycene unit itself.

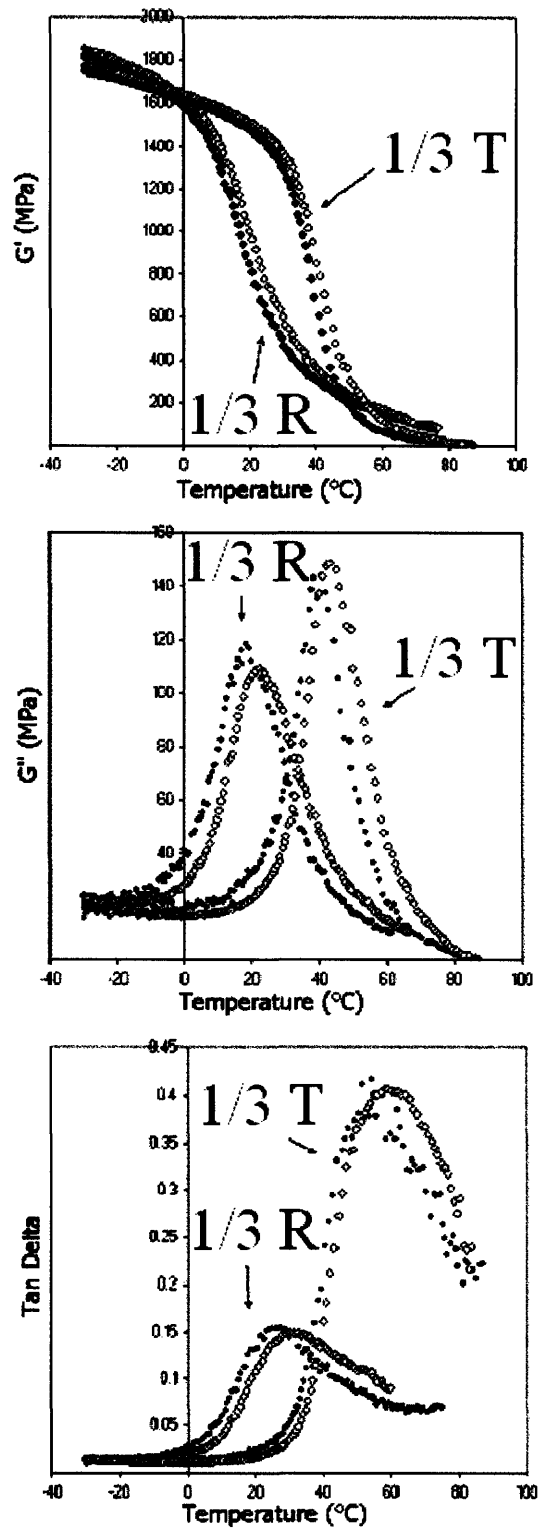
Polymer	$M_n$ (g/mol)	$M_w$ (g/mol)	PDI	No. repeats
1/3 R	31,900	62,000	1.94	27
1/3 T	40,300	75,500	1.87	30

**Table 4.2:** Number average molecular weight ( $M_n$ ), weight average molecular weight ( $M_w$ ), and polydispersity ( $PDI = M_w/M_n$ ) data on polyesters from GPC. Number of monomer repeats calculated from  $M_n$  values.

Clear and colorless films of about 100 microns in thickness for both samples were obtained by slow solvent casting. Dynamic mechanical analysis (DMA) plots of storage modulus ( $G'$ ), loss modulus ( $G''$ ), and tan delta of these films are shown in Fig. 4-5. The frequency dependence obeys the expected behavior. The 10 Hz curve is slightly shifted

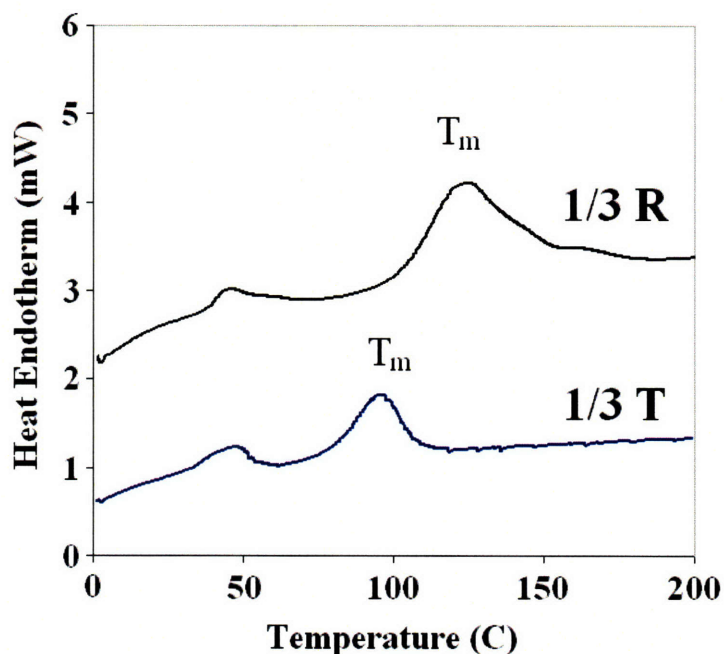
such that the values for storage modulus, loss modulus and tan delta are higher than for the 1 Hz curve. It is noticeable that the tan delta curve for the triptycene polyester is much more intense than the tan delta curve for the non-triptycene polyester, demonstrating its improved dampening properties. This difference in intensity is also indicative of the more amorphous character of the triptycene polyester as compared to the non-triptycene polyester (*vide infra*). The triptycene polyester displays an increased glass transition temperature ( $T_g$ ) from 25 °C to 55 °C (taken from the 1 Hz tan delta curve).





**Figure 4-5:** DMA of triptycene containing polyester (1/3 T) versus non-triptycene polyester (1/3 R) at 10 Hz (open circles) and 1 Hz (closed circles).

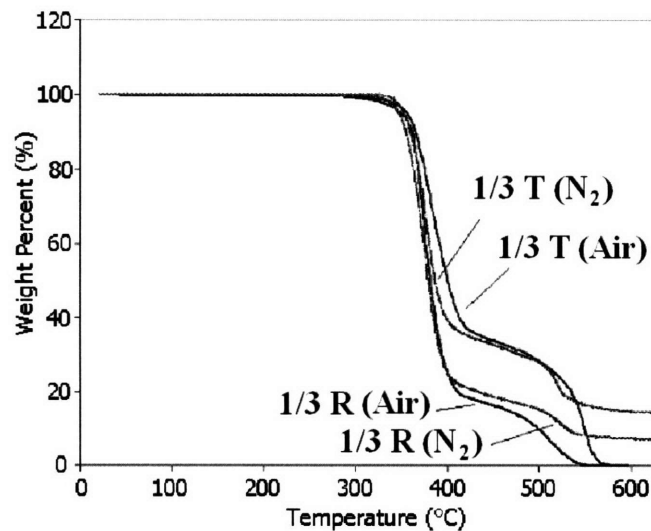
DSC results show a decreased melting temperature from 119 °C to 93 °C and a reduced heat of melting with respect to the non-triptycene polyester, indicating that the inclusion of the bulky triptycene unit decreased crystallinity in the samples (Fig. 4-6). Data shown is from first cycle scans of the films. Interestingly, in both samples, there is a small peak around 45 °C for which the origins are unknown. This peak was not consistently present in either sample for first or second cycle runs and represents a relatively low amount of energy. Therefore, it was ignored, but it is shown here for the benefit of future researchers.



**Figure 4-6:** Shifted DSC curves for triptycene (1/3 T) and non-triptycene (1/3 R) polyesters with the endotherms up. Melting points ( $T_m$ ) are labeled but  $T_g$  was not readily identifiable.

The thermal properties from DMA and DSC are summarized in Table 4.3 along with thermal gravimetric analysis (TGA) of the degradation of the polyesters. Thermal degradation in both air and nitrogen can be seen in Fig. 4-7. In both atmospheres, the

tritycene containing polyester degraded at slightly higher temperatures than the non-tritycene polyester. There were some interesting phenomena after the main degradation. The triptycene polyesters retained more mass than the non-tritycene polyester before burning off completely in a secondary degradation phase. In nitrogen, a more inert atmosphere than air, this secondary degradation did not result in the complete vaporization of material. These observations are interesting but unlikely to affect the mechanical properties as over 50% of each material is lost in the first phase of degradation.



**Figure 4-7:** TGA curves for polyester samples in both air and nitrogen atmospheres.

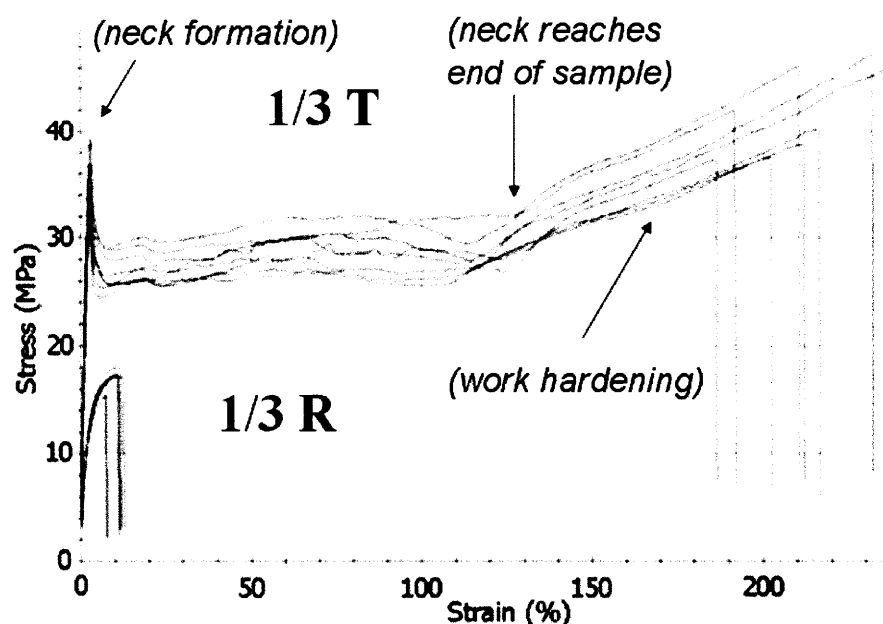
From the storage modulus curves in Fig. 4-5, it can be seen that, at room temperature, the triptycene polyester displays a significantly higher modulus value than the non-tritycene polyester. The addition of triptycene extends the glassy plateau well past room temperature, while the non-tritycene polymer has its glass transition around room

temperature. However, DMA indicates that when both polymers are in their glassy regimes, their modulus values are comparable.

Polymer	T <sub>g</sub> (°C)	T <sub>m</sub> (°C)	ΔH <sub>m</sub> (J/g)	T <sub>d,air</sub> (°C)	T <sub>d,N<sub>2</sub></sub> (°C)
1/3 R	25	119	27.9	375	376
1/3 T	55	93	11.8	382	378

**Table 4.3:** Summary of the thermal properties as assessed by DMA, DSC, and TGA.

Tensile tests conducted on the solvent cast films showed sample moduli in agreement with the observations from the DMA. Comparative tensile stress-strain curves are shown in Fig. 4-8, and the tensile mechanical properties data are summarized in Table 4.4. The presence of triptycene resulted in average percent increases of 180% for modulus (1.62 GPa compared to 0.58 GPa), 150% for strength (42 MPa compared to 17 MPa), and over 2000% for strain to failure (211% compared to 10%). While the difference in modulus between the two samples at room temperature may be mostly attributed to the shift in glass transition temperature, the triptycene polyester also displayed significantly higher strength and strain to failure. The latter behavior was a particularly unexpected result, since the triptycene polyester is still in its glassy plateau at room temperature. Additionally, the non-triptycene polyester, despite being beyond its glassy plateau, displayed low ductility compared to the triptycene polyester.



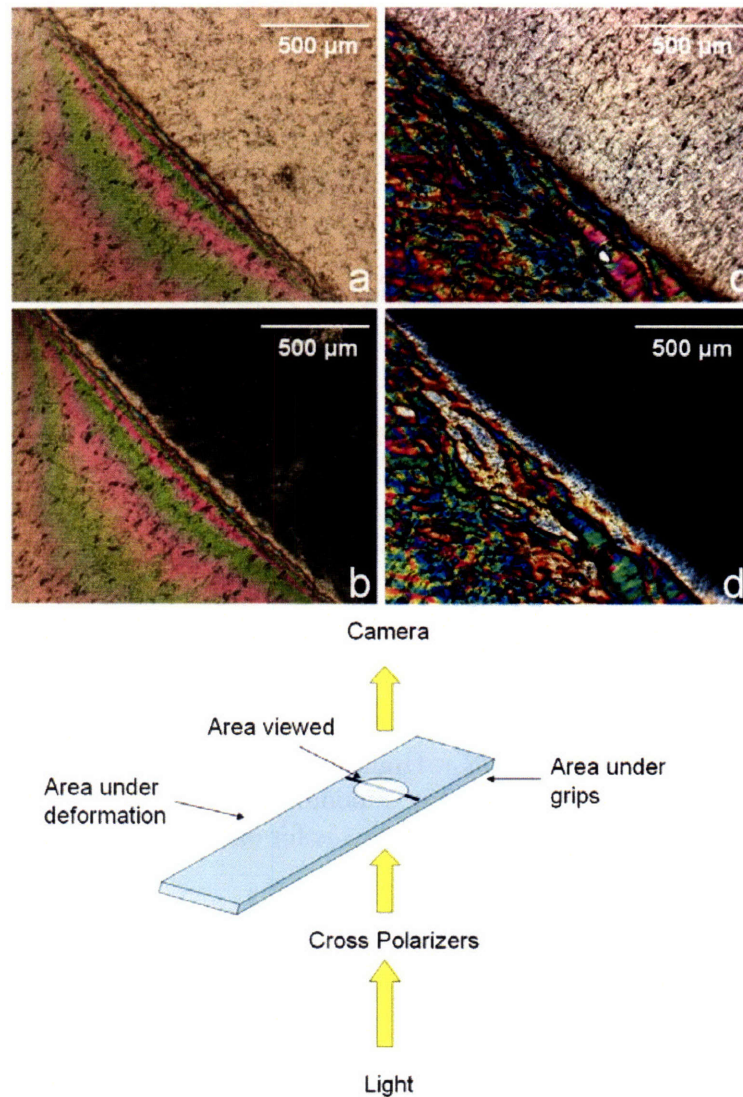
**Figure 4-8:** Tensile properties of triptycene (1/3 T) and non-triptycene (1/3 R) polyester films at room temperature.

Polymer	$\rho$ (g/cc)	E (GPa)	$\sigma_y$ (MPa)	$\sigma_{UTS}$ (MPa)	$\epsilon_b$ (%)	Work (J/cm <sup>3</sup> )
1/3 R	1.20 ( $\pm$ 0.01)	0.58 ( $\pm$ 0.03)	17 ( $\pm$ 1)	17 ( $\pm$ 1)	10 ( $\pm$ 2)	1.50 ( $\pm$ 0.25)
	HIR:	0.70	23	23	11	2.50
1/3 T	1.18 ( $\pm$ 0.01)	1.62 ( $\pm$ 0.11)	35 ( $\pm$ 3)	42 ( $\pm$ 4)	211 ( $\pm$ 17)	66.25 ( $\pm$ 8.25)
	HIR:	1.95	45	62	224	83.75

**Table 4.4:** Summary of film tensile tests 1/3 R films of  $80 \pm 3$   $\mu$ m thickness and 1/3 T films of  $87 \pm 13$   $\mu$ m thickness. HIR = Highest Individual Result (not plotted in Fig. 4-8 to avoid clutter),  $\rho$  = density, E = Young's modulus,  $\sigma_y$  = yield strength,  $\sigma_{UTS}$  = ultimate tensile strength, and value given in parenthesis is for one standard deviation.

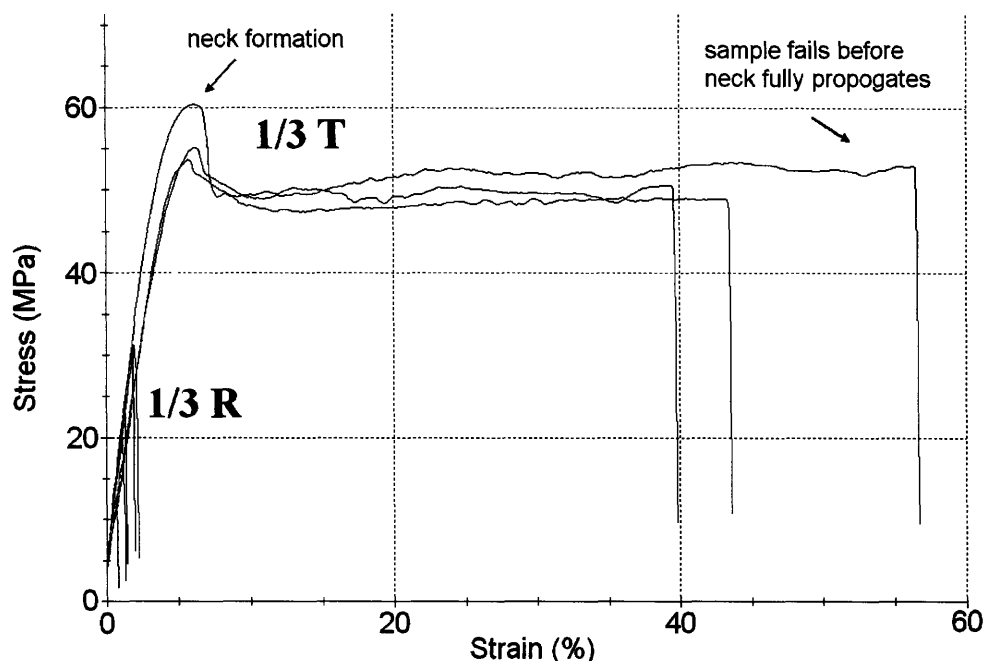
Deformed samples were viewed under an optical microscope with cross-polarizers. Fig. 4-9 contains characteristic images of both the triptycene and non-triptycene polyesters at the areas where the samples were gripped during tensile testing. There is a distinct line between the deformed regions (which exhibit multiple colors) and the undeformed regions that marks where the grips pinched the samples. The films were

oriented diagonally in the microscope, and the drawing direction was perpendicular to the grip line visible in the pictures. The triptycene polyester films exhibit a patterned birefringence indicative of the molecular orientation imparted on the sample from high drawing strains. In contrast, the non-triptycene polyester films exhibit no such ordered patterning. The birefringence visible in these samples merely indicates the sections of the film that deformed versus the sections that were under the grips.



**Figure 4-9:** Representative optical microscope pictures at 5X magnification with cross-polarizers oriented at various degrees for film samples strained to failure: a) triptycene at 0°, b) triptycene at 90°, c) non-triptycene at 0° and d) non-triptycene at 90°.

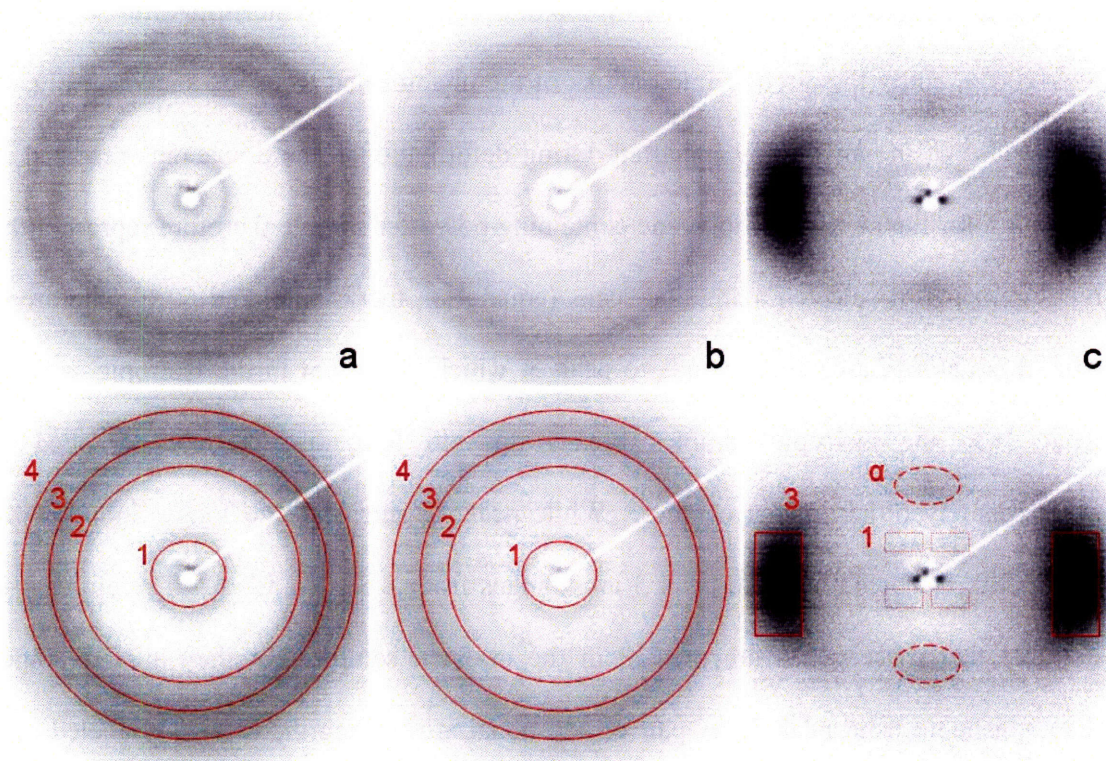
To ensure that the low strain failure of the non-triptycene polyester films was not due to some sort of solid-to-viscoelastic fluid transition around  $T_g$ , tensile tests were also conducted at  $-30^\circ\text{C}$ , a temperature well below the  $T_g$ 's of both polymers. These stress-strain curves are shown in Fig. 4-10. At  $-30^\circ\text{C}$ , the modulus of the non-triptycene polyester increased in accordance with the DMA results, and the ductility dropped sharply (from 10% at room temperature to  $\sim 1.4\%$  at  $-30^\circ\text{C}$ ) as would typically be expected for a polymer transitioning into its glassy regime (see Fig. 4-5). The sub- $T_g$  environment's failure to enhance the ductility confirmed that the non-triptycene polyester's lack of ductility at room temperature had nothing to do with a transition to a viscoelastic fluid because of the proximity to its  $T_g$ . As expected, the triptycene sample maintained a similar modulus (the mean of 1.58 GPa at  $-30^\circ\text{C}$  was slightly lower than the room temperature mean of 1.62 GPa, but this is attributed wholly to statistical variation as 0.04 GPa is well within one standard deviation of either measurement) while producing higher strengths at the point of neck formation. This increase in strength was due to the yield point (neck formation) occurring at a higher strain at  $-30^\circ\text{C}$  ( $\epsilon \sim 6\%$ ) than at room temperature ( $\epsilon \sim 2\text{-}3\%$ ), a side effect from the reduced molecular motions at lower temperatures. The triptycene samples failed prematurely in the grips before necking had reached both ends of the sample. Therefore, no work hardening was seen because of the increased defect sensitivity at the lower temperatures.



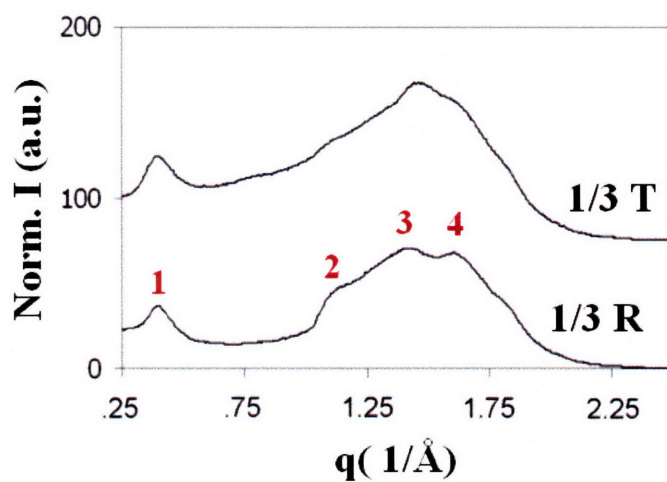
**Figure 4-10:**  $-30^{\circ}\text{C}$  tensile properties of non-triptycene films yield a modulus ( $E$ ) of  $1.61 \pm 0.10$  GPa, strength ( $\sigma_{\text{UTS}}$ ) of  $24 \pm 8$  MPa, and strain to failure ( $\epsilon_b$ ) of  $1.4 \pm 0.5$  % while triptycene polyester films exhibit a modulus ( $E$ ) of  $1.58 \pm 0.13$  GPa, strength ( $\sigma_{\text{UTS}}$ ) of  $55 \pm 6$  MPa, and strain to failure ( $\epsilon_b$ ) of  $47 \pm 9$  %.

Wide-angle x-ray scattering (WAXS) showed that the addition of the triptycene units (while lowering the crystallinity) did not appear to change the type of crystal formed, since nearly the same d-spacings were present for both samples. WAXS images of the as-cast non-triptycene polyester and triptycene polyester films along side a triptycene polyester film strained to failure are presented in Fig. 4-11. Images of non-triptycene polyester films strained to failure were omitted due to the lack of change in orientation commensurate to the low breaking strains. WAXS patterns of the as-cast films were circularly integrated (Fig. 4-12) to measure the d-spacings summarized in Table 4.5. Both types of as-cast films displayed isotropic diffraction rings as expected.





**Figure 4-11:** WAXS of (a) non-triptycene polyester as-cast film, (b) triptycene polyester as-cast film, (c) triptycene polyester strained over 200% along the vertical axis. The bottom row displays the identical patterns but with the peaks labeled.



**Figure 4-12:** Integrated circularly averaged scans of the patterns in Fig. 4-11 a and b.

Fig. 4-11 includes an x-ray pattern taken of a triptycene polyester film after stretching over 200%. Only the circular integrations of the undeformed films are shown in Fig. 4-12 because of the anisotropy imparted during deformation. The d-spacings reported in Table 4.5 for the stretched triptycene containing polyester sample therefore represent the measurements of selected azimuthal scans (equatorial, meridional, and 60°). The broad pair of equatorial arcs corresponds to peak 3, which is present in the isotropic sample. Peak 1 in the isotropic samples breaks up into four distinct spots oriented at approximately 60° from the equator. While peaks 2 and 4 are no longer individually noticeable, the breadth of the peak 3 arcs ranges from 3.5 Å to 5.7 Å. Therefore, it is possible that these peaks are present in the oriented sample, but they are no longer distinguishable from peak 3. A pair of additional arcs (along the meridian labeled  $\alpha$  in Fig. 4-11) also appeared that was not evident in the isotropic samples. The presence of arcs and spots indicate the anisotropy imparted during the deformation process. The azimuthal scans used to measure these d-spacings will be discussed in greater detail in the next section which focuses on oriented samples.

Polymer Film	Peaks				
	<i>1</i>	$\alpha$	<i>2</i>	<i>3</i>	<i>4</i>
1/3 R	15.9 Å	-	5.5 Å	4.4 Å	3.9 Å
1/3 T	16.0 Å	-	5.5 Å	4.3 Å	3.9 Å
1/3 T (S)	15.9 Å	6.5 Å	-	4.3 Å	-

**Table 4.5:** WAXS d-spacings of the polymers of as-cast films, except where indicated otherwise by an (S). The strained sample (S) was elongated over 200% before failure.

The unique mechanical enhancements and structural properties observed must have their origins in the triptycene unit. To recapitulate what was introduced in Chapter 3,

these dramatic effects are best described by the chain-chain interactions induced by the system's desire to minimize its internal molecular free volume (IMFV). The mere presence of pendant rigid triptycene units along the backbone of a polymer coupled with the occupation of triptycene cavities with portions of neighboring polymer chains would be expected to reduce dramatically the molecular chain mobility. In accordance, there was a large increase in the glass transition temperature of the triptycene polyester relative to the non-triptycene homologue. While the enhancement of the stiffness of the polyester with triptycene is therefore expected, the increases in strength and strain to failure were not. The high strength values of the triptycene polyesters at room temperature can be attributed to the work hardening that occurs at high strains ( $\epsilon > 130\%$ ). As suggested previously, this study asserts that the enhanced work hardening occurs due to triptycene-triptycene interactions. Typical bulky groups will slide by one another during the deformation process without large interactions because they are not directed into an interlocking structure by IMFV. However, triptycene units mutually threading along each other's chains will tend to interlock at high strains (recall Fig. 3-8: "molecular interlocking"). The particular strain level at which this occurs and the extent to which it increases the strength will depend on the relative amount of triptycene in the backbone.

We also observe a large region of deformation (the neck propagation) before work hardening initiates. Neither necking nor work hardening occurs in the non-triptycene polymer. We attribute this behavior to triptycene-chain interactions (Fig. 3-8: "molecular threading"). In the non-triptycene polymer, the lateral chain interactions are relatively weak. This is why the strain to failure is so low despite the sample being above its  $T_g$  at room temperature. The polymer chains threading through the triptycene units give the

tritycene polymer enhanced lateral interactions without the loss of ductility that would accompany inter-chain covalent bonding. This promotes the large deformations observed. Mutual threading of triptycene units would also induce parallel alignment of the neighboring chains, further aiding in the orientation process during deformation. The triptycene units, and therefore their effects on the mechanical properties, are randomly and homogeneously distributed throughout the system, and the mechanical properties observed are an average over all chain segment motions and interactions. Thus, the influence on chain segment movement appears macroscopically as similar to enhanced chain entanglement. In the necking region, the dominant interaction was that of threading, but as the interlocking mechanism became more prominent at high strains, the work hardening regime reflected that in a new and homogeneous influence on mechanical properties. The threading of polymer chains through triptycene clefts does not generate a characteristic signal in WAXS as such a spatial correlation would be too weak to resolve in the presence of crystalline peaks. Density measurements show that the non-triptycene polyester as-cast film has a slightly higher density than the triptycene polyester as-cast film. However, the increase in density associated with the threading of polymer chains through triptycenes must compete against the decrease in density resulting from the loss in crystallinity. The most compelling evidence for molecular threading and molecular interlocking is the mechanical properties that result from the addition of triptycene.

The ability for threading and interlocking to affect the mechanical properties of a polymer depends on the percentage of the contour length of the chain that is influenced by the minimization of IMFV. As shown in Fig. 4-4, there are 3 major components to the triptycene polyester: 1) the triptycene, 2) a long aliphatic decane, and 3) a terephthaloyl

connector. The long aliphatic component is the most likely candidate at equilibrium for threading through the triptycene cavities. Using a triptycene cavity width of 7.4 Å (see Chapter 3) and the overall contour length of the mer of about 76 Å, about 10% of the contour length of the chain is affected by the threading of one triptycene cavity. Since *both* chains are affected by threading, in the case of two chains mutually threading one another's triptycene units, 20% of the contour length of the chain is now affected. Since, the triptycene in actuality has three available cavities and three aliphatic components per mer, this model can be extended in three dimensions allowing each mer to participate in four threading interactions. Therefore, a possible 40% of the contour length of a polymer chain can be under the influence of IMFV. During deformation, the occupation of the triptycene cavities is no longer restricted to the aliphatic components. Even though the terephthaloyl connector is a bulkier unit and thus may not reside as "deeply" inside of a triptycene cavity, it is still susceptible to the attractive force related to the minimization of IMFV.

#### 4.1.4 Conclusion

The incorporation of triptycene units into the backbone of a polyester at 21 wt. % significantly increased the modulus, strength, and strain to failure for solvent cast films, marking the simultaneous improvement of both stiffness and ductility. This was an unusual result because it is typically observed that enhancements in stiffness lead to sacrifices in ductility. There exists no general method of achieving such simultaneous enhancements exclusively with a homopolymer. These results indicated that the steric influence of rigid, pendant units may facilitate new advances in the enhancement of the

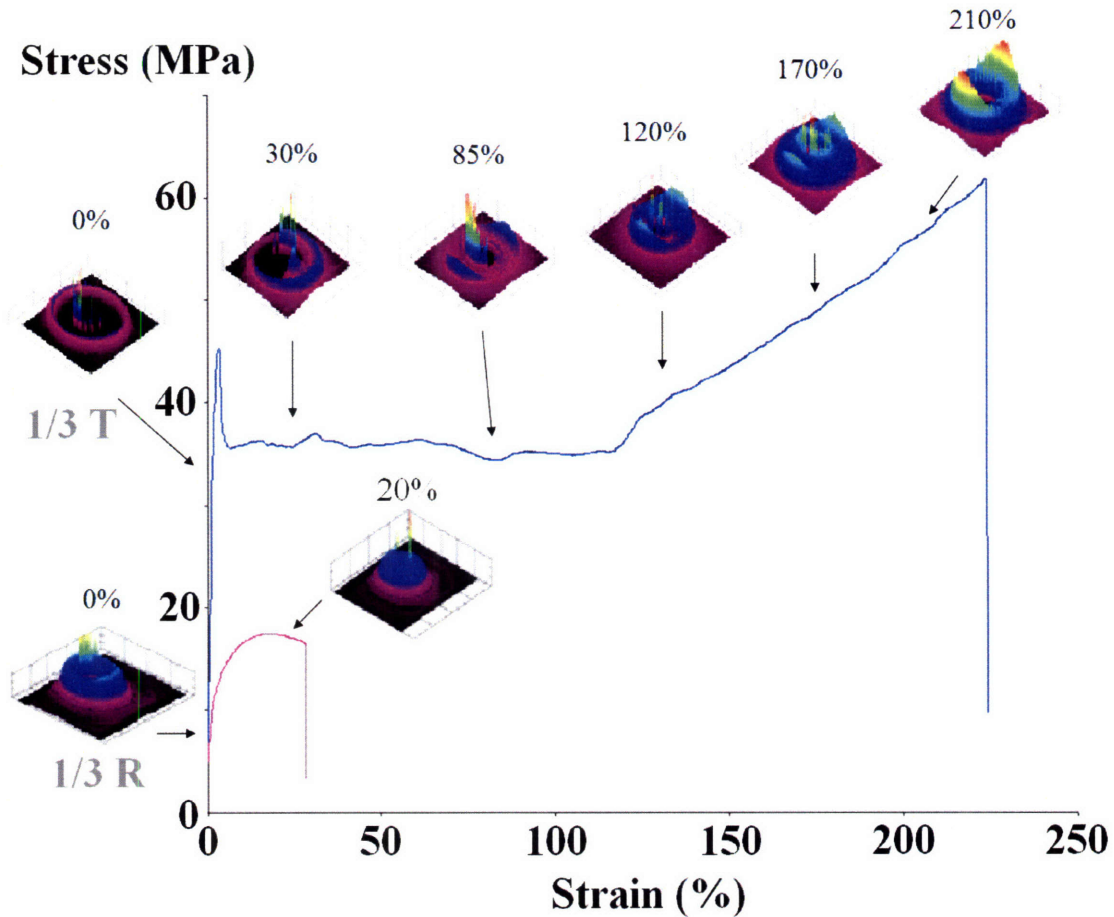
mechanical properties of polymers. The specific types of steric interactions suggested in Chapter 3 (molecular threading and molecular interlocking) are directed by the system's desire for the minimization of internal molecular free volume about the triptycenes and may allow access to combinations of properties that are not presently accessible from conventional systems that rely on chain-chain interactions arising from crosslinking, hydrogen bonding, ionic bonding or crystallization to achieve high strength. This work represented this first random copolymer system to exploit the minimization IMFV successfully to enhance the mechanical properties of a polymer.

## 4.2 Oriented Films and Fibers

### 4.2.1 *Background*

The novel steric interactions induced by the minimization of IMFV become particularly influential during deformation. Therefore, the evolution of the structural and mechanical properties during deformation was of interest. In-situ deformation experiments of film samples at the Brookhaven Synchrotron Light Source were able to pair structural data from WAXS with specific points on the stress-strain curves. It can be seen in Fig. 4-13, that very little (if any) structural orientation took place in the non-triptycene polyester samples because of the low strain to failure. But for the triptycene polyester samples, which deformed significantly before failure, the evolution of molecular orientation is evident from the development of arcs from the isotropic rings. It is important to note that the triptycene polyester samples necked and that necks form and propagate in an

uncontrolled manner during deformation while the beam spot was able to record only a fixed point. Still, this plot provides a useful impetus for the study of oriented samples.



**Figure 4-13:** The in-situ deformation that shows how the WAXS evolves on the stress-strain curve for both triptycene and non-triptycene polyesters. The key point here is that observable structural change does not occur at relatively low deformations (<30%).

It is clear that samples undergo significant structural change (specifically, molecular orientation) after deformation to high strains. Oriented samples are of particular interest not only because of the different structure but because highly oriented fibers also find application in specialized clothing designed to withstand projectile impacts, as was detailed in Chapter 1. This section examines two types of oriented samples: films and

fibers. The experiments sought to examine the effects of triptycenes on oriented polymer samples as well as determine suitability for producing wearable fabric.

#### 4.2.2 *Experimental Methods*

Tension heat treated (THT) films of the materials used in section 4.1 were produced in the Zwick temperature chamber described in Chapter 2. Triptycene polyester film samples were heated to 70 °C, strained 400%, and then held in tension as the chamber was allowed to cool back to room temperature. The films were then removed, measured and tested for mechanical properties. This procedure produced oriented films roughly 40 microns in thickness. These films were cut with razor blades into strips roughly 50 mm in length and 4 mm in width. The non-triptycene polyester samples could not be strained past 20% even at 70 °C. As such small strains would be unlikely to impart significant microstructural changes (Fig. 4-13), non-triptycene polyester films were not tension heat treated for mechanical testing.

Fibers were obtained from an experimental-scale DuPont melt press spinner that was customized to spin small quantities of materials, i.e. 2-5 grams. A monofilament 381 micron spinneret hole was used in conjunction with a variable speed take-up wheel. Polymer powder samples were vacuum dried at 65 °C for 24 hours. Approximately two grams of polymer were brought to the melting point as indicated by DSC in the spinner barrel under a vacuum and nitrogen purge. After about 20-30 minutes in the melt, the temperature was raised to the spin temperature. The spin temperature was obtained by placing polymer powder along a hot strip with a temperature gradient. Using a glass rod to pull fibers, the optimal temperature to spin polymer was qualitatively observed. Once



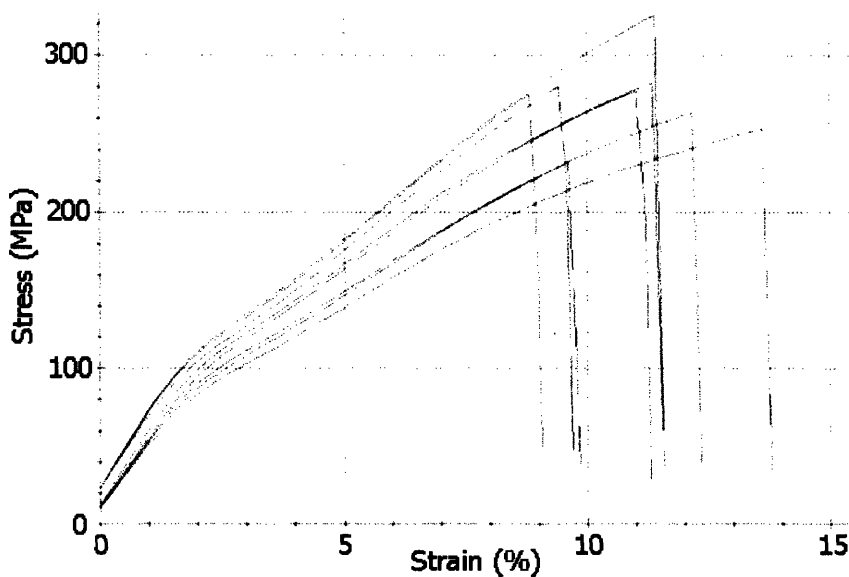
at the spin temperature, polymer was immediately extruded at speeds yielding pressures of 100-300 psi. Fiber diameters of around 40 microns were obtained using this method marking draw ratios,  $(D/D_0)^2$ , of about 90. Fibers bundles were collected off of the take-up wheel and stored in dessicators.

Structural and mechanical characterization of the films was identical in methodology to the procedures described in section 4.1.2. Single fibers were carefully separated from the bundles by hand, and the fiber diameters were measured by optical microscopy. Single fibers were then mounted onto custom tabs and held in place by Loctite® Fast Cure Epoxy. The tabs were cut from Smead manila folders such that an area in the center of the tab was cut away to expose the gauge lengths leaving only two thin edges of the paper holding the tab together. This is shown pictorially as Setup **III** in Fig. 2-10. Fibers mounted on these tabs were also stored in a dessicator until tested. A pre-load of 0.01N was used. 9 samples of non-triptycene fibers of gauge length 38 mm were tensile tested at 38 mm/min. 8 samples of triptycene fibers of gauge length 25 mm were tensile tested at 25 mm/min. Young's modulus, strength and elongation values were obtained using the Zwick software. WAXS patterns of the fiber bundles were attained at the Brookhaven National Synchrotron Light Source on beamline X27C with 300 second exposure times. As was done for the films, images were normalized for samples thickness, exposure time, beam flux, and d-spacings were calibrated with  $Al_2O_3$  using Polar Software and Fit2D.

#### 4.2.3 *Results and Discussion*

Both of the as-cast polyester films were optically clear; however, the tension heat-treated (THT) triptycene polyester films had varying levels of opacity down the length of the

film. This was probably due to sample necking. During the THT process, the parts of the film that first undergo necking contain chains in more extended conformations at the elevated temperature for longer periods of time than other parts of the film due to the neck propagation. This resulted in the variation of crystallinity along the length of the stretched film (> 25 cm long), which caused the varying levels of opacity in individual film samples tested (4 cm gauge length samples). Tensile tests of the THT films at room temperature yielded average values of 4.63 GPa for modulus, 274 MPa for strength, and 11% for strain to failure. The results are summarized in Table 4.6, and the stress-strain curves are plotted in Fig. 4-14. The highest individual THT film results exhibited a modulus of 5.10 GPa, strength of 326 MPa and a strain to failure of 12%. As expected, this oriented film displayed a higher density than the as-cast triptycene film.



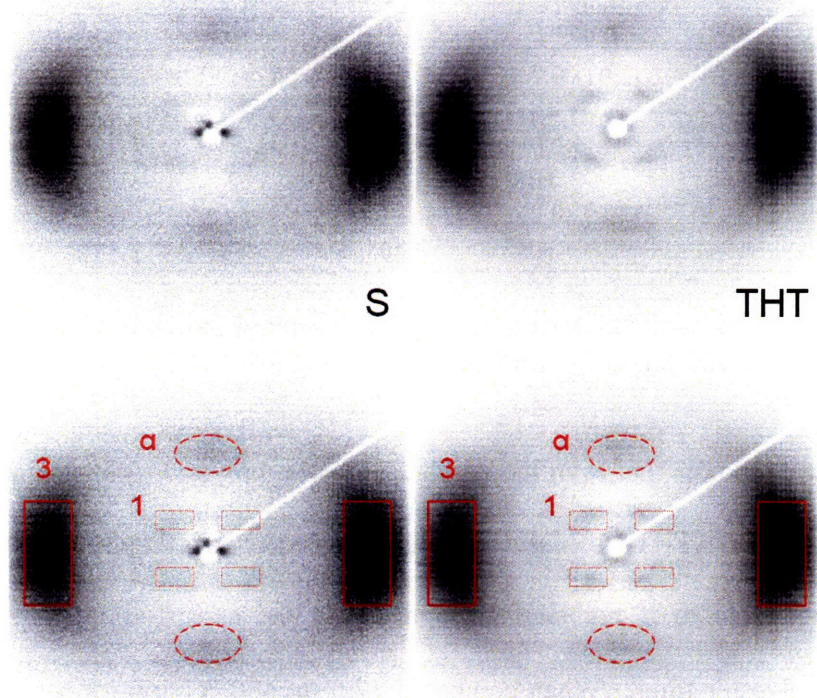
**Figure 4-14:** Room temperature tensile properties of THT triptycene polyester films.

Polymer	t ( $\mu\text{m}$ )	$\rho$ (g/cc)	E (GPa)	$\sigma$ (MPa)	$\epsilon_b$ (%)	Work ( $\text{J}/\text{cm}^3$ )
1/3 R	80 ( $\pm 3$ )	1.20 ( $\pm 0.01$ )	0.58 ( $\pm 0.03$ )	17 ( $\pm 1$ )	10 ( $\pm 2$ )	1.50 ( $\pm 0.25$ )
			HIR: 0.70	23	11	2.50
1/3 T	87 ( $\pm 13$ )	1.18 ( $\pm 0.01$ )	1.62 ( $\pm 0.11$ )	42 ( $\pm 4$ )	211 ( $\pm 17$ )	66.25 ( $\pm 8.25$ )
			HIR: 1.95	62	224	83.75
1/3 T (THT)	38 ( $\pm 8$ )	1.21 ( $\pm 0.01$ )	4.63 ( $\pm 0.36$ )	274 ( $\pm 27$ )	11 ( $\pm 2$ )	18.50 ( $\pm 3.25$ )
			HIR: 5.10	326	12	22.50

**Table 4.6:** Summary of film tensile tests. HIR = highest individual result, t = thickness, and the values in parentheses report standard deviations.

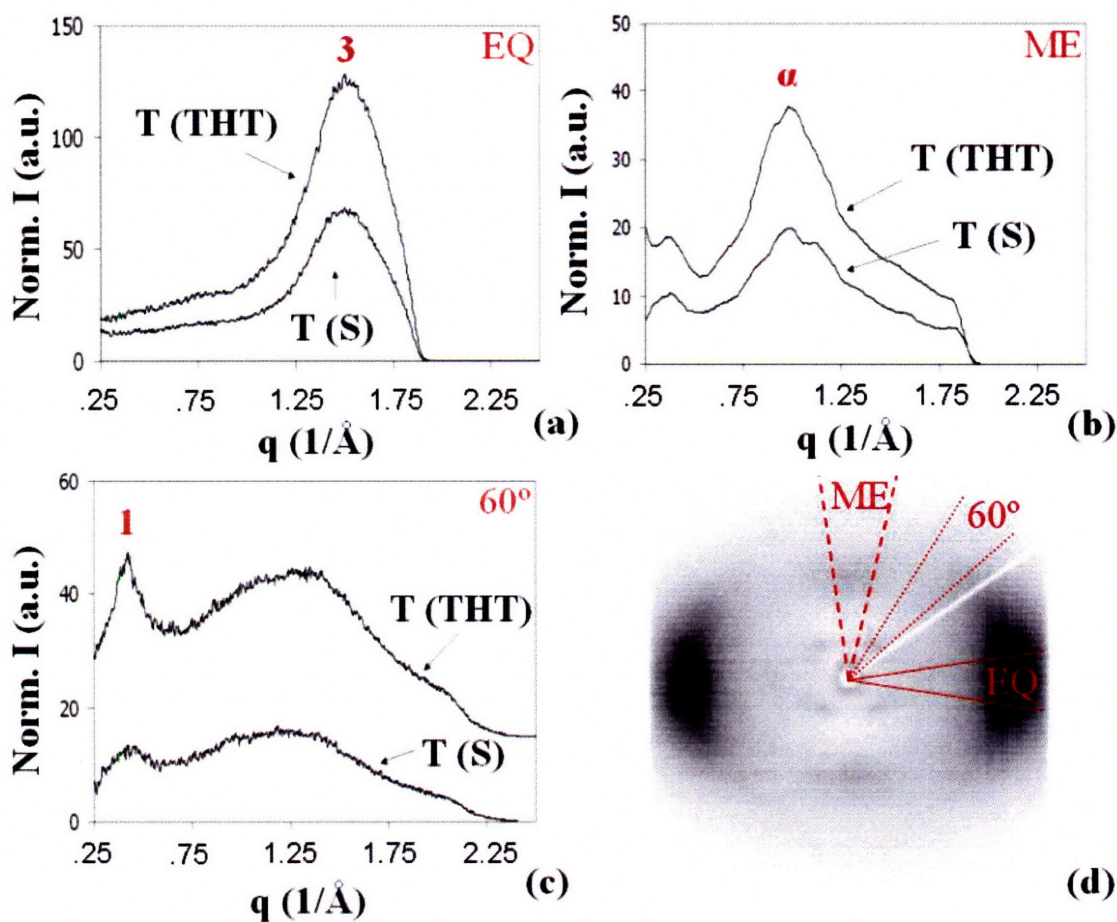
It is interesting to note that even though the triptycene polyester films lost a great deal of ductility during the THT processing (which was expected), they still exhibited failure strains comparable to if not slightly higher than the as-cast room temperature non-triptycene polyester films. When compared with the  $-30\text{ }^\circ\text{C}$  non-triptycene films (from section 4.1), the THT triptycene polyester films displayed on average almost three times the modulus, over eleven times the strength, and almost eight times the strain to failure.

Fig. 4-15 shows the WAXS of a THT triptycene polyester film with labels consistent with section 4.1. The pattern is nearly identical to that of the room temperature strained triptycene sample, but the four inner spots at about  $16\text{ \AA}$  (peak 1) are more intense. The full-width half-maximum of the  $4.3\text{ \AA}$  equatorial peak (peak 3) for both samples also confirmed that the THT process produced films with slightly higher levels of orientation as the azimuthal spread was five degrees for the THT film and six degrees for the room temperature strained triptycene film.



**Figure 4-15:** Representative WAXS pictures of room temperature strained to failure (S) versus undeformed tension heated treated (THT) triptycene polyester films taken at ISN. The deformation axis is the y-direction.

It was mentioned in section 4.1 that due to the anisotropy present in the strained and THT triptycene polyester samples, additional sector integrations were performed to probe the d-spacings in each direction. Three scans were taken with an angular width of 10 azimuthal degrees about a particular direction: equatorial, meridional, and at an azimuthal angle of 60°. The sectors are shown in Fig.4-16, and the observed d-spacings are reported in Table 4.7.



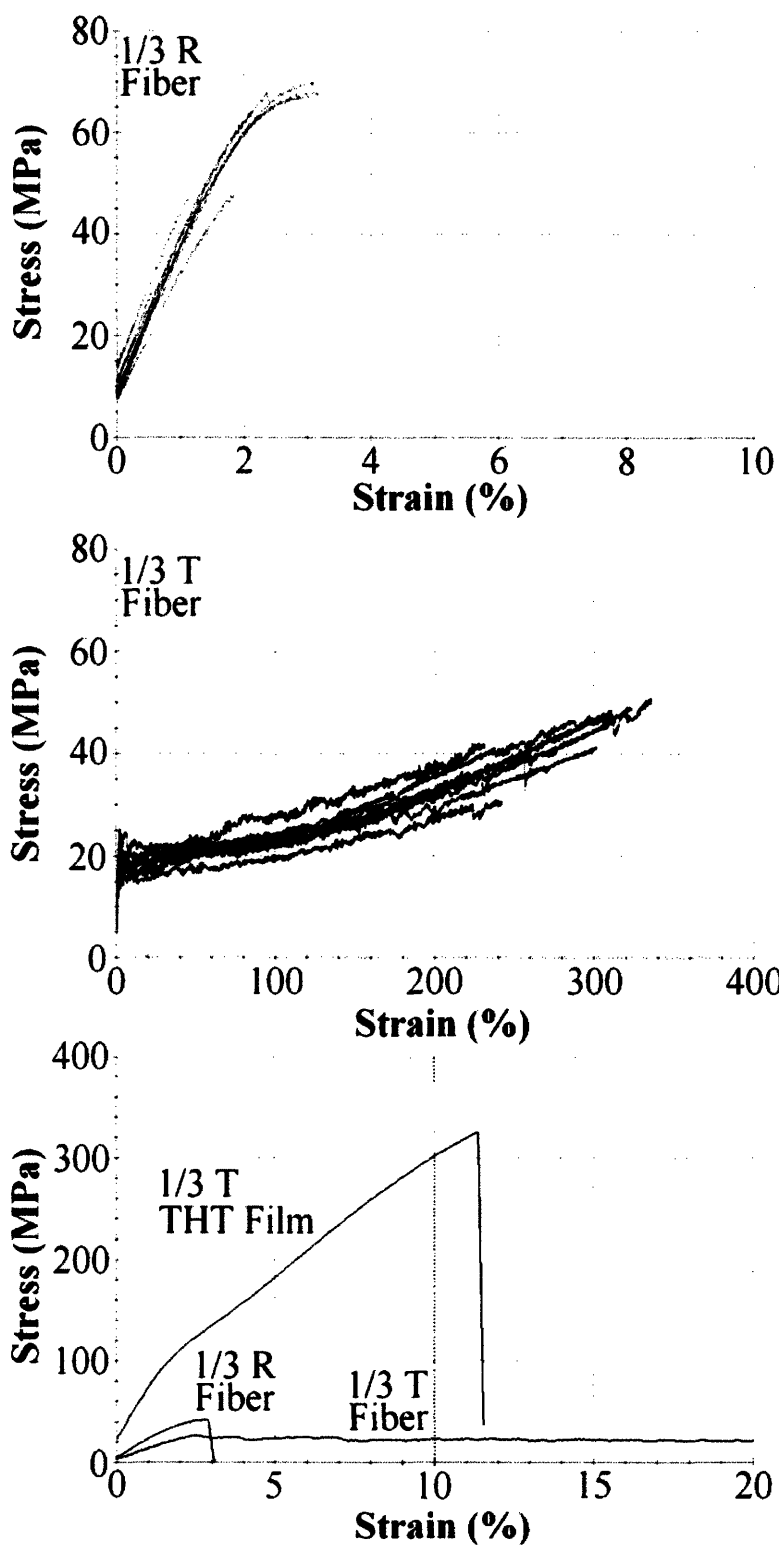
**Figure 4-16:** (a) EQ: Equatorial, (b) ME: meridional, and (c) 60° sector scans in WAXS of strained and THT triptycene polyester films with the peaks of interest labeled in accordance with section 4.1. Part (d) shows the angular definitions of each scan.

Polymer Film	d-spacings		
	EQ (peak 3)	ME (peak α)	60° (peak 1)
1/3 T (S)	4.2 Å	6.5 Å	15.9 Å
1/3 T (THT)	4.2 Å	6.5 Å	15.9 Å

**Table 4.7:** WAXS results from equatorial (-5° to 5°), meridional (85° to 95°), and 60° azimuthal angle (55° to 65°) scans.

Fibers were melt spun from both polymer samples. The non-triptycene polyester was found to spin fiber at 180 °C based on the hot strip procedure detailed in Experimental

Methods. However, despite the lower melting point, the triptycene polyester could not spin fiber until 300 °C. Additional attempts were made to spin fiber at 150 °C, 200 °C and 250 °C. Polymer could be extruded at 250 °C but would not draw. While 300 °C is a relatively high temperature, TGA (Table 4.3) indicated that the polymer should be thermally stable. Additionally, the fibers did not display any noticeable yellow or brown coloring typical of degraded polymer. Single fiber tensile tests are shown in Fig. 4-17.



**Figure 4-17:** Single fiber tensile tests for non-triptycene polyester (1/3 R) and triptycene polyester (1/3 T) melt spun fibers. The bottom plot shows a superposition of representative samples compared to 1/3 T THT film.

The fiber spinning process was intended to impart high levels of axial orientation which should have resulted in high tensile stiffness and low tensile ductility as compared to films. Single fibers with comparable final diameters (and thus draw ratios) were chosen for assessment, as this indicated that each polymer should have experienced roughly the same levels of extensional forces that result in molecular orientation. Compared to solvent cast films of the non-triptycene polyester, single fibers displayed the typical increased modulus (2.82 GPa versus 0.58 GPa) and strength (53 MPa versus 17 MPa) with decreased strain to failure (3% versus 10%). However, the opposite case was apparent for the triptycene polyesters. Single fibers exhibited a lower modulus, equivalent strength, and a higher strain to failure. The values are stated in Table 4.8. It would seem that the fiber spinning process served the opposite effect from what was expected.

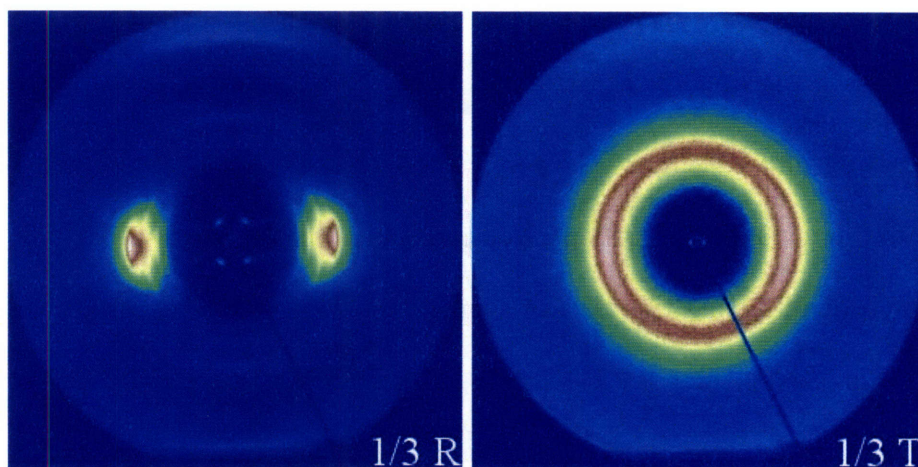
Polymer	T <sub>spin</sub> (°C)	d (μm)	E (GPa)	σ (MPa)	ε <sub>b</sub> (%)
1/3 R fibers	180	40 (± 6)	2.82 (± 0.26)	53 (± 14)	2.4 (± 0.9)
		HIR:	3.10	70	3
1/3 T fibers	300	43 (± 6)	1.02 (± 0.12)	42 (± 7)	279 (± 44)
		HIR:	1.10	49	321

**Table 4.8:** Single fiber tensile properties. HIR = highest individual result, d = fiber diameter, and the values in parentheses report standard deviations.

WAXS of fiber bundles was consistent with the mechanical data observed. The non-triptycene polyesters fibers exhibit well defined arcs and spots characteristic of an oriented polymer system, while the triptycene polyester fibers have only the slightest amount of visible orientation in one pair of diffuse arcs (Fig. 4-18). At first glance, it could be noted that the arcs in Fig. 4-15 are even more diffuse despite being very well



oriented samples. However, the pictures in Fig. 4-18 were taken at a synchrotron and present a higher resolution. The view field is also significantly larger. These scans reach out to q-vectors of  $3.25 \text{ \AA}^{-1}$  in contrast to  $2.25 \text{ \AA}^{-1}$  at the ISN facilities. Therefore, this pattern represents very little molecular orientation in the triptycene fibers.



**Figure 4-18:** WAXS of fiber bundles oriented in the y-direction.

It is suspected that the triptycene polyester must have degraded during the spinning process. But as mentioned earlier, there were no obvious optical signs of degradation. The melt spinning process was conducted under vacuum and nitrogen purge, and TGA indicated that degradation onset was above  $300 \text{ }^\circ\text{C}$ . However, isothermal TGA conducted in Nitrogen at  $300 \text{ }^\circ\text{C}$  revealed that the polymer does in fact degrade slowly (about 1% per 10 minutes) at that temperature. It is worth noting here that TGA measures degradation by mass loss. Therefore, it is possible for a polymer to be degrading well in advance of any indications from the TGA. Given the results from the

mechanical properties and WAXS patterns, degradation seems the most likely explanation.

#### 4.2.4 *Conclusion*

Oriented samples of both non-triptycene and triptycene polyesters were characterized. The non-triptycene polyester remained brittle at 70 °C. Therefore, the THT process could not be employed on this sample, but fibers were able to be melt spun at 180 °C. The opposite case held for the triptycene polyester which could form well oriented THT films but not well oriented fibers. A loose comparison between the two successfully oriented samples yields intriguing results. On average, the THT triptycene films demonstrated over 60% higher modulus, over 400% high strength, and over 350% higher strain to failure compared to the non-triptycene fibers. While the comparison of samples oriented by two different methods limits the evaluation, the superiority of the triptycene polymer to the non-triptycene polymer is qualitatively consistent with the data seen for the isotropic samples discussed in section 4.1.

It was surprising that the triptycene polyester required such high temperatures for melt spinning fibers. In contrast to the cursory experiments on low molecular weight triptycene polyesters discussed in the introduction to this chapter, the higher molecular weight sample displayed a much greater melt viscosity despite a relatively low melting point. Melt viscosity typically increases with molecular weight. The very large melt viscosity relative to the non-triptycene polyester suggest some sort of increased entanglement density, perhaps arising from the minimization of IMFV. Overall, the ability to produce oriented triptycene polyester samples that retained their toughness was

an encouraging result with regards to the possibility of fiber applications, despite the degradation issues encountered here in the melt.

## 4.3 Varying Composition and Type of Iptycene Unit

### 4.3.1 *Background*

It is established that the incorporation of triptycene at 21 wt % resulted in the simultaneous enhancements of stiffness, strength and ductility. These findings were attributed to the unique structure of triptycene units, which contain internal molecular free volume (IMFV), and the novel “molecular barbed wire” architecture created by the integration of these units into a polymer backbone. This particular case has shown that the proposed mechanism of the minimization of IMFV might induce novel steric interactions in polymer systems.

But only one concentration has been presented. This section reports on a different concentration of triptycene in the same polyester system. In addition, other types of iptycene units with different amounts of inherent IMFV were also incorporated into the polyester. Therefore, it was possible to observe the effects of varying inherent IMFV and test the robustness of the preliminary conclusions of the previous sections. Finally, processing conditions were slightly altered, again to probe the consistency of the enhancements attributed to IMFV. It was already seen in section 4.2 that oriented samples of triptycene polyesters were superior to oriented samples of non-triptycene polyester. The results here further strengthen conclusions that the enhancements brought

about by iptycenes and IMFV remain effective across composition, iptycene type, and processing conditions.

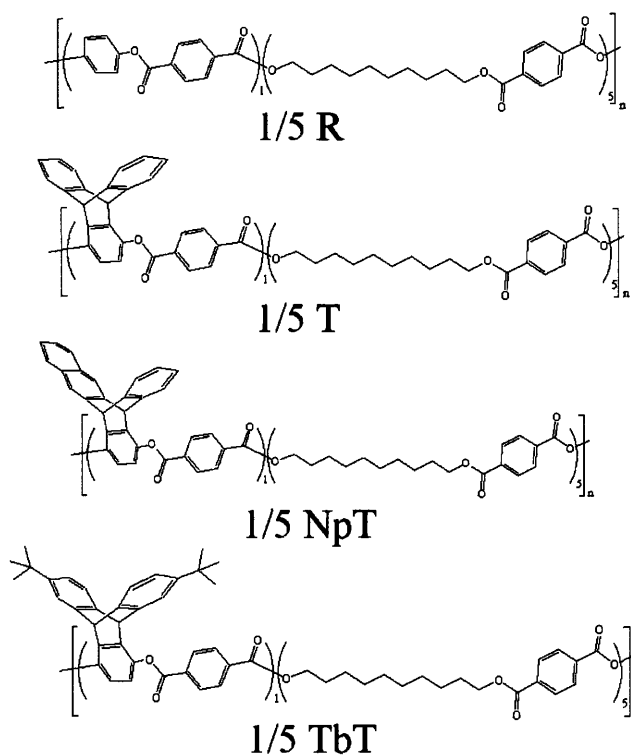
#### 4.3.2 *Experimental Methods*

The materials used in this section were provided by Dr. Lokman Torun (MIT Chemistry, post-doctoral researcher) and are described in detail in Chapter 2. Polymer samples were dissolved in dichloromethane, filtered and transferred to Teflon® boxes, and then, through the slow evaporation of solvent by the identical procedure given in section 4.1.2, isotropic cast films were formed. These films were dried in a vacuum oven to ensure the removal of both excess solvent and water. Films were then melted at 150 °C in a hot press by a procedure explained in section 2.2.2. 150 °C was chosen based on DSC data as the lowest temperature by which all crystals should melt. Films were held in the melt for approximately 5 minutes under light pressure (almost 0 psi) before being quenched to room temperature by cold water cooling coils. This produced melt processed films that were stored under vacuum for one month before testing. The iptycene containing films were transparent, while the non-iptycene film was cloudy.

Films were tested for structural, thermal and mechanical properties according to the experimental procedures in section 4.1.2. WAXS was performed at Brookhaven National Laboratories under identical conditions as those in section 4.2.2.

### 4.3.3 Results and Discussion

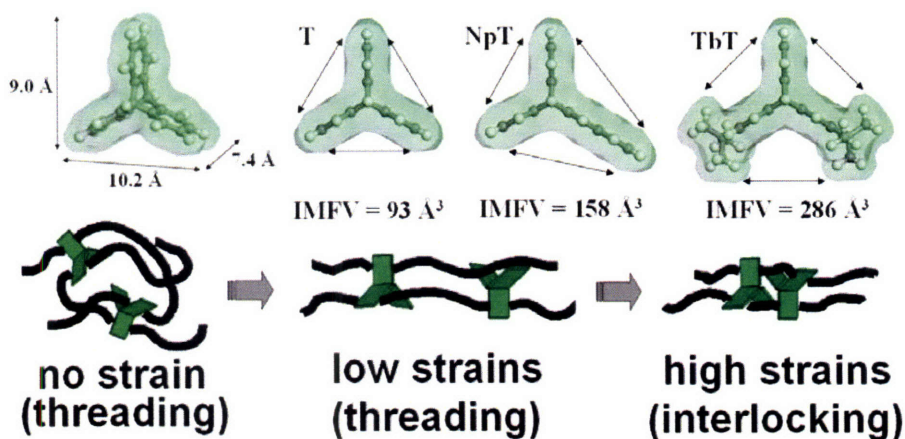
Three types of polyesters with various iptycene units were prepared and characterized against an analogous reference polyester backbone with a para-linked benzene unit instead of an iptycene (Fig. 4-19).



**Figure 4-19:** Chemical structures of the reference non-iptycene polyester (R), triptycene polyester (T), naphthalene-modified triptycene polyester (NpT), and tert-butyl-modified triptycene polyester (TbT).

The first two polyesters (reference and triptycene) were similar to those studied previously but with a lower triptycene content (Fig. 4-19:  $x/y = 1/5$  here vs.  $1/3$  for samples described in sections 4.1 and 4.2). Two new types of iptycene units were synthesized and incorporated into the polyester backbone (naphthalene-modified

tritycene and tert-butyl-modified triptycene) to create a range in size and shape of the pendant units, resulting overall in one reference polyester and three different types of iptrycene polyesters. Fig. 4-20 displays the three iptrycene units along with the schematic of the network morphology of molecular barbed wire and the steric interactions activated during deformation: molecular threading and molecular interlocking.



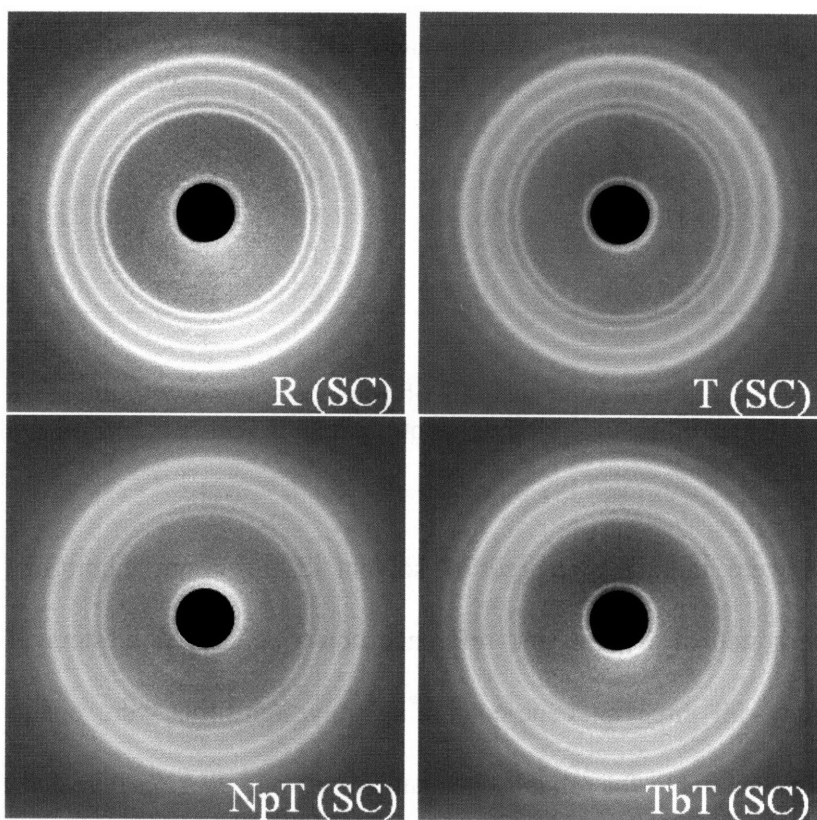
**Figure 4-20:** Triptycene (T), naphthalene-modified triptycene (NpT), and tert-butyl-modified triptycene (TbT) along with inherent IMFV calculations from Chapter 3. Also shown is a schematic of the steric interactions induced by the minimization of IMFV.

The aromatic components (which include the pendant units) are distributed through approximate statistically random copolymerization; therefore, the chemical structures represented in Fig. 4-19 reflect this approximation. The molecular weights and PDI's of the two previous polymers and four new polymers are listed in Table 4.9.

Sample	$M_n$ (g/mol)	$M_w$ (g/mol)	PDI	No. Repeats	C. L. (Å)
1/3 R	31,900	62,000	1.94	27	2040
1/3 T	40,300	75,500	1.87	30	2230
1/5 R	32,000	61,900	1.93	18	2070
1/5 T	31,200	56,700	1.82	16	1830
1/5 NpT	29,500	62,200	2.11	15	1690
1/5 TbT	26,800	49,600	1.85	13	1490

**Table 4.9:** Measured molecular weights of polyesters along with the calculated number of monomer repeat units and polymer contour length (C.L.) based on number average molecular weight ( $M_n$ ).

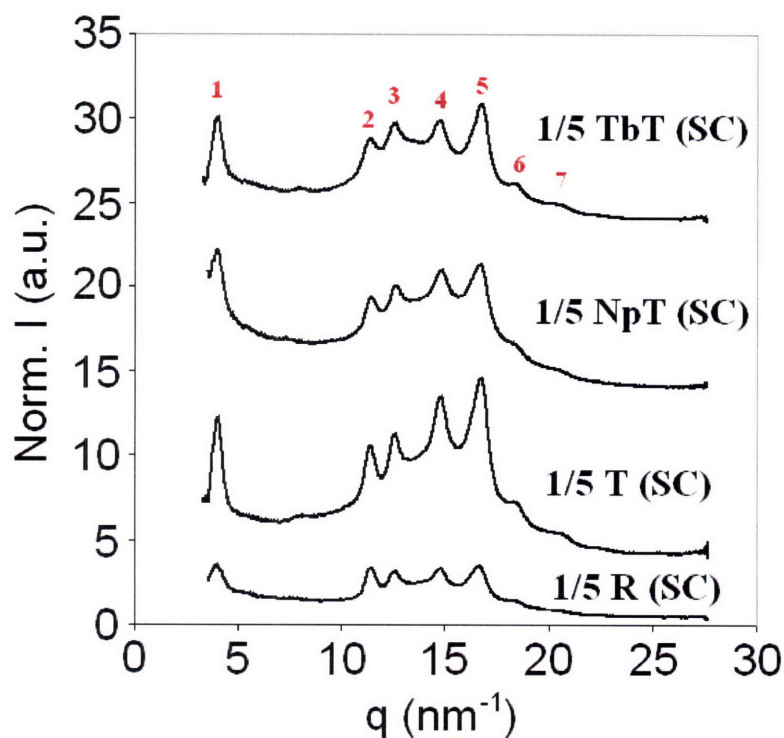
Samples were initially prepared by solvent casting from dichloromethane, as in previous work with triptycene and reference non-triptycene polyesters. But unlike the previous study, all three iptycene-containing polyester films were opaque and brittle, making them unsuitable for reliable mechanical testing. WAXS revealed these films to be highly crystalline.



**Figure 4-21:** WAXS of 1/5 solvent cast (SC) films of reference (R), triptycene (T), naphthalene-modified triptycene (NpT), and tert-butyl-modified triptycene (T) polyesters.

It is interesting that the triptycene containing films were able to achieve crystallinities comparable to the reference film. Circular integrations were used to calculate the peaks in Table 4.10 and are shown in Fig. 4-22.





**Figure 4-22:** Circular integrations of WAXS of solvent cast (SC) films with crystalline peaks numbered in red.

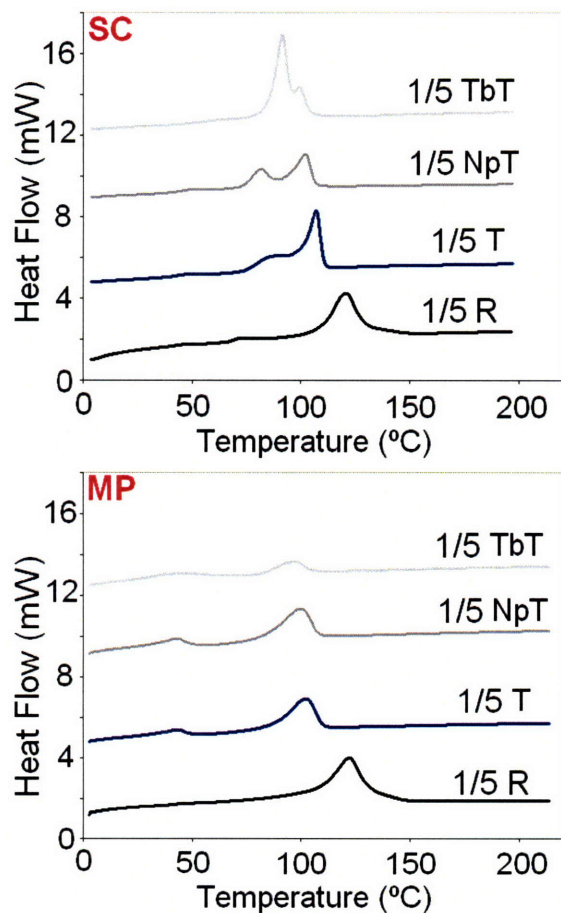
Sample	Peaks						
	1	2	3	4	5	6	7
1/5 R (SC)	15.7 Å	5.5 Å	5.0 Å	4.3 Å	3.8 Å	3.4 Å	3.1 Å
1/5 T (SC)	15.7 Å	5.5 Å	5.0 Å	4.2 Å	3.8 Å	3.4 Å	3.0 Å
1/5 NpT (SC)	15.7 Å	5.5 Å	5.0 Å	4.2 Å	3.8 Å	3.4 Å	3.1 Å
1/5 TbT (SC)	15.7 Å	5.5 Å	5.0 Å	4.3 Å	3.7 Å	3.4 Å	3.0 Å

**Table 4.10:** Crystalline peak d-spacings measured from circular integrations of WAXS of solvent cast films.

Since each of the peaks present in the iptycene samples is accounted for in the reference polyester, it can be assumed that the type of crystal formed is the same for all four samples. It is not expected that the iptycene units contribute to the crystalline regions, so

this solvent-induced crystallinity was likely due to the lower molecular weights and lower iptycene content of the 1/5 iptycene containing polyesters. Molecular threading might still be present in these samples, and, in fact, could aid in the crystallization process through the directive ordering of the shorter polymer chains.

Solvent cast films were melt processed at 150 °C in order to depress the crystalline component evidenced in DSC (Fig. 4-23). This treatment produced robust films suitable for reliable mechanical testing. From this point on, the discussion of 1/5 polyester films will refer to the melt pressed films unless specifically stated otherwise. The melt pressed film of the reference polyester was cloudy-white due to its crystallinity.



**Figure 4-23:** DSC of solvent cast (SC) and melt pressed (MP) 1/5 polyester films.

The iptycene films were all clear but had a slight yellowish tint. TGA (Table 4.11) indicated that these polymers were stable in air at temperatures well above the processing conditions, so this yellow tint was due to residual triptycene hydroquinone from the synthesis [63].  $\Delta H_{m,U}$  values in Table 4.11 indicate the relative levels of crystallinity present in each sample. The melt processed 1/5 series was seen to crystallize more than the solvent cast 1/3 pair, which was probably due to the lower iptycene content. The addition of triptycene in both cases was seen to depress crystallinity. In the 1/5 series, modifications to the triptycene unit (NpT and TbT) further depressed crystallinity.

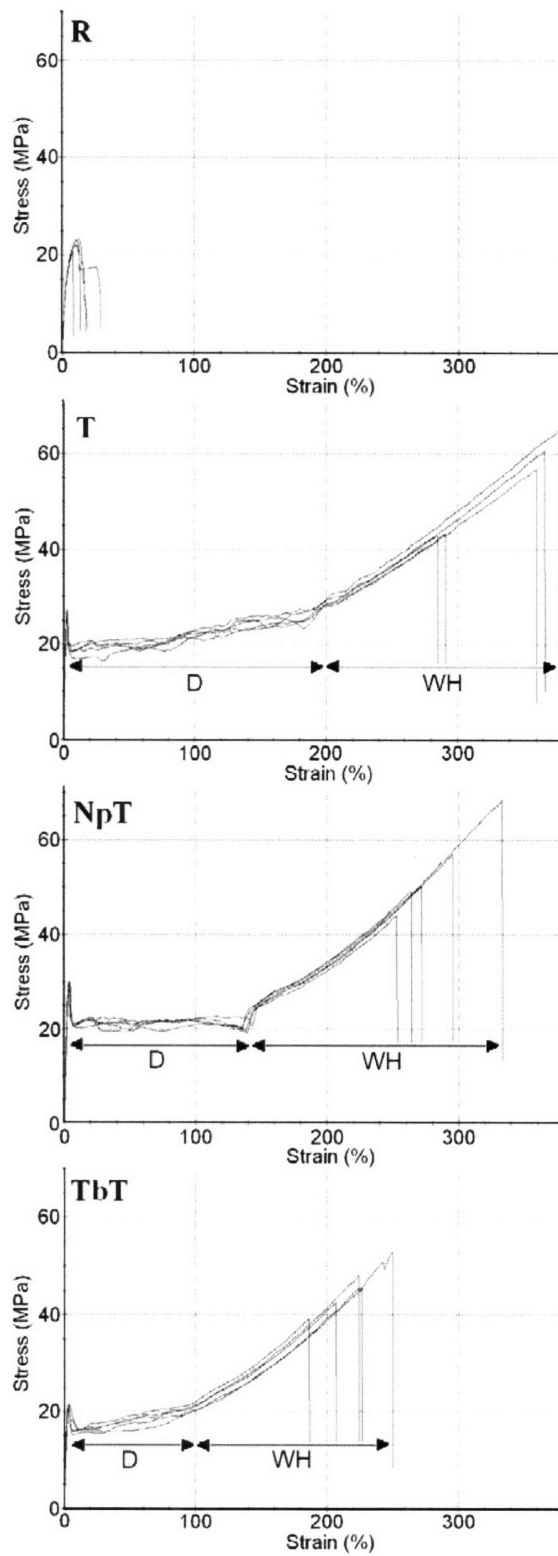
Sample	$\rho$ (g/cc) <sup>a</sup>	$T_g$ (°C) <sup>b</sup>	$T_m$ (°C) <sup>c</sup>	$\Delta H_{m,U}$ (J/g) <sup>c</sup>	$\Delta H_{m,S}$ (J/g) <sup>c</sup>	$T_d$ (°C) <sup>d</sup>
1/3 R *	1.20	25	119	28	-N/A-	375
1/3 T *	1.18	55	93	12	-N/A-	382
1/5 R	1.19	26	123	35	-N/A-	372
1/5 T	1.18	52	102	27	34	380
1/5 NpT	1.17	55	100	24	29	384
1/5 TbT	1.14	57	97	9	12	376

**Table 4.11:** Thermal properties of polyesters. <sup>a</sup> Taken by researchers at DuPont ( $\pm 0.01$ ). <sup>b</sup> 1 Hz tan delta curve of DMA. <sup>c</sup> DSC – U: unstretched isotropic films; S: films that were strained to failure; N/A: data not taken. <sup>d</sup> TGA of powders in air and assumed to be independent of processing conditions. \* Solvent cast films from section 4.1. The rest of the films were melt pressed.

The results of the tensile mechanical testing of melt pressed films are summarized in Table 4.12. All three iptycene-containing polyesters displayed about twice the Young's modulus, more than twice the strength, and 14-20 times the strain to failure as compared to the reference polyester (Fig. 4-24).

Sample	E (GPa)	$\sigma$ (MPa)	$\epsilon_b$ (%)	Work (J/cm <sup>3</sup> )	$m_{WH}$ <sup>a</sup>
1/3 R *	0.58 ± 0.03	17 ± 1	10 ± 2	1.5 ± 0.3	-
1/3 T *	1.62 ± 0.11	42 ± 4	211 ± 17	66.3 ± 8.3	0.15 <sup>b</sup>
1/5 R	0.63 ± 0.09	22 ± 1	16 ± 8	2.7 ± 0.6	-
1/5 T	1.39 ± 0.27	54 ± 10	336 ± 45	101.0 ± 11.3	0.20 <sup>b</sup>
1/5 NpT	1.38 ± 0.63	54 ± 10	284 ± 32	83.8 ± 0.6	0.26 <sup>b</sup>
1/5 TbT	1.15 ± 0.56	46 ± 5	219 ± 24	56.2 ± 4.2	0.24 <sup>b</sup>

**Table 4.12:** Tensile properties of polyester films. <sup>a</sup>  $m_{WH}$  = slope of stress-strain curve in the work hardening regime. <sup>b</sup> Standard deviations for these values were all around ± 0.005. \* Solvent cast films from section 4.1. The rest of the films were melt pressed.

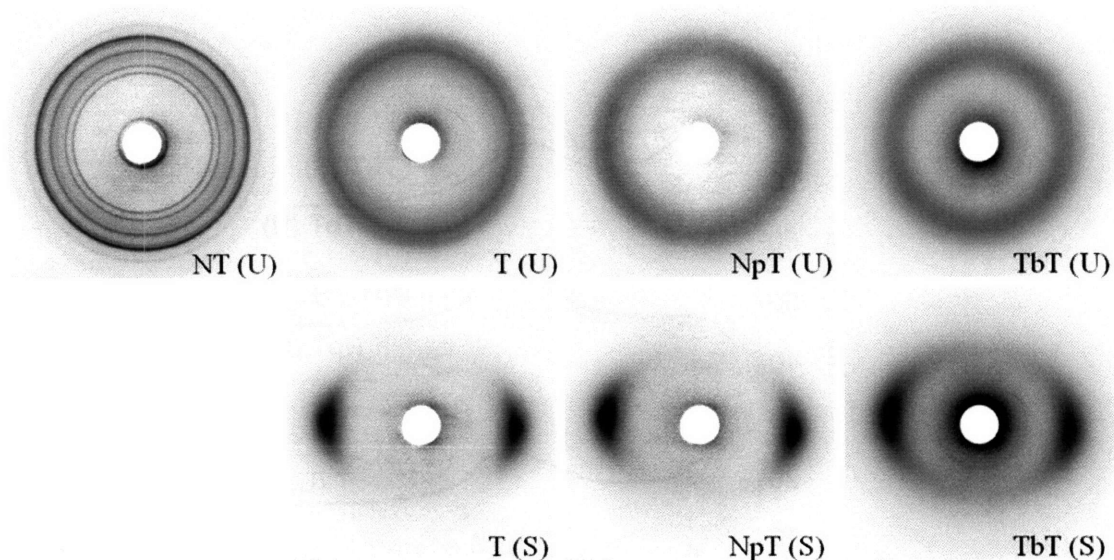


**Figure 4-24:** Tensile stress-strain curves of melt pressed 1/5 polyester films. Two deformation regimes are specified in the ductile films (D = drawing; WH = work hardening).

As was the case with the solvent cast films, the addition of iptycene units to the backbone of the polyester did not change the type of crystal formed since all detectable reflections in WAXS matched those already present in the reference polyester (Table 4.13). The reflections in the melt pressed samples match with the peaks in the solvent cast samples (Table 4.10) and are thus numbered the same with the exception of the emergence of two new peaks (4' and 5'). This again indicated that the non-iptycene segments were responsible for the crystallization.

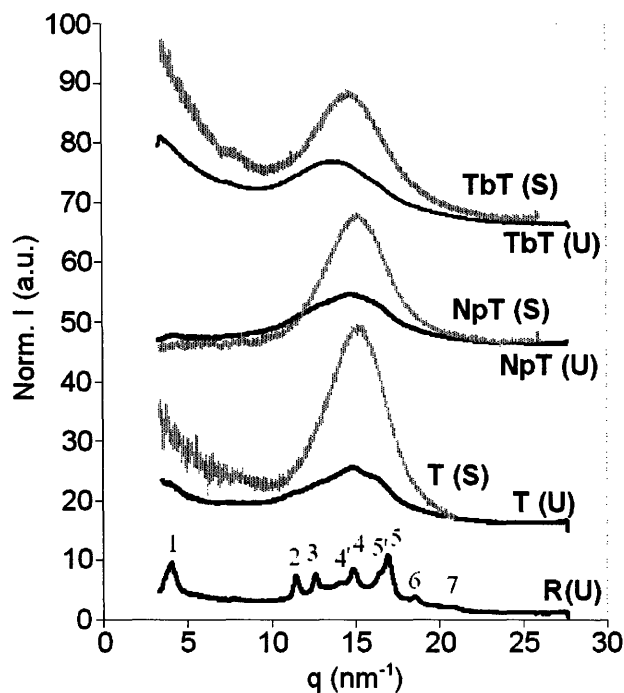
Sample	Peaks (Å)								
	1	2	3	4'	4	5'	5	6	7
1/5 R <sup>a</sup>	15.7	5.5	5.0	4.5	4.2	3.8	3.7	3.4	3.0
1/5 T <sup>a</sup>	15.6	5.5	5.0	-	4.2	3.9	-	-	-
1/5 NpT <sup>a</sup>	15.6	-	-	-	4.2	-	-	-	-
1/5 TbT <sup>a</sup>	-	-	-	4.6 <sup>b</sup>	-	-	-	-	-

**Table 4.13:** WAXS d-spacings of melt pressed 1/5 polyester films. <sup>a</sup> Measured from circular integrations in Fig. 4-26. <sup>b</sup> Could be a superposition of peaks 3 and 4.



**Figure 4-25:** 2D WAXS patterns of unstretched (U) and strained to failure (S) 1/5 melt pressed films. R(S) was not taken due to the low failure strains. The stretching direction is vertical.

WAXS images are shown in Fig. 4-25, and equatorial scans of the strained films were superimposed onto circular integrations of the unstrained films in Fig. 4-26. The reference non-iptycene polyester did not strain significantly before failure, so an x-ray pattern of that strained sample was not taken. The decrease in sharpness and relative number of rings evident in Fig. 4-25 confirmed the trend of decreasing crystallinity with size of iptycene unit shown by DSC. The peak (equatorial arcs) positions from the strained samples were 4.1 Å, 4.1 Å, and 4.3 Å for the triptycene polyester, the naphthalene-modified triptycene polyester, and the tert-butyl-modified triptycene polyester, respectively. The full-width half-maximums (FWHM) of this peak from equatorial scans (Fig. 4-26) were  $3.9 \text{ nm}^{-1}$ ,  $4.1 \text{ nm}^{-1}$ , and  $4.6 \text{ nm}^{-1}$  for T, NpT, and TbT, respectively. This confirmed that the films that strained less before failure exhibited less molecular orientation in the loading direction, as expected.



**Figure 4-26:** WAXS circular integrations of unstretched (U) 1/5 films and equatorial integrations with a width of 10 azimuthal degrees after strain to failure (S). X-ray patterns of R(S) were not taken due to the low failure strains in the non-triptycene polymer.

The triptycene polyester presents the best combination of enhanced stiffness, strength and ductility. The increased stiffness of the iptycene-containing polyesters occurred despite the decrease in crystallinity (compared to the reference polyester) because the iptycene units stiffened the chain backbone, which was evident from the rise in  $T_g$ . It might be tempting to attribute the higher stiffness and ductilities of the iptycene-containing polyesters solely to the increase in  $T_g$  and decrease in crystallinity. But this correlation was not supported when comparing the iptycene-containing polyesters to one another. The 1/3 triptycene polyester had a higher  $T_g$  and lower crystallinity than the 1/5 triptycene polyester. But, although the modulus of the 1/3 was increased, the ductility suffered significantly. Additionally, amongst the 1/5 iptycene-containing polyesters (T, NpT, TbT), the increase in  $T_g$  and decrease in crystallinity lead to decreased modulus *and*



decreased strain to failure. The two reference polyesters also negated such a suggested correlation as the 1/5 R exhibited better stiffness, strength and ductility compared to the 1/3 R despite having higher crystallinity and about the same values for  $T_g$ , molecular weight, and chain contour length.

To explain the variations in the mechanical behavior of these polymers, we focus on the effects of the presence of pendant iptycene units with IMFV and the tendency for molecular threading and interlocking. The bulky iptycene units stiffen the backbone of the polymer chain itself, but the minimization of IMFV also results in the occupation of iptycene clefts by neighboring polymer chains. This combination together significantly restricts chain dynamics which accounts for the large increase in  $T_g$  as compared to the reference polyester. The differences in  $T_g$  between the various iptycene-containing polyesters was relatively insignificant compared to what might be expected given the large differences in the inherent IMFV calculated for the various types of isolated iptycene units (Fig. 4-20). The variation of the mechanical stiffnesses of the 1/5 iptycene films seemed to correlate with their differences in crystallinity. However, this was not the case with ductility.

The naphthalene-modified triptycene polyester failed at notably smaller strains than the triptycene polyester, and the tert-butyl-modified triptycene polyester failed at even lower strains. As expected, all three polymers exhibited levels of molecular orientation commensurate to their respective strain to failure values. Typically, less oriented samples yield lower stress levels because the stress-strain behavior in the work hardening regime is almost entirely due to the entropic penalty associated with the uncoiling and alignment of polymer chains [96-101]. This explanation assumes no effects from crystallinity. A

polymer developing less chain orientation with applied strain generally has a lower work hardening slope ( $m_{WH}$ ). However, our experimental values showed the opposite trend. Both the naphthalene-modified triptycene and tert-butyl-modified triptycene polyesters exhibited increased work hardening slopes (Table 4.12) despite lower final orientation states. These results cannot be attributed to crystallinity since both the naphthalene-modified triptycene and tert-butyl-modified triptycene polyesters have less crystallinity than the triptycene polyester (with no signs of strained-induced crystallinity). Therefore, we attribute the increase in slope to the more extensive molecular interlocking of iptycene units, which represents an additional (and new) work hardening mechanism specific to these types of molecular barbed wire polymers.

To investigate the interlocking mechanism further, the post-yield deformation was divided into two distinct behavioral regimes: drawing (D) and work hardening (WH). These regimes are labeled on the stress-strain curves in Fig. 4-24, using the abrupt change in slope of the stress-strain profile to identify each region. These two regimes correspond to particular types of behavior directly related to the ideas of threading and interlocking induced by the “molecular barbed wire” contour of the polymer chains. The drawing regime relates to the threading mechanism. The onset of iptycene-iptycene interlocking likely occurs during the latter stages of drawing. The work hardening region begins when the combination of entropic forces and this new interlocking mechanism dominates the mechanical response of the material. It can be seen that, as the size of the pendant iptycene unit increased, the total drawing strain (D) decreased and was accompanied by an earlier initiation of the work hardening regime. The naphthalene-modified triptycene polyester displayed significantly less total drawing strain than the triptycene polyester but

maintained the same level of total work hardening strain (WH) representing a greater contribution of the work hardening regime to the total post-yield deformation. The shortening of the drawing regime could be anticipated, as the naphthalene-modified triptycene is a physically larger unit. The molecular interlocking of such units would contribute to the mechanical behavior at lower strains than the triptycene unit because of the greater resistance to deformation. This is also likely to be why the naphthalene-modified triptycene polyester has the larger  $m_{WH}$  despite exhibiting less chain orientation. In this case, the additional resistance to deformation from molecular interlocking dominated over the reduced entropic force (from less chain orientation) resulting in the higher measured stress levels at any given strain in the WH regime.

The tert-butyl-modified triptycene polyester transitioned into its work hardening regime at even smaller strains but then expressed a much-shortened total work hardening strain. The slope of this regime for the tert-butyl-modified triptycene polyester was slightly lower than for the naphthalene-modified triptycene polyester but was still notably higher than for the triptycene polyester. This again can be attributed to the interplay between the entropic penalty of uncoiling/aligning polymer chains and the molecular interlocking of triptycene units. The interlocking of the larger units results in the earlier initiation of the WH regime and a lower degree of final chain orientation. It can be seen from Fig. 4-26 that the *unstrained* tert-butyl-modified triptycene had a WAXS halo centered on a higher d-spacing (lower q vector: peak 4 for T, NpT vs. peak 4' for TbT in Table 4.13) than the other triptycene samples, which could be an indication that the tert-butyl-modified triptycene unit was not as effective at promoting molecular threading as either the triptycene or naphthalene-modified triptycene units in the prepared isotropic

samples. Therefore, we suggest that the decrease in the drawing regime was not only because of the earlier significance of interlocking but also because of decreased amounts of threading. The  $m_{WH}$  of the tert-butyl-modified triptycene polyester was higher than that of the triptycene polyester because the increased stress contribution from the molecular interlocking of bigger triptycene units dominated over the reduced entropic force from less chain orientation. However, the  $m_{WH}$  of the tert-butyl-modified triptycene polyester was slightly lower than that of the naphthalene-modified triptycene polyester. In comparing these two, the reduced entropic force must have outweighed the gain in stress produced by the molecular interlocking of the larger triptycene unit.

Why were the triptycene and naphthalene-modified triptycene polymers more suited for molecular threading than the tert-butyl-modified triptycene polymer? Although structural units with higher amounts of inherent IMFV (Fig. 4-20) might be expected to induce greater amounts of molecular threading, it is critical to note the accessibility of the cavities that are assumed to be occupied by neighboring chains. In the case of the naphthalene-modified triptycene, the IMFV of a pendant unit probably has the same accessibility as a triptycene unit. However, a somewhat larger cavity may not promote any more threading than is already present in the triptycene. The tert-butyl-modified triptycene has even larger amounts of inherent IMFV, but, in this case, accessibility might be a significant problem because of the rotational freedom of the tert-butyl groups. The molecular dynamics of these groups could sterically obstruct the occupation of empty cleft spaces by shielding the opening. It is possible that during deformation, tert-butyls could momentarily cease to obstruct a cleft space. Once a chain slides into that cavity, it can then begin threading along the triptycene, and it is unlikely to vacate that

space. The x-ray peak (4') shift to higher  $q$  for the tert-butyl-modified triptycene polyester during deformation was greater than for both of the other samples ( $\Delta q_{\text{TBT}} \approx 3\Delta q_{\text{T}}$ ,  $\Delta q_{\text{T}} \approx \Delta q_{\text{NpT}}$ ) which could be an indication that threading was indeed increasing during deformation. However, given the early initiation of the WH regime, it is likely that some of the triptycene clefts remained unoccupied even at failure. Therefore, even though the tert-butyl-modified triptycene polyester here had the most *inherent* IMFV, that calculation only considers a static, isolated structural unit. An *effective* IMFV would take into account chain dynamics and the particular incorporation into a polymer backbone. In this case, the effective IMFV may have been much less than the inherent IMFV calculation.

The contribution of molecular interlocking to a sample's ability to resist applied load will also depend on the concentration of pendant units. The  $m_{\text{WH}}$  of the 1/3 triptycene polyester was much lower than any of the 1/5 triptycene polyesters studied, despite having more units presumably capable of interlocking (1/3 T  $\approx$  21 wt % triptycene vs. 1/5 T  $\approx$  15 wt % triptycene). This was again due to the lower strain to failure, which reduced the entropic contribution to the stress in the work hardening regime. The pendant concentration also affects other structural and mechanical characteristics, as might be expected. Integration of the crystalline peak in DSC ( $\Delta H_{\text{m,U}}$ ) showed that the greater concentration of triptycene resulted in a larger depression of crystallinity relative to each polymer's reference non-triptycene counterpart. Specifically, the addition of 15 wt % triptycene produced a 23% decrease in relative crystallinity, while the addition of 21 wt % triptycene produced a 57% drop in relative crystallinity. The greater concentration of triptycene also slightly increased the glass transition temperature, but only by 3 °C. Most

interestingly, despite the greater reduced crystallinity, the 21 wt % triptycene content produced an almost three times higher modulus than the reference polyester while the 15 wt % triptycene content produced closer to two times higher modulus than its reference polyester. It is interesting to note that the relative contributions of each deformation regime to the total sample strain (D:WH ratio) were approximately the same for the 1/3 and 1/5 triptycene polyesters. In a system where the contributions of chain orientation to the deformation resistance in the WH regime are known, it would be possible to isolate the additional forces associated with molecular interlocking. Once empirical values for the contribution of molecular interlocking are attained, an *interlocking index* can be created to correlate the size, shape and frequency of pendant units to the stress-strain behavior in the WH regime.

#### 4.3.4 Conclusion

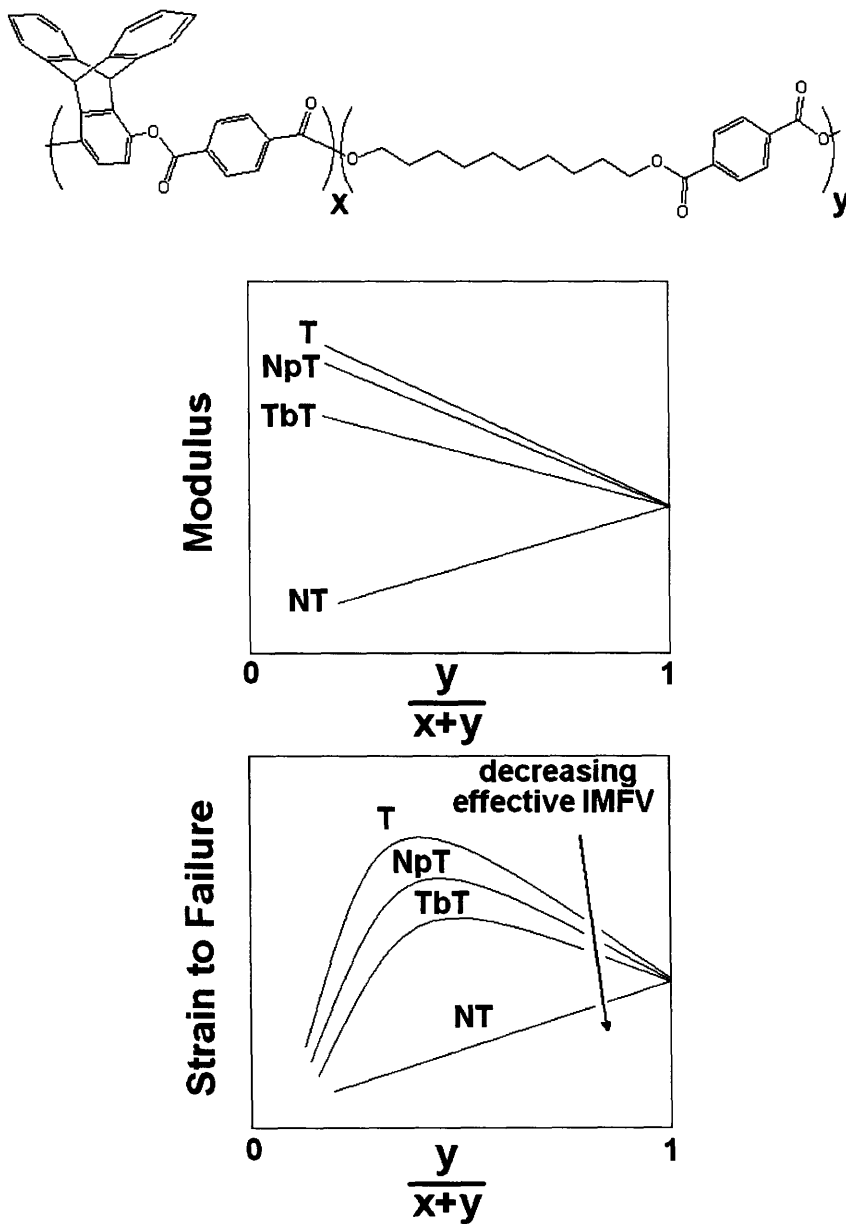
The incorporation of rigid pendant units with IMFV (in contrast to conventional smooth polymer chain contour systems) significantly improved the mechanical properties of a family of polyesters. The results in this section further established the idea that threading and interlocking of polymer chains through molecular level, steric interactions is a novel means to enhance ductility simultaneously with stiffness and strength. The accessibility of the incorporated IMFV plays an important role in exploiting these new mechanisms. Mechanical data suggest that the amount of IMFV, as well as the size and shape of the pendant unit, must be optimized within the polymer system and that larger IMFV units are *not* necessarily better. Additionally, it was demonstrated that molecular interlocking can create a stronger system than can be made considering only chain orientation and

crystallinity. The stress response at any particular strain was enhanced by simply modifying the triptycene unit. Therefore, these types of systems can be used to meet different application requirements for particular strength values by specific strains by making only minor changes to the iptycene unit. Finally, the degree of molecular threading and the onset of molecular interlocking determine the ratio of the drawing to work hardening regimes (D:WH) which were found to be dependent on the size and shape of the particular iptycene unit. In the future, it may be possible to use these ratios to index propensities for certain pendant groups with IMFV to induce molecular threading and interlocking.

## Summary

Multiple polyester systems were thoroughly examined for the effects of iptycenes on the mechanical properties of solid-state films. The covalent incorporation of iptycene units into the polymer chain backbone produced a unique polymer architecture that resembled molecular barbed wire. This architecture was able to utilize successfully the minimization of IMFV about the iptycene units to induce novel steric inter-chain interactions. Specifically, molecular threading and molecular interlocking were identified as lateral chain interactions brought about by the minimization of IMFV. Polyester films containing triptycenes were seen to exhibit simultaneous enhancements to stiffness, strength and ductility. This was unusual as typically improvements to stiffness are accompanied by losses in ductility. The results were shown to be robust across different concentrations of iptycenes, different types of iptycene units, and different processing conditions. Based on the data observed, hypothetical curves for the

dependence of the mechanical properties on concentration and iptycene type were generated in Fig. 4-27.



**Figure 4-27:** Hypothetical curves for the concentration dependence of modulus and strain to failure based on experimental observations for the polyesters studied.



Fig. 4-27 depicts the composition dependence of the modulus as linear, but this is not the only possibility. In fact, it is unlikely that the dependence is linear, but the hypothetical curves are drawn in this way merely to avoid more detailed suppositions as to the nature of the curve other than that the modulus is expected to continue to increase. This is in contrast to the strain to failure curves, which are expected to have an optimization with regards to composition. An optimal composition is predicted because molecular threading that occurs in the polyesters requires both iptycene content *and* aliphatic content; whereas, the increase in iptycene concentration can increase the modulus independent of threading.

The specific polyesters examined in this chapter may not be suitable for ballistic armor as they were prepared here. However, there are many other high strength applications that could benefit from significantly enhanced polyesters. One example relevant to the military might be parachutes [102]. It is also unknown whether or not the mechanisms of threading and interlocking can still behave as described at high deformation rates. It is possible that at very high strain rates, threading may resemble covalent crosslinks and not allow for the high levels of deformation that access interlocking. But most importantly, the polyesters served as a scientific case study motivating the investigation of iptycenes in other polymer systems. The next chapter was a direct result of the encouraging findings from the polyester data.



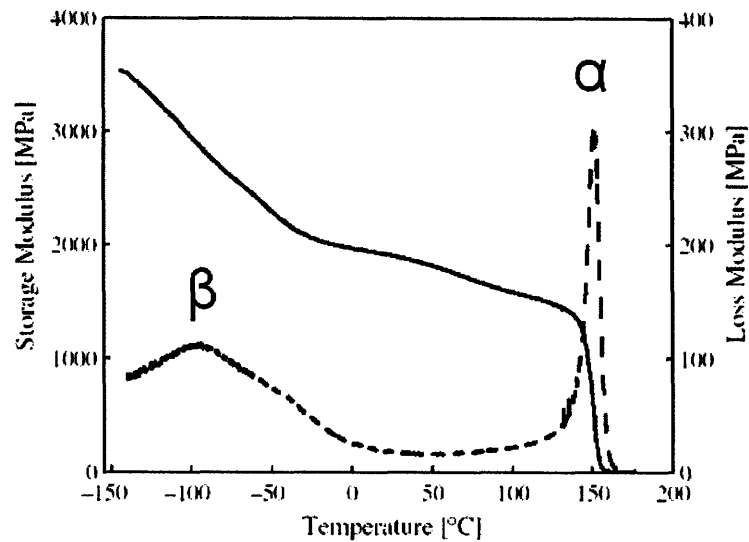
## Chapter 5

# Polycarbonates (PC) and PC Blends

Upon the conclusion of the work done on polyesters, it was determined that triptycene incorporations into polymers could significantly alter the mechanical performance in the solid state. It therefore became desirable to examine another polymer system. Given the motivations of the Institute for Soldier Nanotechnologies (ISN), a polymer suitable for ballistic applications seemed appropriate. Bisphenol-A polycarbonate (PC) was chosen for a variety of reasons.

PC is a high  $T_g$  (~150 °C) engineering thermoplastic with excellent ductility and optical clarity. It is non-corrosive, non-toxic, and resistant to both staining and thermal degradation. Furthermore, it has been found to have exceptional impact resistance. With such advantageous physical properties, the commercial applications of PC are widespread, including automobile parts, DVDs, sport bottles, windows, visors, anti-scratch coatings, and even bullet-proof glass. Improvements to the mechanical behavior of this material would thus garner significant interest from a wide range of industries.

One of the most intriguing properties of PC is the coupling of its high glass transition temperature with high ductility (typical  $\epsilon_b > 100\%$ ). It might be expected that a polymer in its “glassy” state would behave in a rather brittle manner. However, correlations have shown that high  $T_g$  polymers with below ambient temperature thermal-mechanical relaxations will often express ductile mechanical behavior [33]. It can be seen in Fig. 5-1 that PC exhibits such a characteristic transition (the  $\beta$ -transition at about  $-95\text{ }^\circ\text{C}$ ) in its dynamical mechanical spectra.

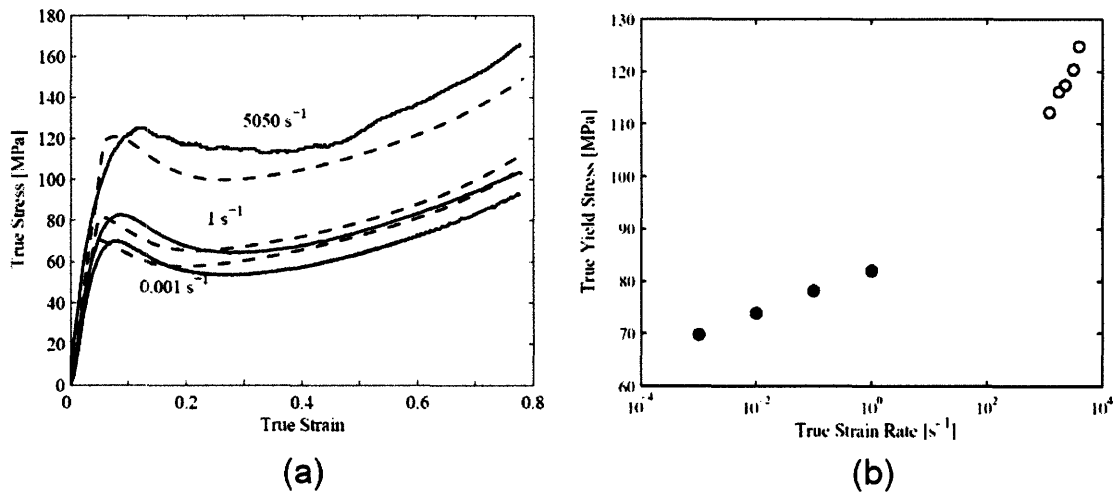


**Figure 5-1:** DMA spectra for Lexan® 9034 PC, adapted from Mulliken [103], showing the storage modulus ( $G'$  - solid line) and loss modulus ( $G''$  - dashed line).

Relaxations (or transitions) in the loss modulus curves are labeled alphanumerically with decreasing temperature, starting with  $T_g = \alpha$  by convention. According to correlations, PC therefore owes its ductility to its salient  $\beta$ -transition.

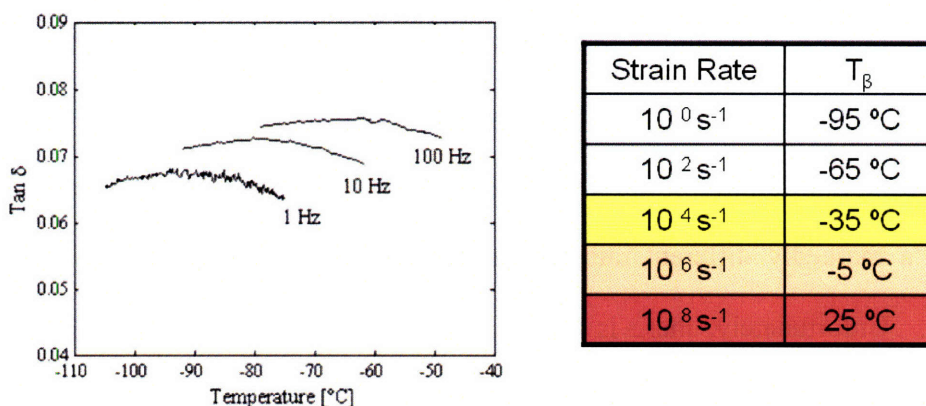
Recently, specific interest has been generated with regards to the high-rate mechanical behavior of PC. A number of researchers have identified a significant

transition in the rate-dependent yield behavior of this material, which ultimately leads to enhanced strength under conditions of high strain rate [103-105]. Fig. 5-2 illustrates the two regimes of behavior. The yield strengths at “low” deformation rates (closed circles) display a markedly different rate-dependence than at “high” deformation rates (open circles). Unfortunately, there is a gap in the data during the actual shift due to the inability to acquire reliable data at those particular strain rates.



**Figure 5-2:** Lexan® data, adapted from Mulliken [103], for uniaxial compression tests at various true strain rates. Plots of characteristic stress-strain curves (a) and rate-dependence of yield strength (b).

This transition in the yield behavior at higher strain rates has been linked to the material’s viscoelastic  $\beta$ -transition [103]. The two related transitions are both thought to be brought on by restrictions to the mobility of short chain segments. Once these molecular motions become restricted, an additional component to the material’s deformation resistance is generated. This was shown by tracking the  $\beta$ -transition through increasing deformation rates.



**Figure 5-3:** Linear dependence of the  $\beta$ -transition with deformation frequency, adapted from Mulliken [103], along with linear extrapolation of peak position at high strain rates (ballistic projectile impact rates  $\geq 10^4 \text{ s}^{-1}$ ).

As shown in Fig. 5-3, the very broad  $\beta$ -transition shifts linearly by about 15 °C per decade of strain rate becoming increasingly relevant for room temperature ballistic deformation rates ( $10^4 \text{ s}^{-1}$  and above). It is this enhanced deformation resistance under conditions of high strain rate, coupled with the intrinsic ductility, which makes PC such an attractive material for impact applications.

Enhancements to the mechanical properties of PC have been attempted repeatedly and span decades of work. As is typical for many systems, it was commonly found that improvements to the stiffness and strength sacrificed ductility [106-109]. With regards to the discussion of rate-dependence, it has been seen that modifications to the  $\beta$ -transition have significant consequences on the mechanical properties. Specifically, dampening of the  $\beta$ -transition has proven detrimental to the deformation resistance of PC at high strain rates [110-112].

Triptycene was incorporated into the molecular backbone of bisphenol-A polycarbonate. The rest of this chapter reports the effects of triptycenes and IMFV on the mechanical properties of bisphenol-A PC.

## 5.1 Low Molecular Weight PC Blends

### 5.1.1 *Background*

Interfacial polymerization is the most prevalent synthesis route for commercial PC [113, 114]. Because this process involves the use of phosgene, a gaseous toxin, many alternative synthesis routes have been developed. Transesterification in the melt [115, 116], direct reaction of bisphenols with carbon monoxide by catalysis [117-119], catalyzed ring-opening polymerization [120, 121], and oxidative carbonylation [122] are amongst the more popular routes that have been investigated.

For a synthesis route to be commercially viable, it must produce both the transparency and the tough mechanical properties [123-125] that make PC such an attractive polymer. The key is to achieve high enough molecular weights to ensure a sufficient number of entanglements. This has been found to occur for molecular weights around 17,000 - 20,000 g/mol [126, 127]. Most commercially available PCs have molecular weights of 25,000 - 30,000 g/mol. While it is known that the lower molecular weight PCs exhibit brittle behavior, little has been reported as to possible commercial uses of these materials. This is probably because there have always been multiple known synthesis routes for higher molecular weight PC.

This section examines the effects of low molecular weight PCs blended with a commercially available bisphenol-A PC. The mechanical properties studied will be reported with a particular focus on rate dependence and relation to the  $\beta$ -transition.

### 5.1.2 Experimental Methods

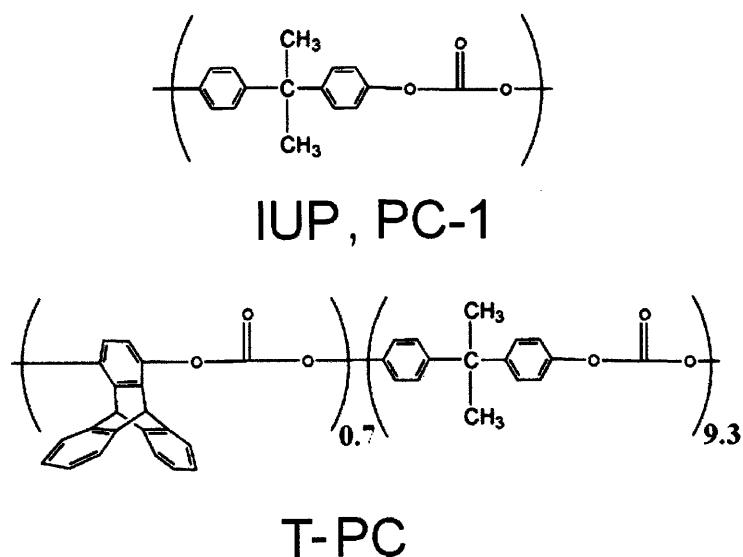
Table 5.1 lists the three different types of polycarbonates that were used to prepare the materials characterized in this work. IUP is a high viscosity grade bisphenol-A PC supplied by Mitsubishi Engineering Plastics under the commercial name Iupilon® E2000. PC-1 and T-PC were both synthesized by Triton Systems, Inc. (TSI) through processes referenced in Chapter 2.

Polymer	$M_n$ (g/mol)	$M_w$ (g/mol)	PDI
IUP	29,900	67,000	2.2
PC-1	13,100	30,100	2.3
T-PC	5,900	22,000	3.7

**Table 5.1:** Average molecular weight values ( $M_n$  and  $M_w$ ) and polydispersity index (PDI) determined via gel permeation chromatography (GPC) with THF eluent by Yong Yang (MIT Chemistry, graduate student).

PC-1 was intended to replicate IUP, but it can be seen that TSI was not able to achieve molecular weights comparable to that of the Iupilon® commercial standard. The T-PC copolymer was synthesized with approximately 7.7 wt % triptycene hydroquinone, corresponding to a 7/93 (or about 1/13) molar ratio in the x/y notation used in Chapter 4. The chemical structures of the monomers are given in Fig. 5-4.





**Figure 5-4:** Chemical Structures of IUP, PC-1, and T-PC monomers.

This section presents only one composition of triptycene, so the x/y notation will not be necessary here. The triptycene containing PC will be simply referred to as T-PC.

From the three PC variants listed in Table 5.1, three different materials were prepared for mechanical characterization. The first material (IUP) was pure, commercial Iupilon® PC. The second material (PC Blend) was a 25 wt % blend of PC-1 with IUP. The third material (T-PC Blend) was a 25 wt % blend of T-PC with IUP, yielding an overall triptycene concentration of about 1.9 wt %. The blend process was used for two reasons: first, PCs with molecular weights this low are brittle and second, blending conserves sample. The particular value of 25 wt % was arbitrary. The blends were prepared by dilute solvent mixing with a spinner in dichloromethane at room temperature overnight. Solutions were allowed to evaporate in a fume hood for 2-3 days in Teflon dishes, leaving behind crystallized films. These films were ground into a fine powder and then stored at 120 °C overnight in a vacuum oven, along with fine powder of IUP, before melt

processing. For all three polymers, disks of about 50 mm in diameter and 3 mm in thickness were compression molded at 265 °C (a temperature above the crystalline melting point for PC [128, 129]). Finally, the compression molded disks were machined into three specified sample geometries: cylinders, rectangular bars, and dogbones. All samples were dried at 55 °C under vacuum for a week before mechanical testing.

Uniaxial compression tests were conducted over a span of six decades in strain rate, ranging from about  $10^{-3} \text{ s}^{-1}$  to  $2000 \text{ s}^{-1}$ . Specimens for all compression tests were of right circular cylinder geometry, with a diameter of approximately 5 mm and a height of 2.5 mm. Low to moderate rate testing ( $10^{-3} \text{ s}^{-1}$  to  $10^{-1} \text{ s}^{-1}$ ) was conducted on a Zwick/Roell Z010 servo-hydraulic testing machine at constant engineering strain rates, in accordance with Fig. 2-11. High strain rate testing ( $1000 \text{ s}^{-1}$  to  $2000 \text{ s}^{-1}$ ) was performed on a compressive split-Hopkinson pressure bar (SHPB) test apparatus described in Chapter 2. Data from three tests per sample per rate were averaged to produce curves shown in figures.

The same circular specimens were also used to acquire data in parallel plate rheology. The rheometer at ISN was designed for 25 mm diameter disks. Therefore, the following scaling factor had to be employed during data analysis:

$$\tau = G \gamma$$

$$\text{and} \quad \begin{array}{l} \tau \sim r^{-3} \\ \gamma \sim r \end{array}$$

$$\therefore G \sim r^{-4}$$

Samples were tested at frequencies of 100 to 0.1 rad/sec at 10 °C intervals from 210 °C to 160 °C. TA Analysis software was then utilized to perform time-temperature superposition with a 190 °C reference temperature. The room temperature bulk density was used in the calculations for entanglement molecular weight because a melt density was not available. It was found that data from three samples provided sufficient reproducibility.

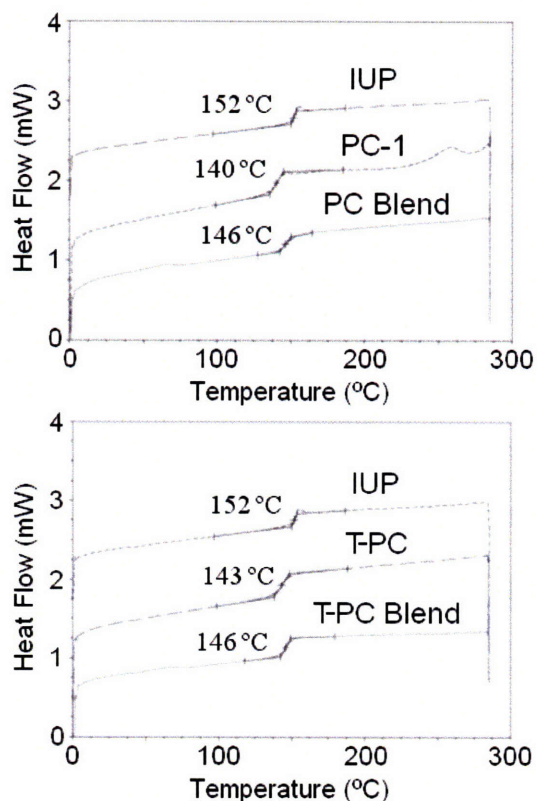
DMA was performed on rectangular bar specimens (approximately 20 mm x 2 mm x 1.6 mm) with a tensile pre-load (0.01 N) and scanned at 2 °C/min. Displacement control mode was used to oscillate about the pre-strain level such that total strain levels never exceeded 0.1 % at temperatures below  $T_g$ . Materials were tested at frequencies of 1 Hz over the temperature range of -140 to 170 °C. Materials were then tested at 100 Hz over the specific ranges in temperature around identified material transitions. Curves shown in figures again represent the average of three sample runs.

Uniaxial tension tests were performed on dogbone samples of 17 mm gauge length in the Zwick/Roell Z010 at a constant displacement rate of 5 mm/min (setup II in Fig. 2-10). An extensometer applied to measure true strain within the gauge length was found to induce premature failure in the specimens. Thus, it was necessary to estimate engineering strain from crosshead displacement. This estimated strain is reported in the figures as “apparent engineering strain.” Without an accurate strain measure, modulus values could not be calculated. However, modulus is provided by the DMA experiments for a wide range of temperatures.

DSC was used to cycle samples between 0 to 290 °C twice at 10 °C/min while holding isothermal for 5 minutes in between each half cycle. Room temperature bulk density measurements were taken with a pycnometer by researchers at DuPont.

### 5.1.3 *Results and Discussion*

Polymers PC-1 and T-PC exhibited depressed  $T_g$  values compared to IUP, as might be expected from their lower molecular weights. Blending resulted in one visible  $T_g$  that was equivalent for both the PC Blend and T-PC Blend (Fig. 5-5). DSC showed no signs of crystallinity in the blends, and all three polymer samples exhibited optical transparency (Fig. 5-6). There was a slight endotherm visible at the end of the glass transition for the 2<sup>nd</sup> cycle of the IUP powder. This is the free volume “release” of aging induced by the cooling cycle. This was not present in the fast quenched IUP samples, but additional DSC scans are not shown since this was the only difference. The room temperature densities of the materials were comparable at 1.19, 1.20 and 1.20 g/cc for IUP, PC Blend and T-PC Blend, respectively.



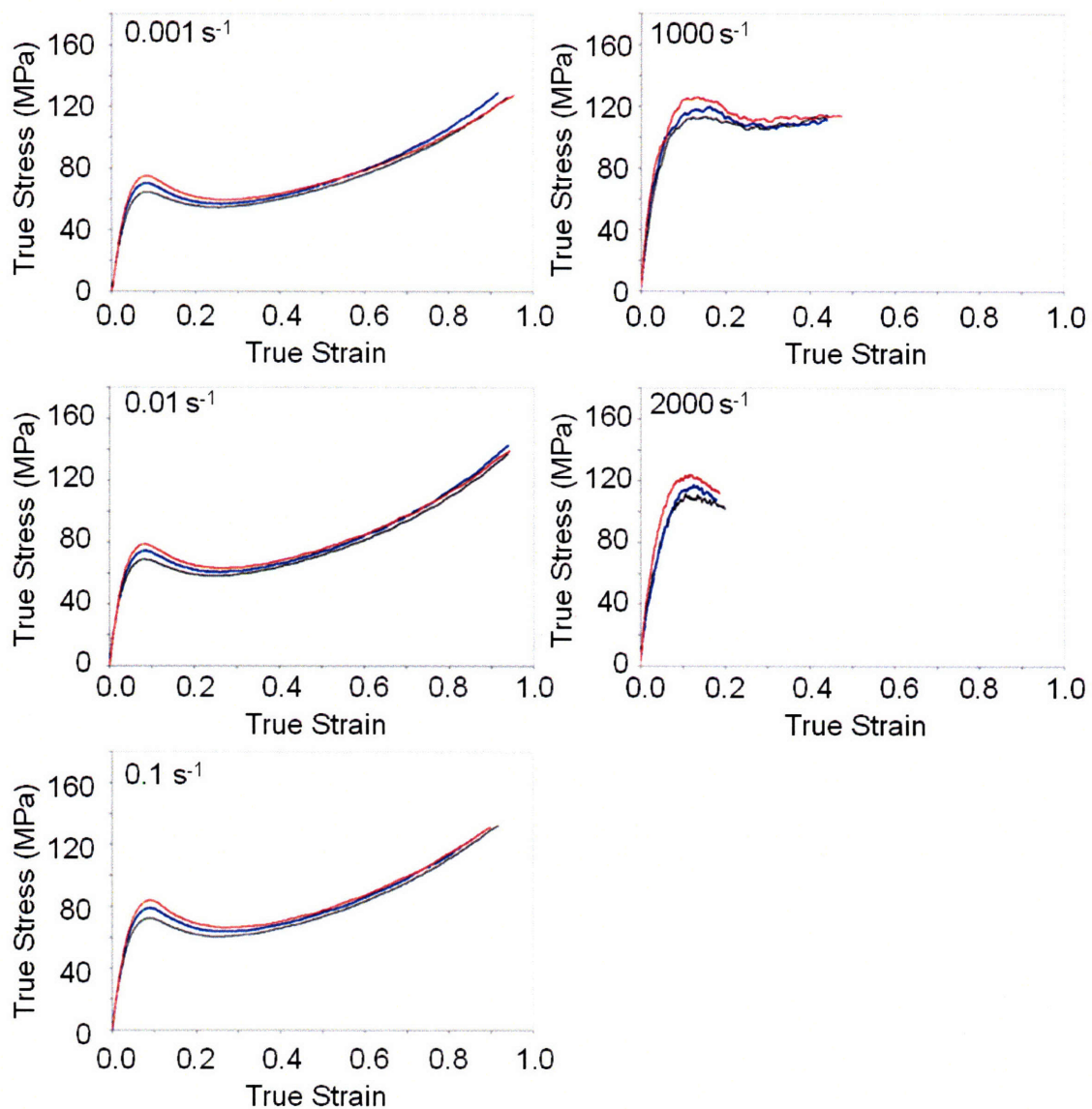
**Figure 5-5:** 2<sup>nd</sup> heat cycle DSC scans of powders of IUP, PC-1, and T-PC along with the 1<sup>st</sup> heat cycle scans of the blends after compression molding. 1<sup>st</sup> heat cycle scan of compression molded IUP (not shown) was identical to the powder's 2<sup>nd</sup> heat cycle scan (shown) only without the small endotherm just after the T<sub>g</sub>. T<sub>g</sub>'s are labeled next to the curves.



**Figure 5-6:** PC and T-PC Blends display the same level of optical transparency as IUP. Specimens shown are approximately 6 mm in diameter and 2 mm in height.

Stress-strain curves comparing all three polymers in uniaxial compression tests are shown in Fig. 5-7. At every strain rate measured, the PC Blend exhibited yield strengths

superior to that of IUP while the yield strengths of the T-PC Blend were greater still. At the strain rate of  $0.001 \text{ s}^{-1}$ , the stress-strain curve of the T-PC Blend began to overlap with that of IUP above strains of approximately 75% (true strain). The PC Blend still exhibited higher stresses even at strains as high as 90%. This was not the case at  $0.1 \text{ s}^{-1}$ , where by about 50% strain, the stress-strain curves of both blends overlapped and were slightly higher than IUP. The  $0.01 \text{ s}^{-1}$  curve was an exact intermediary where the PC Blend still had the highest strength at high strains but by very little over the T-PC Blend, which was superior to IUP. The SHPB was able to achieve much higher strain rates but much lower overall strains. Therefore, the stress-strain behavior at high strains *and* high strain rates could not be observed.



**Figure 5-7:** Uniaxial compression curves at various engineering strain rates of IUP (black), PC Blend (blue) and T-PC Blend (red).

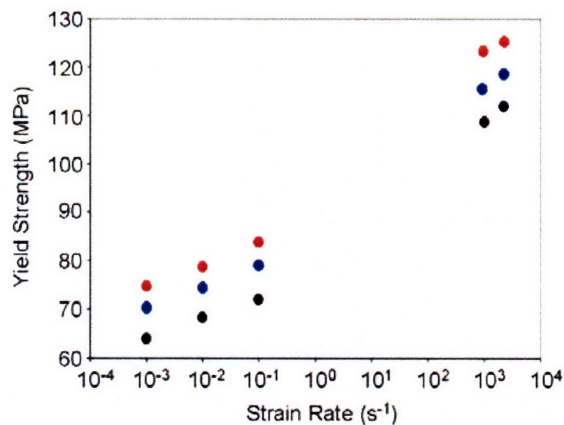
Yield strength results are summarized in Table 5.2. All three materials displayed two distinct regimes of rate-dependent yield behavior, with a significant transition occurring over the range of strain rates ( $10^0 \text{ s}^{-1}$  to  $10^2 \text{ s}^{-1}$ ) not accessible by either testing instrument. In the high-rate regime ( $> 10^3 \text{ s}^{-1}$ ), yield strengths were observed to be significantly

higher than in the low-rate regime ( $10^{-3} \text{ s}^{-1}$  to  $10^{-1} \text{ s}^{-1}$ ). This finding was consistent with published results [103-105] for Lexan®.

Material	Strain Rate				
	$0.001 \text{ s}^{-1}$	$0.01 \text{ s}^{-1}$	$0.1 \text{ s}^{-1}$	$1000 \text{ s}^{-1}$	$2000 \text{ s}^{-1}$
Lexan <sup>a</sup>	70 MPa	74 MPa	78 MPa	112 MPa	117 MPa
IUP	64 MPa	68 MPa	72 MPa	109 MPa	112 MPa
PC Blend	70 MPa	74 MPa	79 MPa	116 MPa	119 MPa
T-PC Blend	75 MPa	79 MPa	84 MPa	123 MPa	125 MPa

**Table 5.2:** Compressive yield strengths at various engineering strain rates. Standard deviations for low strain rates were less than 1 MPa. Standard deviations for high strain rates were about 1 MPa. Data for Lexan® 9034 PC by Mulliken [103].

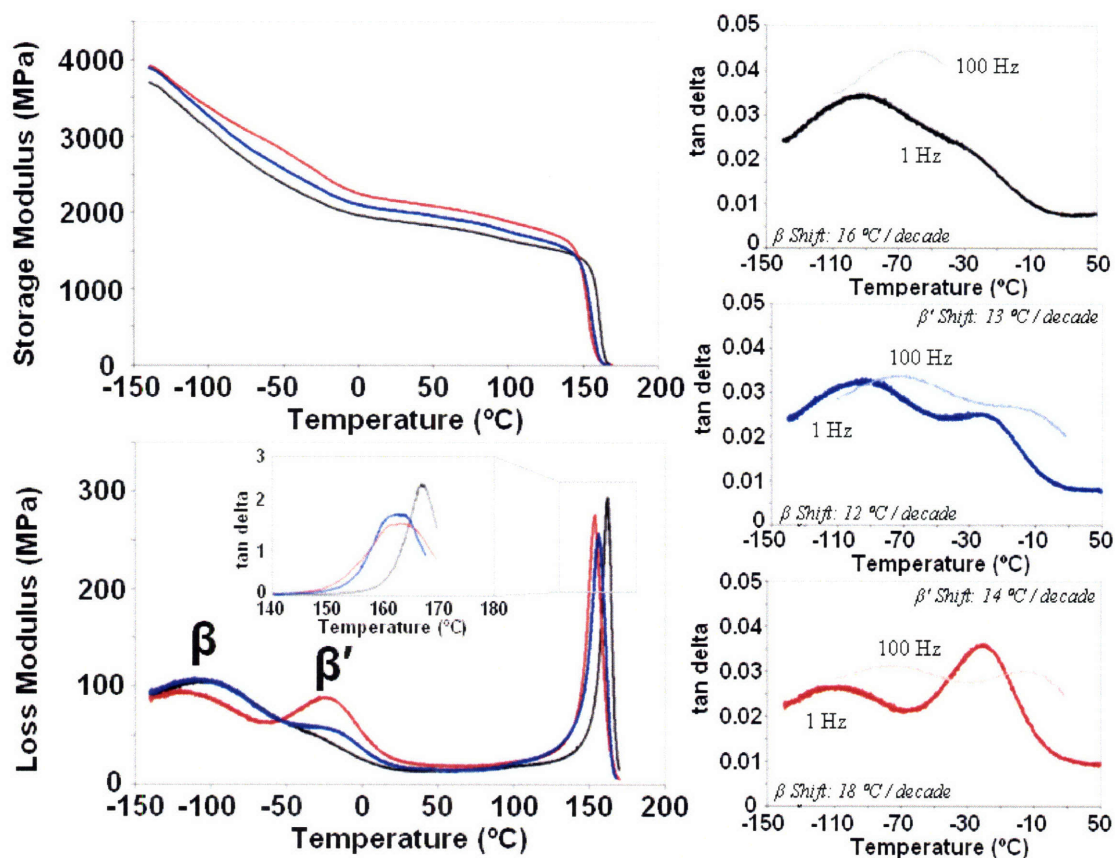
In Fig. 5-8 it is seen that the T-PC Blend had yield strengths as much as 7 % higher than that of the PC Blend and as much as 17 % higher than that of the IUP, for all strain rates tested. It should be noted that, in the literature, Lexan® (tested under all of the same conditions) exhibited higher yield strength values than IUP. As can be seen in Table 5.2, this particular Lexan® has values on par with that of the PC Blend, but still less than the T-PC Blend.



**Figure 5-8:** Engineering strain rate dependence of the yield strengths of IUP (black), PC Blend (blue) and T-PC Blend (red).



Dynamic mechanical testing in tensile mode was used to probe the temperature and frequency dependence of each material's response to deformation. Comparative results for all three polymers are summarized in Fig. 5-9. In general, the character of the storage modulus curve was the same for all three polymers. All three curves exhibited a high glass transition temperature through which the storage modulus changed by three orders of magnitude. Both blends showed a decreased glass transition temperature ( $\approx 162$  °C from tan delta) compared to IUP ( $\approx 167$  °C from tan delta). But despite the lower  $T_g$ 's, both blends displayed enhanced stiffnesses relative to IUP across most temperatures. At all temperatures above  $-75$  °C (and below  $T_g$ ), the PC Blend had a modulus 5-10 % higher than IUP while the modulus of the T-PC Blend was 14-20 % higher. The modulus values at room temperature ( $25$  °C) for IUP, the PC Blend and the T-PC Blend were 1.89 GPa, 2.03 GPa, and 2.15 GPa, respectively.



**Figure 5-9:** DMA of IUP (black), PC Blend (blue) and T-PC Blend (red). Curves are at 1 Hz unless labeled otherwise.

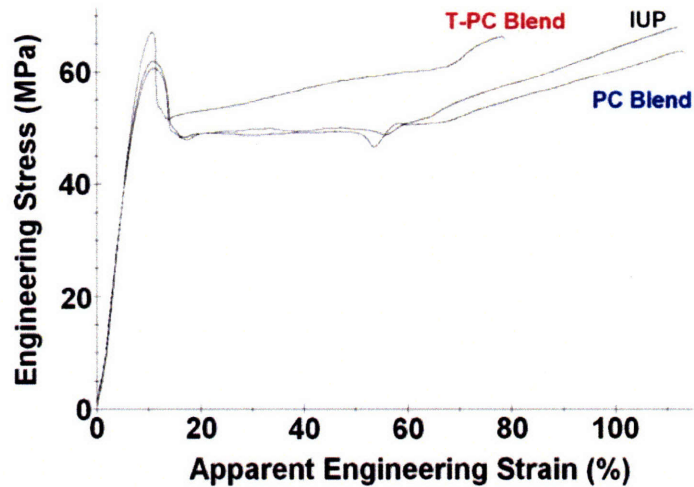
All three curves had a low temperature secondary ( $\beta$ ) transition noticeable in the rate of increase in the storage modulus below 0 °C. For the case of the PC Blend, the  $\beta$ -peak was nearly identical to that of IUP, occurring at -92 °C and -95 °C (from tan delta) for IUP and the PC Blend, respectively. For the T-PC Blend, this peak shifted to a significantly lower temperature, -108 °C. But the most noticeable difference in the loss modulus curves was the emergence of an additional transition at -19 °C, in between the traditional  $\alpha$  and  $\beta$  peaks of PC. This peak, labeled as  $\beta'$  in Fig. 5-9, was seen first in the PC Blend but was still overshadowed by the larger, broader  $\beta$ -peak. However, it became very pronounced in the T-PC Blend with an intensity equivalent to that of its  $\beta$ -peak.

Close examination of the tan delta versus temperature data revealed that IUP indeed has a shoulder (barely discernible) in the  $\beta'$  region.

These secondary transition peaks were followed by tan delta measurements as the frequency was changed from 1 Hz to 100 Hz. In Lexan® PC, the  $\beta$ -peak has been reported to shift linearly with decade of strain rate at about 15 °C/decade from 1 to 100 Hz [103]. The shift in the peak positions per decade was therefore calculated and labeled on the curves in Fig. 5-9. Movements of the shoulder in IUP were not tracked due to the inability to determine accurately an actual peak position. The  $\beta$ -peak was seen to shift about 16 °C/decade in IUP, which is consistent with the reported values for Lexan®. In the PC Blend, the  $\beta$ -peak shifted at a slower rate of 12 °C/decade while the  $\beta$ -peak in the T-PC Blend shifted at a slightly higher rate of 18 °C/decade. The  $\beta'$ -peaks in both blends shifted at comparable rates of 13-14 °C/decade.

Uniaxial tension tests (shown in Fig. 5-10) were conducted on dogbone samples to examine the ductile behavior of these polymers. It was observed that all three polymers displayed characteristic ductile behavior (including necking) with failure strains over 80%. It is interesting to note that at failure, the PC Blend exhibited a lower stress than IUP. In contrast, the T-PC Blend was seen to have higher stresses than either of the other two materials at any given strain. Yield strength values were consistent with trends observed in uniaxial compression tests, with the T-PC Blend having the highest yield strength and IUP having the lowest. Because extensometers caused premature failure in samples, they were not used. Therefore, Young's modulus was not obtained from these tensile tests, and the strain is reported in Fig. 5-10 as an "apparent engineering strain."

Results from the tensile tests are summarized in Table 5.3 along with the tensile modulus measured from DMA.

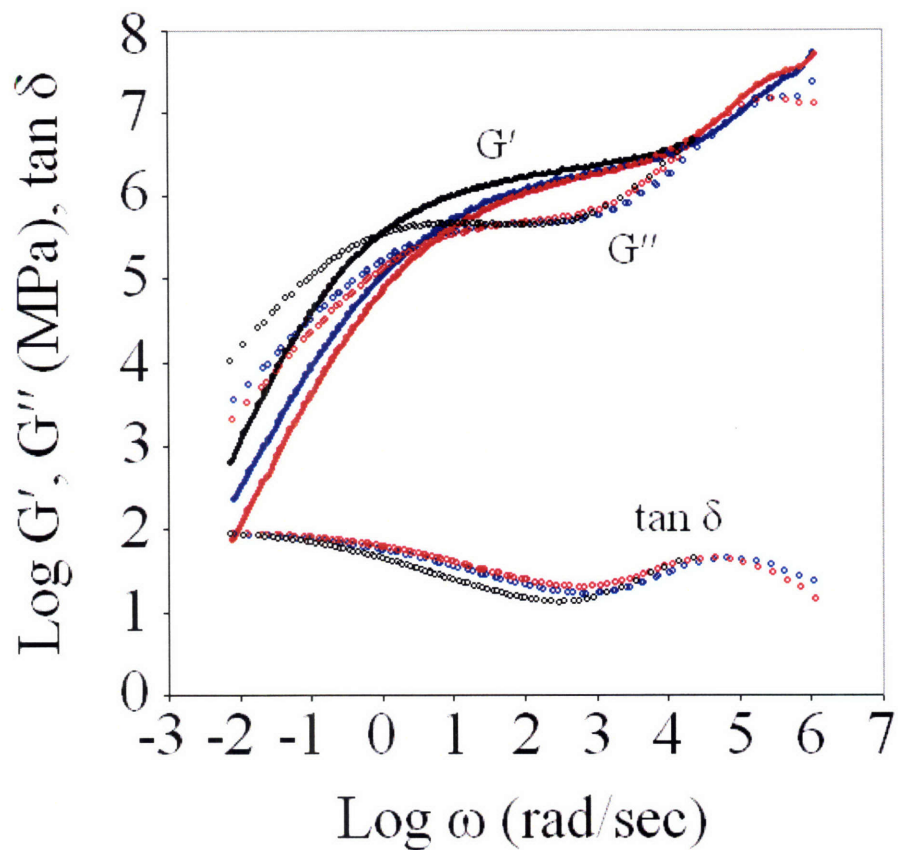


**Figure 5-10:** Representative stress-strain curves from uniaxial tensile tests of dogbone samples.

Material	$\rho$ (g/cc)	E (GPa)	$\sigma_y$ (MPa)	$\epsilon_b$ (%)
IUP	1.19	1.89	61	110
PC Blend	1.20	2.03	63	110
T-PC Blend	1.20	2.15	67	80

**Table 5.3:** Tensile mechanical properties:  $\rho$  – density at room temperature, standard deviations  $\approx 0.01$  g/cc; E - Young’s modulus from DMA (1Hz at 25 °C), standard deviations  $\approx 0.02$  GPa;  $\sigma_y$  - tensile yield strength, standard deviations  $\approx 1$  MPa;  $\epsilon_b$  - strain to break, highest value observed.

Results from parallel plate rheometry are displayed in Fig. 5-11. Terminal flow is seen to correspond directly with molecular weight, as expected. This is visible in the  $G'$ ,  $G''$ , and  $\tan \delta$  curves.



**Figure 5-11:** Representative data from parallel plate rheometry of IUP (black), PC Blend (blue) and T-PC Blend (red). The storage modulus curves are accented by bold lines.

Entanglement molecular weights ( $M_e$ ) were calculated for all three materials using methods described in Chapter 2 on identifying the plateau modulus ( $G_N^0$ ). They are reported in Table 5.4 and were consistent with literature values for other PCs [95, 130].  $M_e$  was observed to increase slightly from IUP to the PC Blend to the T-PC Blend.

Material	$G_N^0$ (MPa)	$M_e$ (g/mol)
IUP	$1.92 \pm 0.09$	$1920 \pm 90$
PC Blend	$1.77 \pm 0.12$	$2100 \pm 150$
T-PC Blend	$1.70 \pm 0.17$	$2190 \pm 210$

**Table 5.4:** Measured plateau modulus ( $G_N^0$ ) and calculated entanglement molecular weight ( $M_e$ ) values with standard deviations.

Both DSC and DMA demonstrated that the blending process resulted in homogeneous, amorphous polymer samples. Each blend exhibited a single glass transition, which was an average between the higher  $T_g$  from IUP and the lower  $T_g$  from the lower molecular weight PCs. The density was seen to increase slightly for the blends but within one standard deviation of IUP. Despite these relatively minor differences, the mechanical properties seemed to be very sensitive to composition. Both blends exhibited enhanced values for stiffness and yield strength in both compressive and tensile tests. While the increase in stiffness and yield strength from IUP to the PC Blend can be attributed to blend effects, the additional improvements from the PC Blend to the T-PC Blend are more likely related to the presence of triptycene units. Enhancements brought about by the presence of triptycene units occurred with only 1.9 wt % triptycene content.

Recall that when incorporated into polyesters at levels of 15 wt % and 21 wt %, triptycenes have been shown to induce novel steric inter-chain interactions, such as molecular threading and molecular interlocking through the minimization of IMFV [85, 86], while inhibiting crystallinity. These enhanced lateral interactions resulted in higher stiffnesses and strengths while also improving ductility through an extended sample drawing region believed to be associated with molecular threading. However, due to the pendant methyl side-groups in the bisphenol-A component, the PC chain may not thread through triptycene cavities as efficiently as the polymers containing long aliphatic components used in previous studies.  $M_e$  values were unfortunately complicated by the large variations in molecular weight. Because molecular weights for the PC-1 and T-PC were progressively lower than for IUP, the terminal flow region was expected to have occurred at higher frequencies (which it did). The lowering of the measured  $G_N^0$  values

with polydispersity (especially for the T-PC polymer approaching the  $M_c$ ) is known to exist in all polymer systems [95]. Therefore, this data was not as constructive in drawing conclusions as the other mechanical data. Before discussing the specific compressive and tensile properties, the DMA data will help to build a framework to understand how these molecular level interactions from the relatively small number of triptycene units directed the mechanical properties observed.

The seemingly contradictory ductile behavior (and high impact strength) of some glassy amorphous polymers (e.g., PC) is often correlated with sub- $T_g$  thermally activated mechanical ( $\beta$ ) relaxations [33] that are indicative of accessible deformation modes related to the molecular motions of specific segments of the polymer chain. Specifically for PC, it is debated as to whether the phenyl motions or carbonate motions dominate this relaxation. Modifications to the main chain of PC that affect the mobilities of either the phenyls or the carbonate groups have been shown to alter the shape and position of the  $\beta$ -peak [131-133]. However, it has also been shown that the  $\beta$  relaxation involves intra-chain *and* inter-chain cooperative motions [133-138]; and therefore, any local molecular restrictions would have to influence multiple repeat units in order to affect the  $\beta$  relaxation. The blending process of the pure PC materials did not result in any changes to the  $\beta$  relaxation as the loss modulus curves for IUP and the PC Blend were identical around that transition. Therefore, the shift in peak position of the  $\beta$  relaxation for the T-PC Blend can be attributed solely to triptycene interactions. The bulky triptycene units function as inhomogeneities in the chain backbone and disturb the cooperative motions of the bisphenol-A PC. However, copolymerizations with aromatic groups in as high as 25 mole % that do not chemically alter the phenyls or carbonate groups in the main chain of

PC have been shown to leave the  $\beta$  relaxation unaffected [139, 140]. Therefore, we offer two plausible explanations for the triptycene-induced changes to the  $\beta$  relaxation. First, it is possible that the triptycene units do not engage in the types of molecular threading seen in polyester studies. Instead, the IMFV is left unoccupied increasing the total free volume in the system. This increase in free volume affords greater molecular mobility to the PC chain resulting in a lower  $T_{\beta}$  and  $T_{\alpha}$ . This would imply that there should be a lower density in the triptycene-containing PC. This was not observed, but bulk density can be an insensitive measurement for small changes in free volume.  $M_e$  data imply a lesser degree of entanglements, but it is impossible to know exactly how much of the effects are due solely to molecular weight distribution. Either way, neither an increase in free volume nor low molecular weight (unless below 6-9 units of PC monomer, which T-PC was not) have been documented to dampen the intensity of the  $\beta$ -peak.

The second possibility is that the triptycenes *do* engage in molecular threading with constituents of the PC main chain. Since molecular threading would create localized restrictions, it might be expected that the  $\beta$  relaxation would occur at a higher temperature. However, it was seen to appear at a lower temperature. This could occur for two reasons. First, it has been suggested that the  $\beta$  relaxation consists of two overlapping contributions: a lower temperature peak from carbonate rotation and a higher temperature peak from phenyl rotation [131]. The damping of one of these mechanisms while leaving the other intact narrows the peak appearing as a peak shift. Second, the facility of a particular motion will also lower the temperature at which that peak occurs. The data in Fig. 5-9 implies that the phenyl motions were dampened and carbonate motions were facile. This could not occur from just localized free volume enhancements.



Furthermore, increasing free volume has been shown to *decrease* yield strengths in PCs [139, 141-145] which is in contrast to what was observed. Therefore, the presence of increased inter-chain interactions introduced by molecular threading is more plausible. The data suggests that the triptycenes interacted with the phenyl units and enhanced cooperative motions of the carbonate units. Increased inter-chain interactions would also explain the enhanced yield strengths observed, given the lower  $T_g$ 's.

DMA revealed that both blends had an additional peak ( $\beta'$ ) that existed only as a minor shoulder in IUP. This peak, which occurred at about  $-19\text{ }^\circ\text{C}$ , showed that blending the lower molecular weight PC with the Iupilon® PC created some kind of new relaxation hardly present before. While the exact mechanism is unclear, it could be possible that the lower molecular weight PC had a shifted  $\beta$ -peak which appeared as a separate peak in the blend. It is also possible that the presence of low molecular weight PC induces additional molecular motions in the high molecular weight PC similar to what is seen in polyester-PC copolymers [139]. In either case, the enhancements to Young's modulus and yield strengths of the PC Blend over IUP are accompanied by the emergence of this additional peak. In the T-PC Blend, the  $\beta'$ -peak was even more intense, and the Young's modulus and yield strengths are again increased.

In compression, the effects of blending and of the presence of triptycene units were the most pronounced around yielding. At every strain rate, the yield strengths of the T-PC Blend were higher than those of IUP by about 12-17%, and the PC Blend's yield strengths were higher than those of IUP by about 6-10%. But these differences became less significant post-yield, as the stress-strain curves of all three polymers tended to converge at high strains. It is interesting to note that the T-PC Blend behavior at high

strains changes with the strain rate relative to the other two samples. From  $0.001 \text{ s}^{-1}$  to  $0.1 \text{ s}^{-1}$ , the T-PC Blend stress-strain curves grow steeper compared to the other two samples. This trend must be brought about by the presence of triptycenes. Free volume does not affect the post-yield stress-strain curve [146]; therefore, this serves as further evidence of molecular threading and molecular interlocking present in the triptycene containing samples.

A different behavior was observed in tension. There, the yield behavior again increased in order from IUP to the PC Blend to the T-PC Blend, but only the stress-strain curves of the PC Blend and IUP converged at high strains. The T-PC Blend maintained higher stresses than either of the other polymers at any given tensile strain. Overall, it was seen that the effects of blending (PC Blend) resulted in only minor differences from the Iupilon® PC (IUP), except for the Young's modulus in DMA. However, the triptycene effects were more prominent. Both the Young's modulus and yield strength for the T-PC Blend were about 6% higher than for the PC Blend and 10-14% than for IUP. Post-yield, the stress-strain curve of the PC Blend overlapped with that of IUP, exhibiting flat engineering stress levels for about 40% apparent engineering strain (associated with sample drawing) before the samples began to strain harden. During this transition, some irregularity in the stress-strain profile was noticeable as "dips" or "bumps." This corresponded to the neck propagating to the edge of the gauge length and impinging upon the tapered section just before the grip areas of the dogbone samples. This effect was also present in the T-PC Blend but at higher strains and was followed by sample failure shortly thereafter. However, the T-PC Blend did not exhibit flat stress levels over this same drawing range. The stresses seemed to increase linearly, reaching

as much as 20% higher than either of the other two polymers before the transition to strain hardening. Unlike in the previously studied triptycene polyester systems, there was no observed high strain triptycene-triptycene interlocking region. This was due to failure occurring at the point where the neck propagated to the grips. Most significantly, the tensile data shows that the enhancements to modulus and yield strength did not result in embrittlement.

The difference in the stress-strain behavior between tension and compression at large strains is a result of the differences in the evolution of molecular orientation during uniaxial tension versus that during uniaxial compression. Uniaxial compression results in a preferential biaxial orientation in a plane perpendicular to the loading axis; whereas, uniaxial tension aligns polymer chains in the loading direction. In equi-biaxial extension, the likelihood of triptycene-triptycene interactions during deformation is probably less than for the case of uniaxial extension due to Poisson's ratio affecting only one dimension instead of two.

#### *5.1.4 Conclusion*

This section focused on the changes in mechanical behavior brought about by the substitution of triptycene along the PC main chain. A 25 wt % blend of an 7.7 wt % triptycene-containing PC was found to enhance the stiffness of a commercial Iupilon® PC at all temperatures. Blends of the triptycene-containing PC enhanced the yield strength of the Iupilon® PC by as much as 17%. Loss modulus data revealed that the PC  $\beta$ -transition was significantly altered by the blends and by the inclusion of triptycene, creating two distinct low-temperature loss peaks ( $\beta$  and  $\beta'$ ) where there had only been one

before. The triptycene-containing PC blend was optically transparent, amorphous, and showed no evidence of phase separation. There were notable differences in the stress-strain responses in compression versus tension. Tensile data indicated that the molecular threading in PC might have been less efficient than in the polyesters studied previously. This, combined with the very low concentration of triptycene units (1.9 wt % overall), resulted in no individually detectable region of molecular interlocking. As interlocking is even less probable in biaxial extension, it was consistent that an interlocking region was also not detected in compression. But it was seen that the T-PC Blend displayed more sensitivity to strain rate at high strains than either PC Blend or Iupilon®. It is asserted that this was brought about by enhanced lateral interactions from the minimization of IMFV.

Furthermore, the blending of low molecular weight PC with Iupilon® PC brought about enhancements to the mechanical properties to a somewhat lesser extent than the triptycene containing PC. This was an intriguing result for which an explanation is not obvious. However, any explanation must include the DMA data and, specifically, the emergence of the  $\beta'$  peak. This again emphasized the influence of sub- $T_g$  thermal-mechanical relaxations on the mechanical properties of polymers. Both low molecular weight polymers here were shown to be promising additives to improve the mechanical properties of PC.

## 5.2 Low Molecular Weight Fire-Retardant PC Blends

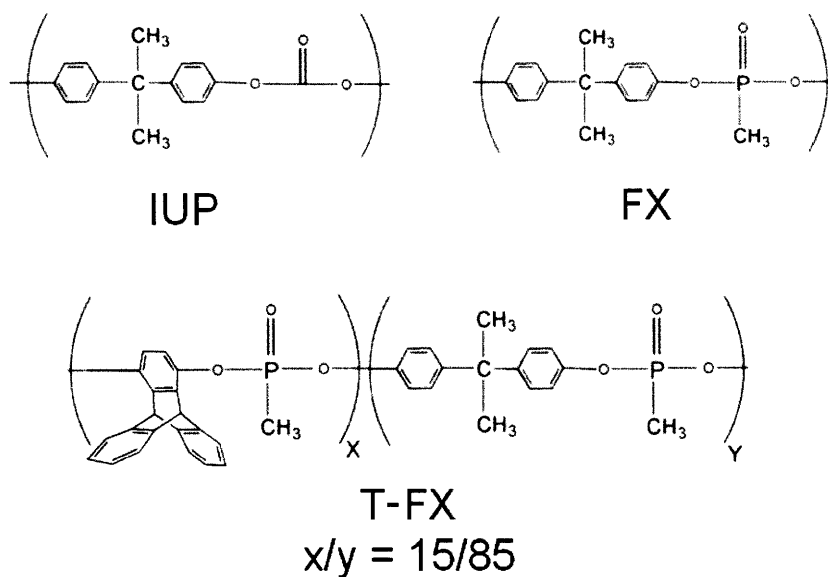
### 5.2.1 *Background*

Phosphorous compounds are often used as additives to enhance the fire retardancy of polymers due to the char that forms during burning [147-153]. It has been found that covalent incorporations of phosphorus units in particular have led to high flame retardancy [154-157]. PC is a widespread engineering thermoplastic used in a variety of applications due to its excellent thermal and mechanical properties, as discussed earlier. Phosphorus containing copolycarbonates exhibit slightly depressed glass transition temperatures (5 to 10 °C) while increasing the degradation temperature by as much as 60 °C and producing up to five times more char [151]. However, little has been reported as to the effects of the addition of phosphorus on the mechanical properties of the PCs.

Here, low molecular weight phosphorus containing polymers with and without triptycene were blended with Iupilon® PC, similarly as in the previous section, and tested for the effects on the low-rate and high-rate compressive properties.

### 5.2.2 *Experimental Methods*

The chemical structures of the monomers of the three materials used are illustrated in Fig. 5-12, and the molecular weights are listed in Table 5.5. The same Iupilon® E2000 PC (IUP from section 5.1) was used as the host polymer for blending. Triton Systems, Inc. supplied both of the phosphorus containing polymers, with triptycene (T-FX) and without triptycene (FX).



**Figure 5-12:** Chemical structures of Iupilon® PC (IUP), phosphorus containing polymer (FX), and phosphorus containing polymer with triptycene (T-FX). As indicated in the diagram, the weight percent of triptycene in T-FX is ~14.4 wt %.

As in the last section, due to there being only one composition of T-FX studied, the x/y notation will not be necessary for the discussion here.

Polymer	$M_n$ (g/mol)	$M_w$ (g/mol)	PDI
IUP	29,900	67,000	2.2
FX	4,100	12,700	3.1
T-FX	2,900	12,500	4.3

**Table 5.5:** Molecular weights of the polymer materials used in this study.

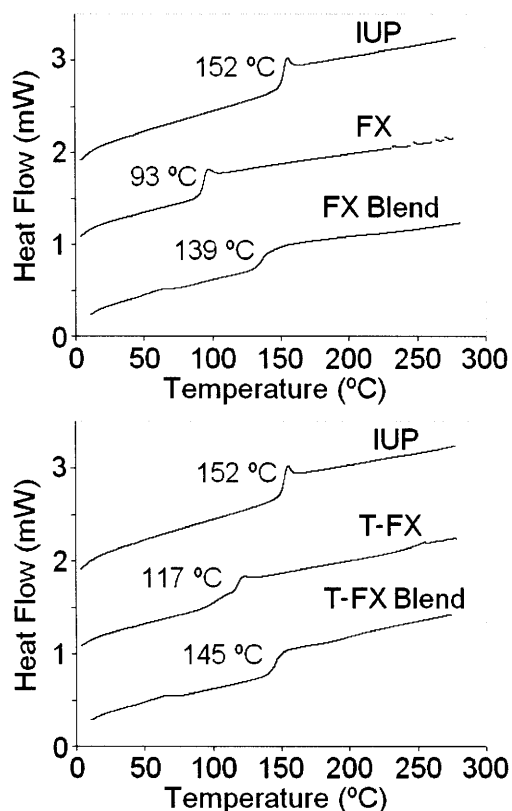
From the polymers listed in Table 5.5, three different materials were prepared for mechanical characterization. The first material (IUP) was again the pure, commercial Iupilon® PC. The second material (FX Blend) was a 10 wt % blend of FX with IUP. The third material (T-FX Blend) was a 10 wt % blend of T-FX with IUP, yielding an

overall triptycene concentration of about 1.44 wt %. The blends were prepared by the same dilute solvent mixing process described in section 5.1.2. The particular concentration of 10 wt % was chosen for sample conservation reasons. For all three polymers, disks of about 50 mm in diameter and 3 mm in thickness were compression molded at 285 °C. Finally, the compression molded disks were machined into cylinders and dried at 55 °C under vacuum for a week before mechanical testing.

Techniques used for characterization also followed the identical procedures outlined in section 5.1.2.

### 5.2.3 *Results and Discussion*

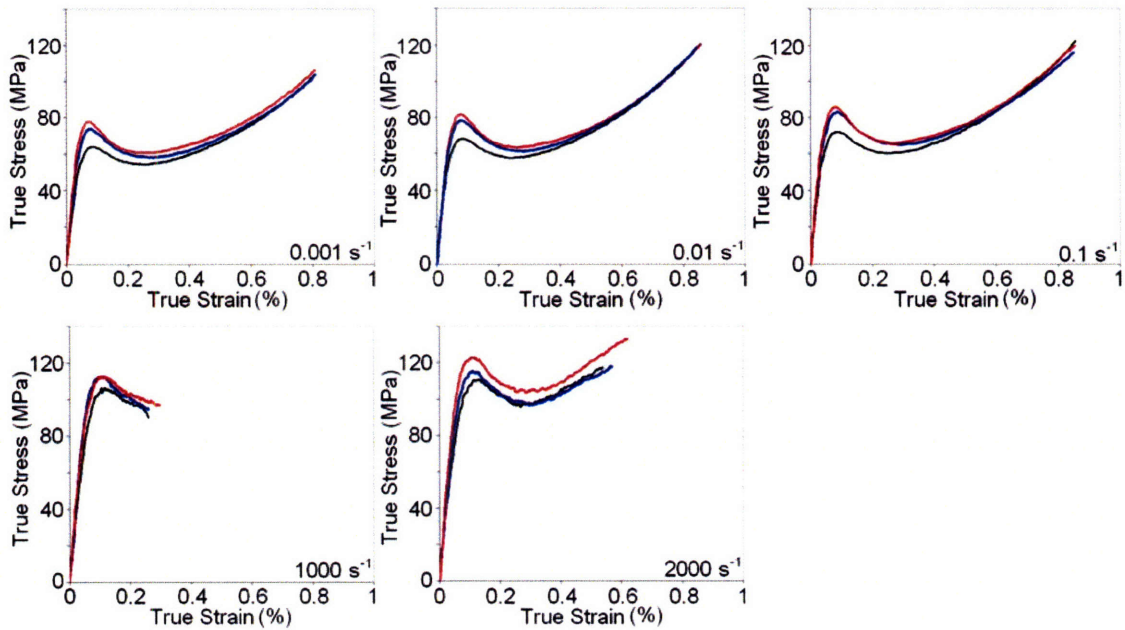
DSC of the samples both before and after processing confirmed homogeneous mixing of the component polymers. It can be seen in Fig. 5-13 that both blends exhibited a single  $T_g$  which lay in between those of the pure starting materials. The absence of any crystalline endotherms verified that the processed disks were amorphous. The powders display a small endotherm just after the  $T_g$  just as in the PCs in the previous section. This was again due to aging induced by the cooling cycle of the DSC. The tested samples were quenched and therefore did not have these endotherms. It can be seen in Fig. 5-13, that neither of the 1<sup>st</sup> heat cycles of the Blends displayed endotherms. Again, the quenched IUP DSC is not shown due to the only difference from the figure being the slight endotherm.



**Figure 5-13:** 2<sup>nd</sup> heat cycle DSC scans of powders of IUP, PC-1, and T-PC along with the 1<sup>st</sup> heat cycle scans of the blends after compression molding. 1<sup>st</sup> heat cycle scan of compression molded IUP (not shown) was nearly identical to the powder's 2<sup>nd</sup> heat cycle scan (shown).  $T_g$ 's are labeled next to the curves.

Densities of both blends and IUP were comparable (Table 5.6). Additionally, all three materials were transparent. Stress-strain curves from uniaxial compression tests indicated that both blends had superior yield strengths compared to the pure Iupilon® PC (IUP). At low strain rates ( $10^{-3} \text{ s}^{-1}$  to  $10^{-1} \text{ s}^{-1}$ ), the yield strengths of the FX Blend were on average about 15-16% higher than those of IUP. T-FX Blend yield strengths were greater still, at a 19-22% enhancement over IUP. Curves are plotted in Figure 5-14.





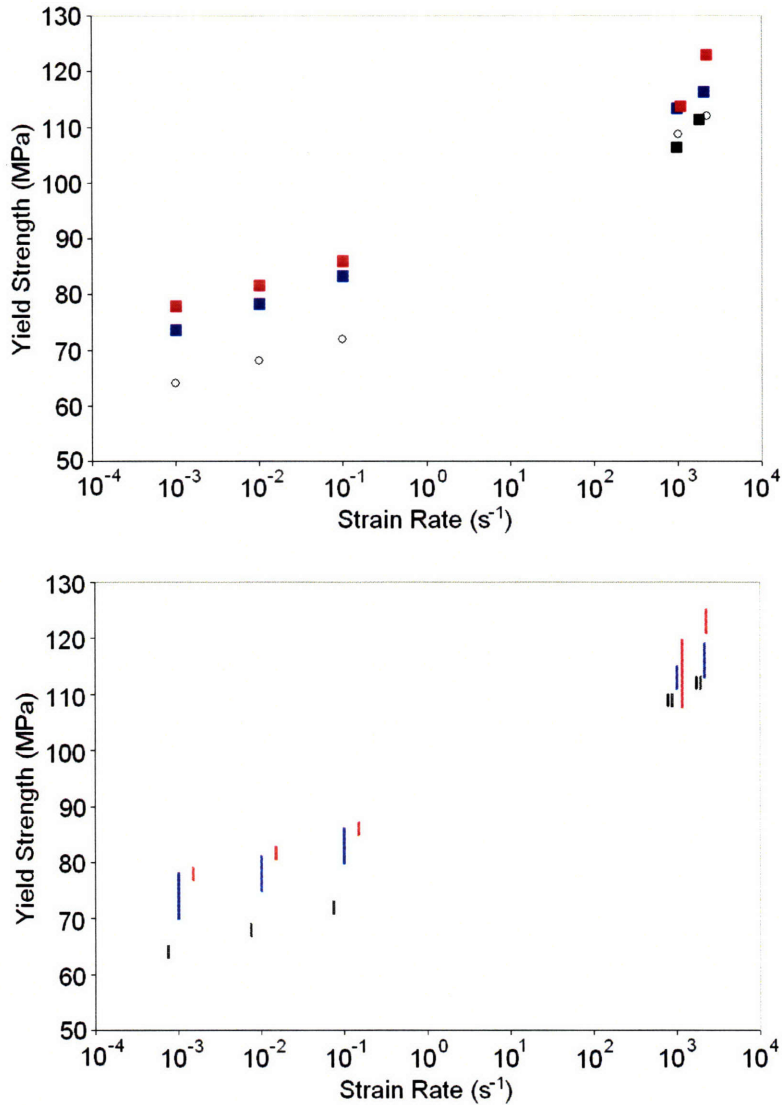
**Figure 5-14:** Uniaxial compression stress-strain data at various engineering strain rates (marked at the bottom right of each plot) for IUP (black), FX Blend (blue) and T-FX Blend (red). Data for IUP at  $0.001 \text{ s}^{-1}$ ,  $0.01 \text{ s}^{-1}$ , and  $0.1 \text{ s}^{-1}$  are from the experiments presented in section 5.1.

As IUP had been tested before in previous work, only the high rate data was repeated to ensure consistency of the testing methods across different testing dates. The IUP data at  $1000 \text{ s}^{-1}$  was slightly lower but still overlapped within one standard deviation of previous results. At  $2000 \text{ s}^{-1}$ , data showed good agreement. Values are reported in Table 5.6.

Material	$\rho$ (g/cc)	Strain Rate				
		$0.001 \text{ s}^{-1}$	$0.01 \text{ s}^{-1}$	$0.1 \text{ s}^{-1}$	$1000 \text{ s}^{-1}$	$2000 \text{ s}^{-1}$
IUP *	1.19	$64 \pm 1 \text{ MPa}$	$68 \pm 1 \text{ MPa}$	$72 \pm 1 \text{ MPa}$	$109 \pm 1 \text{ MPa}$	$112 \pm 1 \text{ MPa}$
IUP	1.19	-	-	-	$106 \pm 2 \text{ MPa}$	$111 \pm 1 \text{ MPa}$
FX Blend	1.20	$74 \pm 4 \text{ MPa}$	$78 \pm 3 \text{ MPa}$	$83 \pm 3 \text{ MPa}$	$113 \pm 2 \text{ MPa}$	$116 \pm 3 \text{ MPa}$
T-FX Blend	1.20	$78 \pm 1 \text{ MPa}$	$82 \pm 1 \text{ MPa}$	$86 \pm 1 \text{ MPa}$	$114 \pm 6 \text{ MPa}$	$123 \pm 2 \text{ MPa}$

**Table 5.6:** True yield strengths at various engineering strain rates. \* represents data from section 5.1, which was taken on a separate occasion from the rest of the data in this section.  $\rho$  – density, standard deviations  $\approx 0.01 \text{ g/cc}$ .

At high strain rates ( $1000\text{ s}^{-1}$  to  $2000\text{ s}^{-1}$ ), the FX Blend exhibited about 4-7% increased yield strengths compared to IUP, while the T-FX Blend displayed 5-11% greater yield strengths over IUP. Though the average values for yield strengths of the blend with triptycene (T-FX Blend) were consistently higher than those of the blend without triptycene (FX Blend), it should be noted that the variability (standard deviations) in the FX Blend data in particular made it difficult to address definitively the effects of triptycenes at any particular rate. Only at the  $2000\text{ s}^{-1}$  rate was the T-FX Blend clearly superior. This is shown in Fig. 5-15, which demonstrates that both of the blends still exhibit the shift in the rate dependence of the yield strength seen in commercial PC.



**Figure 5-15:** Top: Average values for true yield strengths versus engineering strain rates for uniaxial compression tests of IUP (black squares), FX Blend (blue squares), and T-FX Blend (red squares). Previous IUP data (open circles) is superimposed to demonstrate consistency of testing across different dates. Bottom: Range of values slightly offset following the same color scheme as the top.

#### 5.2.4 Conclusion

Special acknowledgement for a significant portion of the work done in this section must be given to Douglas Fraser (MIT DMSE, S.B. 2006). While the breadth of tests here was

not as expansive as in the previous section, there are two conclusions that can be drawn. First, the incorporation of phosphorus containing copolymers into a commercial PC did not adversely affect the compressive mechanical behavior. By contrast, in fact, the compressive yield strengths *increased* without an apparent sacrifice in ductility. This was consistent with our results from previous work with blends of low molecular weight copolymers with Iupilon® PC. Second, while the benefits of adding triptycene to the backbone of the phosphorus containing copolymer additive were not as pronounced (due to the variability in the non-triptycene blend data), the data indicated that triptycene on average had overall positive effects despite the low content of triptycene after the blending process (~1.44 wt %). This work in conjunction with our previous studies strongly supports the continued investigation of the effects of triptycenes in PCs.

## Summary

Bisphenol-A polycarbonate was chosen as a backbone for triptycene incorporation because of its significant use in both commercial and military applications. While there were some challenges involved with synthesis, processing and testing, it ultimately provided an excellent host for the incorporation of triptycenes. The mechanical data in PC blends showed that the incorporation of triptycene units produced outsized enhancements to the stiffness and yield strength relative to the rather small concentrations of triptycenes. The improvements were less than seen in the polyester case, but this was expected given the much lower concentrations of triptycenes in the PCs. It was not, however, observed in the blends that triptycene enhanced the ductility of the PCs. The exact strain to failure values for the PC blends containing triptycene were not definitively

determined. But it was established that the incorporation of triptycene retained the characteristic ductile behavior of PC critical in its applications.

It was seen that the triptycene containing PCs were not only superior at low deformation rates but also at high (ballistic) deformation rates. Therefore, they proved suitable for use as protective materials in military applications. Samples also retained the optical transparency desired in many applications. Aside from the blending process itself, the triptycene containing PCs did not require any unique or additional processing steps. The high compatibility with current industrial processing techniques makes these materials ideal for use in the enhancement of commercial PCs.

One unexpected result was that the blends of low molecular weight polymers *without* triptycenes also generated enhancements to the mechanical properties. While the enhancements were less than those seen with triptycenes, they were still unanticipated. The existing literature did not provide much insight or guidance as to why this might have happened. However, these enhancements were accompanied by noticeable changes in the low temperature thermal-mechanical relaxations (also seen in the triptycene containing blends). This further confirmed the importance of these types of relaxations on the mechanical properties of PCs. In conclusion, it was seen that the incorporation of triptycene units into polycarbonates was able to exploit the minimization of IMFV to produce enhancements to the mechanical properties.



## Chapter 6

# Summary and Future Work

This thesis explored the idea that the minimization of IMFV could be used as a novel means to enhance the mechanical properties of polymers. The endeavor began by first developing the concept of IMFV in polymer systems. A formal qualitative definition for IMFV was established along with the first methods of identifying and quantifying this property. Methods introduced also provided means to compare molecular units on the basis of the amount of inherent IMFV present in the isolated structures. Additionally, the minimization of IMFV was postulated to produce two novel steric inter-chain interactions: *molecular threading* and *molecular interlocking*. Threading resulted directly from the system's desire to minimize void spaces, specifically around the pendant units with IMFV. Interlocking is an interaction between the pendant units triggered during the deformation of the threaded network. These concepts were evaluated by incorporating units with IMFV into polymer backbones and observing changes to the structural, thermal and mechanical behavior.

For the systems studied, various iptycene units were chosen that contained readily identifiable amounts of IMFV according to the methods developed. Additionally, the synthetic chemistry required to incorporate the chosen iptycenes into polymer chain backbones was already known, making them ideal candidates to study. Most of the work here focused on the triptycene unit in particular, although several other variants were also examined. Triptycene was selected because it is one of the “simplest” and most basic of all iptycene structures. Triptycenes were first incorporated into random segmented polyesters where it was seen that the presence of bulky triptycene pendant units depressed the crystallinity (but did not change the crystal type). The stiffer chain backbone coupled with the threaded network formed by the minimization of IMFV raised the  $T_g$  and resulted in significantly enhanced stiffness, strength and (surprisingly and importantly) *strain to failure*. Based on additional work with other polymer backbones these results were seen to be robust across different concentrations, types of iptycenes units, and processing conditions.

Bisphenol-A PCs were examined because they are an amorphous, engineering thermoplastic with considerable usage in both commercial and military applications. Again, it was observed that the presence of triptycene units was able to deliver outsized enhancements to the mechanical properties relative to the concentrations in which they were incorporated. These enhancements amplified in magnitude as the deformation rates were increased from “low” strain rates to ballistic strain rates, indicating that these materials could be suitable for protective armor applications. These trends were accompanied by salient changes in the thermal-mechanical relaxations, recognized as critical factors in the understanding of mechanical behavior. Specifically, a shift in the



well documented  $\beta$ -transition and the emergence of a new peak ( $\beta'$ ) between the  $\beta$ - and  $\alpha$ -transitions. Low molecular weight polymer samples both with and without triptycene were found to be promising for use as additives to commercial PC for enhancement of mechanical properties and fire-retardancy.

In summary, this thesis has achieved its goal of demonstrating that the minimization of IMFV can be exploited to improve the mechanical properties of polymers through novel steric interactions. Additionally, an enhanced PC capable of utilization in ballistic armor applications was identified and developed, in accordance with the objectives of the Institute for Soldier Nanotechnologies and the U.S. Army Research Office. This final chapter contains promising leads and suggestions for further work related to the study of iptycenes in polymer systems. Some of these are covered by U.S. Patent #6,783,814 and another provisional patent filed from this thesis work. Topics span theory, mechanical properties applications and other possible utilizations of IMFV not yet studied.

## 6.1 Effective IMFV

Methods of identifying and calculating IMFV of isolated structures developed in this work can be used to select candidates with potential to enhance the mechanical properties of polymers or to produce some other desired effect. But the calculations presented here do not fully take into consideration the type of incorporation into a polymer backbone. This was already noted in Fig. 1-6 where two different incorporations of triptycene produced very different mechanical responses despite having the same value for what was called inherent IMFV. Therefore, there is a need for the calculation of an *effective* IMFV.

Effective IMFV would consider the manner in which a particular unit is integrated into a host system. Blends, covalent bonding to the backbone, side chain bonding, and many other types of incorporations may not all be expected to result in the same utilizations of IMFV. Fig. 3-9 illustrated one possibility of shielding effects originating from the different methods of tethering triptycene to the backbone of a polymer. Accessibility of the IMFV can also be an issue related to the structural unit itself. In section 4.3, tert-butyl groups attached to the periphery of triptycene units seemed to limit occupation of the triptycene cavities. On the other hand, the enlargement of the cavity space (as in the naphthalene-modified triptycene) may not increase the degree of inter-chain interactions if still only one polymer chain can occupy that space. An effective IMFV would also need to consider the total extent to which induced interactions affect a system. For example, it is likely that a polymer chain occupying a triptycene cavity is influenced over a persistence length beyond just the section directly involved in the minimization of IMFV. Another source of discrepancy between effective IMFV and inherent IMFV is simply molecular dynamics. Even if energetically favorable, it cannot be assumed that the minimization of IMFV will result in the complete occupation of all free IMFV space at any given moment. A measure or calculation of an effective IMFV would take all of these factors into account, and it is obvious that such a task is not trivial.

One method of creating such a value would be to develop correlations between inherent IMFV, types of incorporation of units into systems, and the resultant mechanical properties (or which ever property is of interest). This would provide empirical relationships between the accessibility of inherent IMFV in any particular system arrangement and translation of that accessibility into observable properties. A

hypothetical plot based on the data in Chapter 4 was presented in Fig. 4-27. A considerably larger data set would be necessary to produce a more detailed and informative correlation. Another method would be to use molecular and computational modeling. Again, it would need to be grounded in empirical data and able to reproduce results from known systems. But the strength of such a model would be in its ability to predict (or estimate) behavior in a wider range of systems and a broader range of conditions.

Effective IMFV is directly related to the concepts of molecular threading in polymer systems, and the conversion of inherent IMFV to effective IMFV is a notion that would provide significant insight in the efforts to exploit the minimization of IMFV.

## 6.2 Interlocking Index

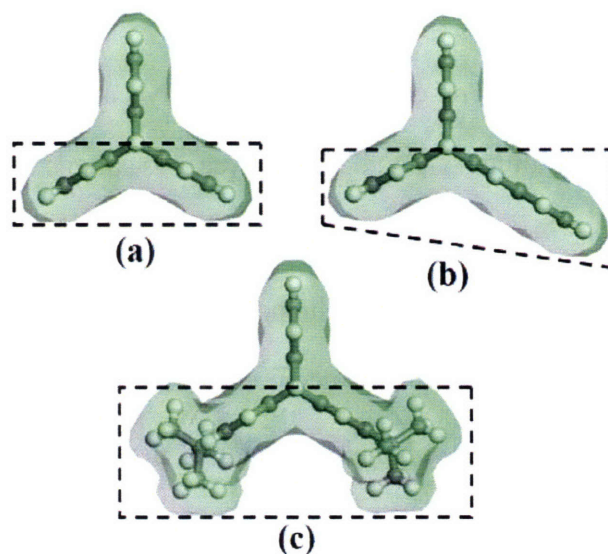
The second inter-chain interaction generated by the minimization of IMFV occurs during deformation. The molecular interlocking of pendant units engaged in a threaded network provides a new work hardening mechanism for polymers at high strain. Thus, it would be desirable to be able to predict the degree to which units might interlock and the effects that would have on the mechanical properties of a system (or again, on any particular property of interest).

Molecular interlocking was presented as a new contribution to strength in the work hardening regime (WH). In amorphous systems, the relationship would be:

$$\text{Stress in the WH regime} \approx \text{entropic penalty} + \text{molecular interlocking}$$

Modeling the behavior in the WH regime based on entropic considerations alone is extremely polymer dependent and was not done in this work. However, a direct comparison of many ductile, amorphous polymers with and without various types of triptycenes could be able to generate a correlation that would allow for a quantifiable value in stress units for the exact contribution of molecular interlocking. The contribution of entropic penalty would be calculated from measuring molecular orientation of the non-triptycene samples (perhaps by x-ray or polarization/birefringence). Degree of orientation of the samples containing triptycene at high deformation would allow the researcher to isolate the stress levels associated solely with the entropic penalty of aligning chains. The difference between the calculated and measured stress values would be the contribution of molecular interlocking.

These quantified values in stress units could then be used to develop an interlocking index by correlating observations back to the size, shape, frequency, and type of incorporation of the pendant units. For example, one possibility would be an interlocking volume that measures each pendant unit's deviation from the backbone (Fig. 6-1).



**Figure 6-1:** Space-filling models of a) T, b) NpT, and c) TbT with the interlocking volume highlighted with dotted lines. Volumes calculated were  $275 \text{ \AA}^3$ ,  $394 \text{ \AA}^3$ , and  $736 \text{ \AA}^3$  for T, NpT, and TbT, respectively. Widths (not shown) were determined using methods from Chapter 3.

Using some measure of the shape and size (such as above), an interlocking index would also need to correlate with the frequency of pendant units (concentration).

An interlocking index would allow a researcher to predict or estimate the stress-strain behavior in the work hardening regime of a polymer containing units with IMFV. As before, molecular modeling is another route to quantifying the effects of molecular interlocking but should still be based on empirical relationships.

### 6.3 Other Iptycene Incorporations

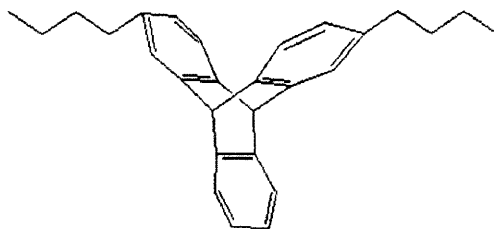
In this thesis, iptycene units were covalently bonded through polymer chain backbones using a benzene substitution (Fig. 1-6). However, there exist many available options regarding the integration of units with IMFV. This section outlines some suggested possibilities often using triptycene as the model.

### 6.3.1 *Blends*

Individual triptycene units and other low molar mass triptycene units were blended into LC systems in chromophore alignment studies. Triptycene is soluble in polar solvents, and so it should be possible to solvent blend with many different polymer systems. It may also be possible to melt blend triptycene with polymers; its melting point is about 240-250 °C [158]. There are many possible outcomes of such experiments. First, it is possible that the triptycene units will phase separate from the host polymer. Second, if each triptycene interacts with only one polymer chain (i.e., only one cavity is occupied), this would not result in the same enhanced inter-chain interactions predicted from this work. However, there may still be some interesting effects on the mechanical properties. And finally, if each triptycene interacts with multiple polymer chains (i.e., more than one cavity is occupied), lateral interactions would be enhanced. Such a threaded network might behave very similarly to the rotaxane “figure-of-eight” dynamic gels described in section 1.1.3.

### 6.3.2 *Alternate Covalent Tethering*

Two different types of substitutions have already been illustrated in Fig. 1-6. However, there are many other possible ways to tether a triptycene unit to the backbone of a polymer chain. One particular method that may be interesting is shown in Fig. 6-2, where the triptycene is tethered through different benzene sites.



**Figure 6-2:** Schematic of triptycene tethered to a polymer backbone through different benzene units.

The purpose of such an incorporation would be to promote the *rotation* of triptycene during deformation. Through the minimization of IMFV, the triptycene unit will orient perpendicular to the polymer chains threading the triptycene cavities. During deformation, the polymer chain backbone will force the 90° rotation (approximately) of the triptycene unit prompting evacuation of the triptycene cavities. This evacuation of polymer chains threading the triptycene unit could result in “auxetic” (or negative Poisson’s ratio) behavior, which is described further in section 6.9.1.

Covalent incorporation of units need not be restricted to the backbone of the polymer chain. Side chain arrangements are also possible. These may be particularly intriguing as side chain motions can have substantial effects on polymer properties. For instance, for some polymers (ex: PMMA), the  $\beta$ -transition is governed by side chain motion as opposed to main chain motions (as in PC). Also, units more complex than triptycene offer many more variations regarding possible incorporations into a polymer system.

## 6.4 Suppression of Novel Mechanisms / Blocking IMFV

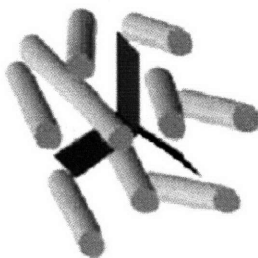
In the search for a full understanding of the nature of IMFV, it may be worthwhile to examine its limitations. Specifically, blocking access to IMFV sites could provide

insights as to how these units really interact with their host system. This section details a few possible methods to demonstrate that the key to triptycene's ability to enhance mechanical properties is via its accessible IMFV.

#### 6.4.1 Carbon Nanotubes (CNTs)

The steric inter-chain interactions promoted by the minimization of IMFV rely on polymer chain occupation of the IMFV of the triptycene. If these chains were forced to evacuate the triptycene cavities, then the mechanisms for enhanced interactions should be disabled. One possible method to achieve this is to introduce another moiety into the system that will compete with polymer chains for the occupation of triptycene cavities. It would be important for such a choice itself not to enhance inter-chain interactions. One example could be a single-walled carbon nanotube.

Fig. 6-3 illustrates a hypothetical diagram of a triptycene unit with its cavities occupied by fictitious cylindrical units. In the example where triptycene is covalently bonded to the backbone of a polymer, these units would compete with neighboring polymer chains during the minimization of IMFV.

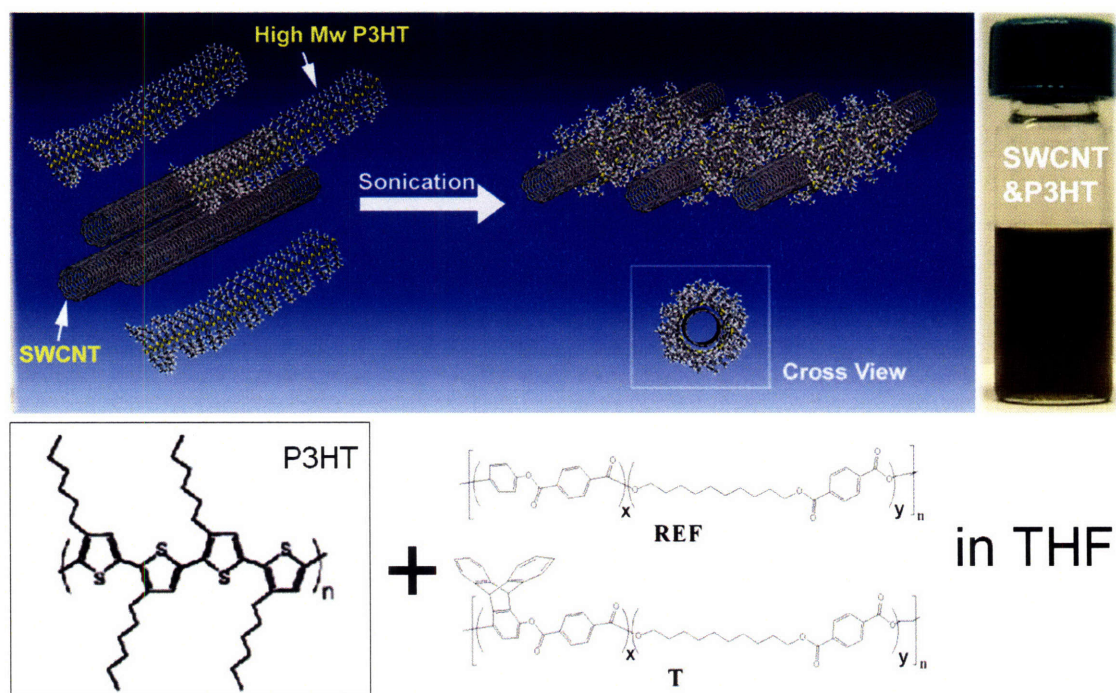


**Figure 6-3:** Schematic of triptycene threaded by high aspect ratio cylindrical units.



If the addition of these units eliminated the enhancements to the mechanical properties, it would further demonstrate the importance of molecular threading.

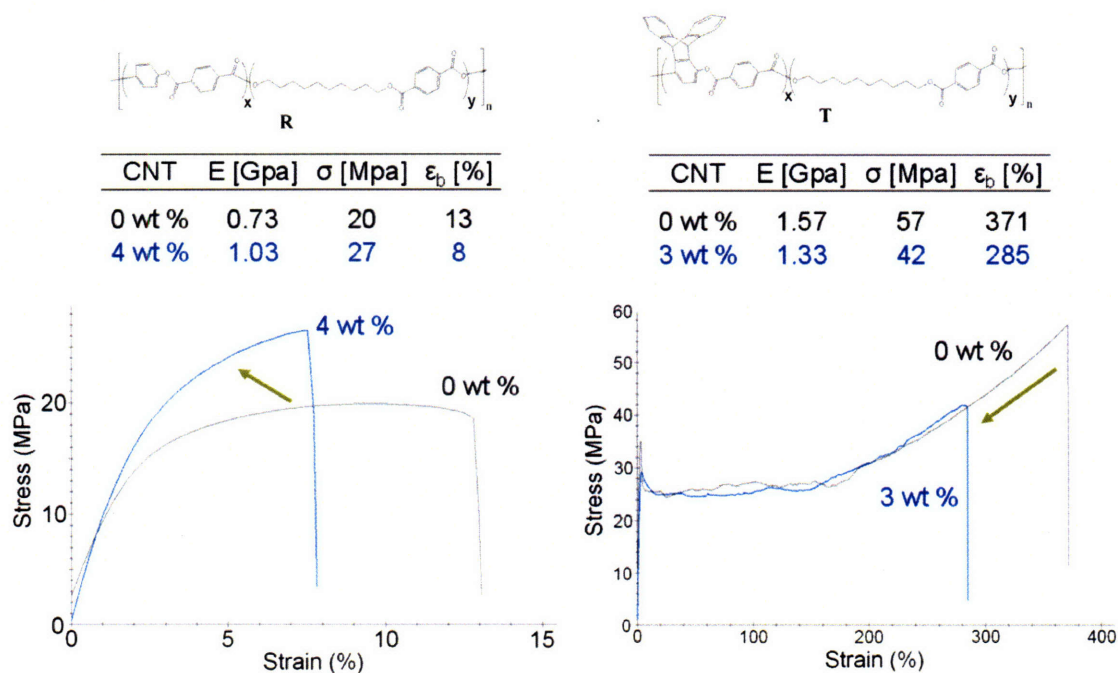
This was the goal of some initial experiments with Dr. Hongwei Gu (MIT Chemistry, post-doctoral researcher). Dr. Gu prepared functionalized single-walled carbon nanotubes (Fig. 6-4) and then blended them with 1/5 polyesters studied in Chapter 4. Solvent cast films were then prepared and mechanically tested. Fig. 6-5 shows the results of the tests.



**Figure 6-4:** Functionalization and blending of single-walled carbon nanotubes (SWCNTs) with 1/5 R and 1/5 T polyester samples in THF.

The non-triptycene polyester (R) was seen to exhibit the expected results from the addition of CNTs. That is, the stiffness enhanced while the ductility decreased. This occurred from a roughly 4 wt % addition (the wt % includes the total weight of the

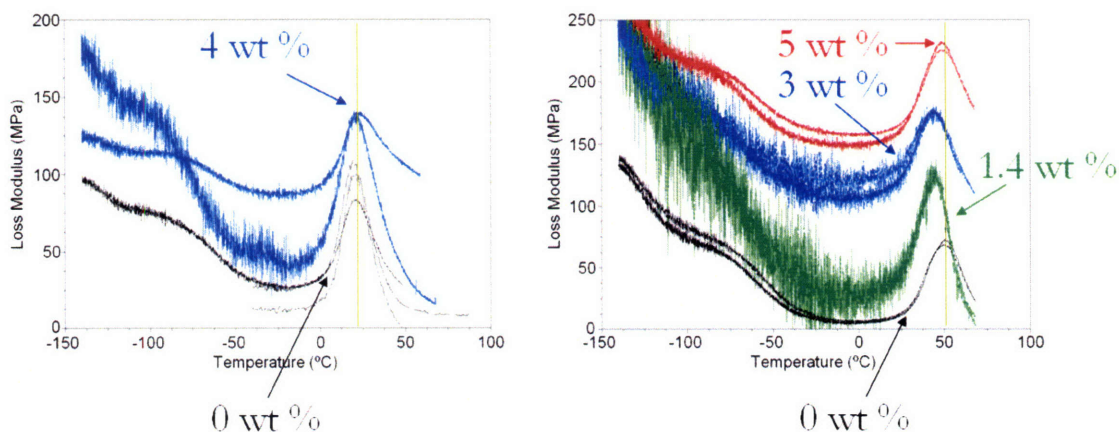
functionalized CNTs, not just the CNTs). The stress-strain curves of the samples containing CNTs are colored blue. It is interesting that the triptycene polyester did not express the same trend with the addition of CNTs. With the addition of about 3 wt % CNTs, the stiffness, strength, and strain to failure values were all seen to decrease. This data was supportive of the hypothesis that the CNTs would compete for the occupation of triptycene cavities.



**Figure 6-5:** Representative curves from tensile mechanical tests of strips of solvent cast films of 1/5 polyesters with and without SWCNTs.

If CNTs were disrupting the threaded network morphology, then it is possible that the  $T_g$  would be affected. Therefore, DMA was used to examine this behavior and is shown in Fig. 6-6. In the non-triptycene case, the addition of CNTs did not affect the glass transition temperature. This is expected behavior as there is no reason why the small percentage of added CNTs would alter the inherent polymer chain dynamics. However, in the case of the triptycene polyester, it was seen that the addition of CNTs at 1.4 wt %

and 3 wt % resulted in a depression in the glass transition temperature. This is again consistent with the notion of the disruption of the threaded network. Unfortunately, at 5 wt %, the  $T_g$  appeared to return to its original temperature. This could have been a result of CNT aggregation.

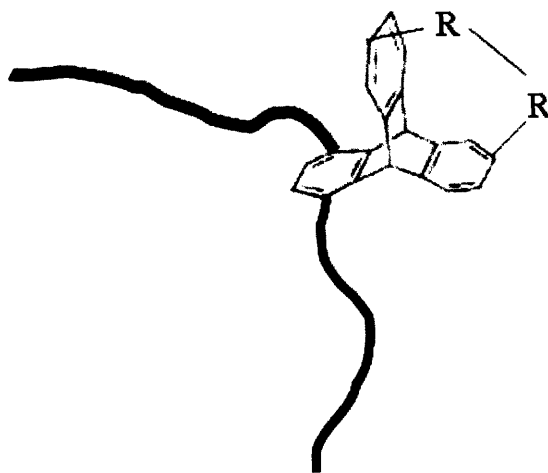


**Figure 6-6:** DMA of solvent cast films of 1/5 R (LEFT) and 1/5 T (RIGHT) with varying amounts of CNTs colored and labeled accordingly.

The initial data shown here are promising but inconclusive. More needs to be done in this regard to show definitively whether or not CNTs can disrupt the threaded network by competing with polymer chains during the minimization of IMFV. However, experiments are certainly not restricted to CNTs. In fact, in these experiments, it is not certain that the CNTs themselves occupied the triptycene cavities. It could also have been the functionalized polymer chains around the CNTs that competed with the polyester chain backbones for occupation. Therefore, there are many viable options that could be used to verify this theory.

#### 6.4.2 Closed Structures

Another method of demonstrating that the mechanical properties enhancements do indeed occur because of the minimization of IMFV (and not from some other consequence of the unique geometry of iptycene units) might be to alter the iptycene unit itself to block access to the IMFV. This would create a nanoporous structure with virtually the same shape but without the possibility of minimizing the IMFV. An example of such a closed structure is shown in Fig. 6-7.



**Figure 6-7:** Schematic of triptycene with one cavity closed off by hypothetical modifications made to the periphery of the benzenes

Comparing such an example polymer with non-triptycene and unmodified triptycene versions of the same backbone would isolate the effects of the minimization of IMFV from other influences that the triptycene may have on the system.

## 6.5 High Molecular Weight PCs

Chapter 5 utilized low molecular weight triptycene-PC copolymers as additives to enhance the mechanical properties of bisphenol-A PC. Outsized percentage improvements were observed combined with significant changes in the thermal-mechanical relaxation behavior. It would be insightful to investigate different triptycene concentrations in blends. This could be done either through changing the x/y ratio in T-PC or by different wt % blends. However, the blending process was only employed because of the low molecular weights TSI, Inc. was able to attain in synthesis. Blending would not be necessary if high molecular weight triptycene-PC copolymers could be synthesized. This would enable processing and testing of monolithic samples of much higher triptycene content. As in the case with the polyesters, higher weight percents of triptycene could result in considerably larger improvements to the properties. Section 5.1.1 references some of the different synthetic routes that might make this possible.

In addition to the potential benefits to the mechanical properties, higher triptycene content could also have intriguing effects on the thermal-mechanical relaxation behavior. It was already seen in the blends that the presence of triptycene not only shifted the  $\beta$ -transition but also was conducive to a new  $\beta'$ -transition. This occurred with only 1.9 wt % triptycene. In monolithic samples with triptycene contents of 5-25 wt %, these trends could be greatly exaggerated. Additionally, it was noted in Chapter 5 that the mechanisms that control the beta relaxation in PC require 6-9 monomer units to activate. This corresponds roughly to a 15/85 T-PC (Fig. 2-6) composition. Therefore, a comprehensive study of high molecular weight T-PC polymers of varying triptycene content around this critical composition could prove very insightful to the relationships of

mechanical properties, the  $\beta$ -transition, and triptycenes' effects on both. Such a set of triptycene PCs has been successfully synthesized by Yong Yang (MIT Chemistry) and is in the process of characterization. These are shown in Table 6.1.

T-PC Composition	$M_n$ (g/mol)	$M_w$ (g/mol)	PDI
5/95	28,200	55,700	1.98
15/85	29,600	60,700	2.05
25/75	29,900	67,500	2.26

**Table 6.1:** Composition and molecular weights of triptycene polycarbonates, following x/y notation for T-PC chemical structures shown in Fig. 2-6.

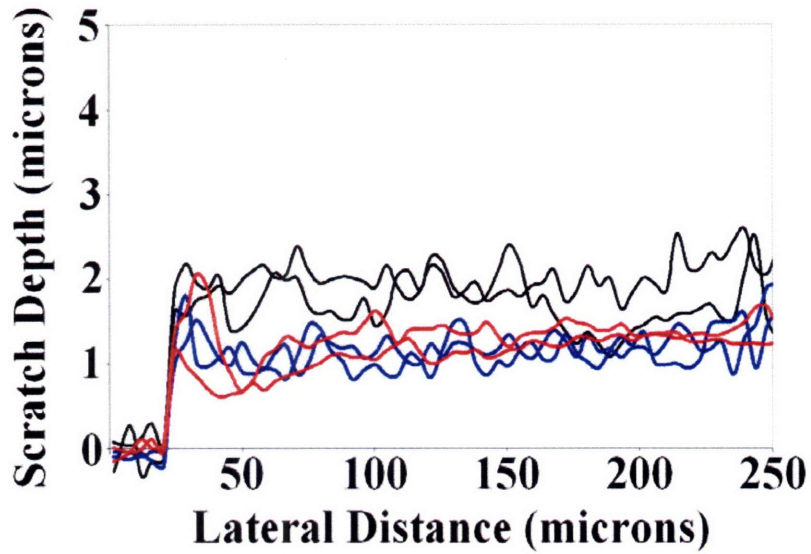
High molecular weight T-PC samples might also deliver more accurate  $M_e$  measurements. Finally, another method of testing that has not been examined in this work is the three-point bending mode of DMA. This could provide useful data in regards to the mode of deformation during impact scenarios.

## 6.6 Scratch Resistance

PC and the modified PCs discussed in Chapter 5 have primary use in applications requiring transparency. Resistance to scratching is often an important attribute for these kinds of materials. There are many tests related to scratch resistance, most of which require a rather large amount of sample. A very common test used is the Taber method, which uses an abrasion wheel. Another common “field test” is sand blasting.

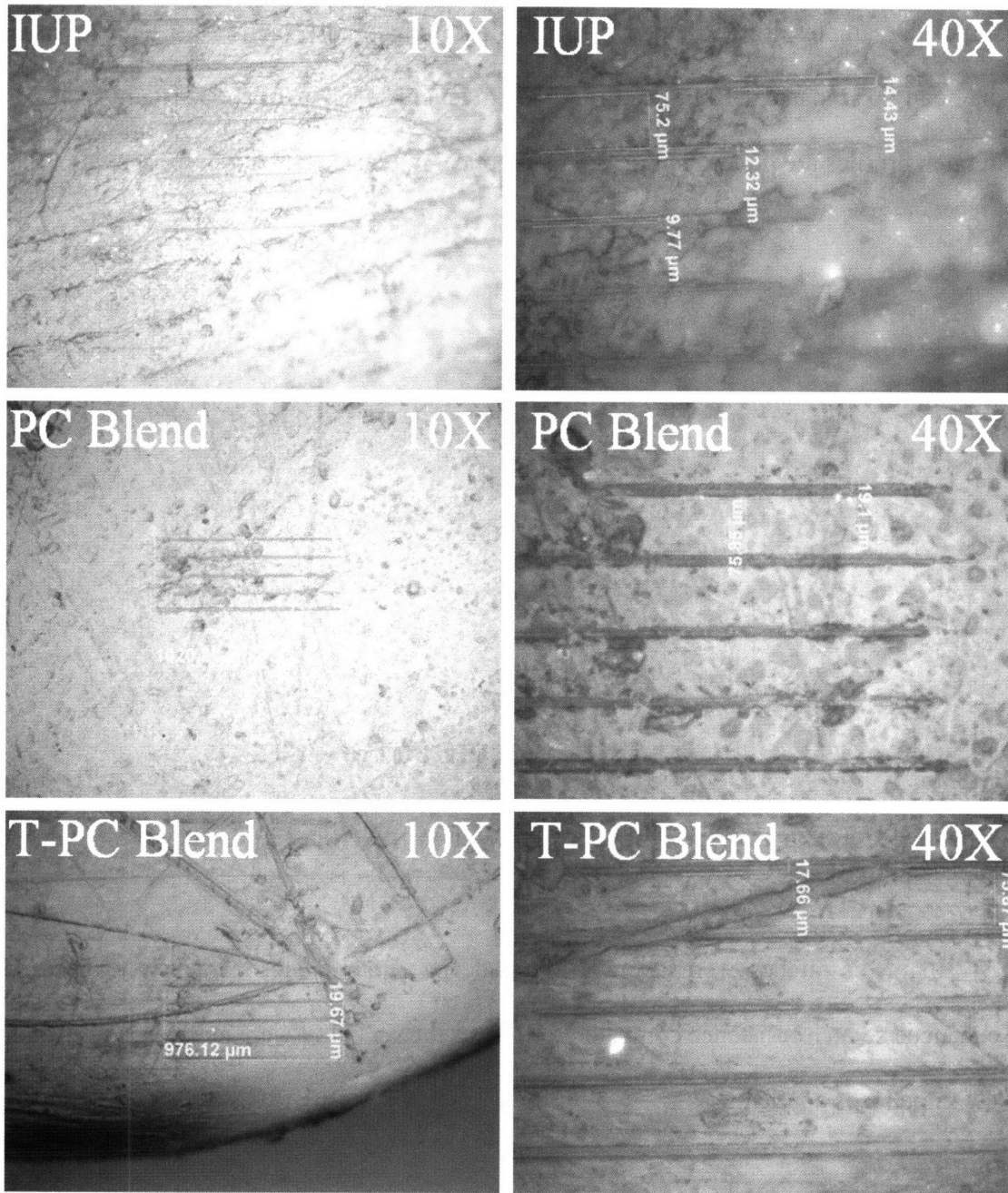
One laboratory test that requires minimal sample is nanoindentation. Using a conical diamond tip (or a Berkovich tip), force can be applied to a very small sample and then maintained as the tip is dragged laterally across the surface. Initial data was taken on

some PC samples from Chapter 5 using a Micromaterials NanoTester with a conical diamond tip at loads of 10 mN to form 500  $\mu\text{m}$  length scratches at about 10  $\mu\text{m}/\text{sec}$ . Scratch profiles are plotted in Fig. 6-8, and optical microscope pictures are shown in Fig. 6-9.



**Figure 6-8:** Depth vs. lateral distance of scratch for IUP (black), PC Blend (blue) and T-PC Blend (red).

At 10 mN, scratches were about 1-2  $\mu\text{m}$  deep. Both blends demonstrated possible enhanced scratch resistance compared to IUP, as the scratches were about half as deep for the same loads applied.



**Figure 6-9:** Optical microscope pictures of scratches made through nanoindentation.

There were a number of noticeable observations from the optical microscope pictures. First, the scratches made were comparable to the roughness already present in the samples. The PC samples were polished beforehand with silica particles through a



process typically used to polish hard metals. This did not prove effective for the soft PC materials. Secondly, some silica particles became imbedded into the PCs, and they can be seen as shiny spots in some of the pictures. It is suspected that a number of silica particles may even rest in the troughs of the scratches. This complicates analysis of the scratch depth data. However, it was shown that nanoindentation indeed can be used to create highly controlled scratches in PC materials. With alternative methods of polishing, this method could provide a large amount of useful scratch resistance data from a relatively small amount of sample. Nanoindentation can also measure sample Hardness, although this was not performed here.

## 6.7 Fluorescent Tags

Fluorescence and absorption are common methods of spectroscopy and can be utilized to probe the orientation of iptycene units. It would greatly be beneficial to “tag” iptycenes in some way such that they express unique fluorescence when their cavities are occupied versus when they are not. Similarly, fluorescence activated by iptycene units in contact with one another would be insightful. Both of these would be useful to probe molecular threading and molecular interlocking in polymer systems.

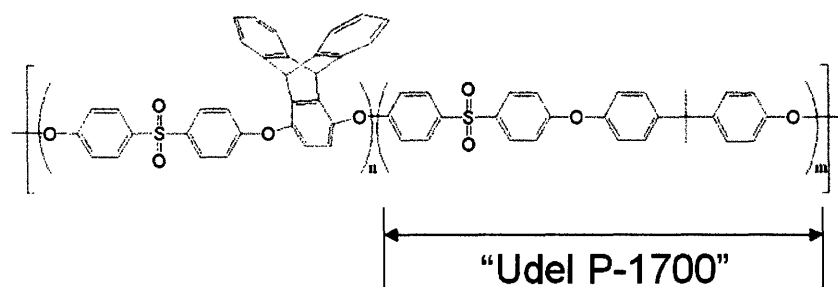
## 6.8 Other Polymer Systems

In developing an understanding of the behavior of units with IMFV in polymer systems, it would be advantageous to observe as many host polymers as possible. Many polymers derive their particular structural, thermal and mechanical properties from characteristics

specific to that polymer or polymer class. This section lists a few systems that would be of interest both scientifically and commercially.

### 6.8.1 Polysulfones (PSU)

PSUs are a very similar to PCs and can be utilized in many of the same applications. Both contain bisphenol-A as a primary chemical constituent. Both exhibit pronounced  $\beta$ -transitions along with the rate-dependent mechanical behavior discussed in Chapter 5. Moreover, both polymers are amorphous, transparent engineering thermoplastics with high  $T_g$ 's and high ductility. This could be a useful system to test the robustness of the effects of triptycene on the  $\beta$ -transition seen already in the PC case. One possible incorporation is a copolymerization substituting in triptycene hydroquinone for bisphenol-A. This is similar to what was done with PC and is shown in Fig. 6-10.



**Figure 6-10:** Integration of triptycene into the PSU backbone through copolymerization with commercially available Udel® P-1700.

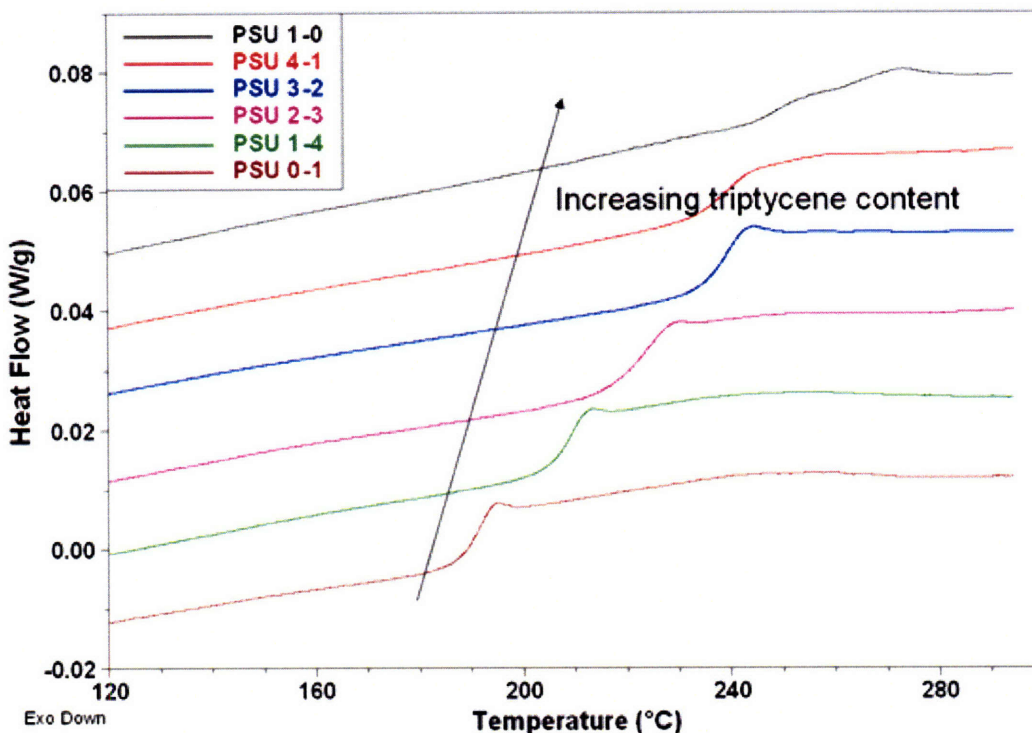
Methods for this particular synthesis were developed by Dr. Lokman Torun and readily achieved very high molecular weights (Table 6.2).

<b>m</b>	<b>n</b>	<b>Mn</b>	<b>Mw</b>	<b>PDI</b>	<b>% Yield</b>	<b>Amount (g)</b>
1	0	91,080	148,200	1.63	96	14.0
4	1	207,700	380,800	1.83	86	24.5
3	2	114,500	186,300	1.63	96	28.1
2	3	94,000	149,300	1.59	95	20.9
1	4	72,300	131,100	1.81	92	26.4
0	1	65,500	115,800	1.77	94	46
UDEL <sup>a</sup>		39,060	63,450	1.96		

<sup>a</sup>UDEL (commercial polysulfone) (UDEL P-1700 NT 11) from Solvay Advanced polymers, L.L.C.

**Table 6.2:** Molecular weights and other characteristics of PSUs synthesized containing various amounts of triptycene.

Unlike PCs, PSUs do not crystallize readily out of solution. Therefore, it is difficult to produce a dense powder ideal for melt processing. One suggested method is to solvent cast films and then manually cut up the films into pieces as small as possible for compression molding disks. Due to the higher  $T_g$ 's, PSUs must be processed around 300 °C. DSC of the samples from Table 6.2 showed an increase in  $T_g$  with increasing triptycene content (Fig. 6-11).



**Figure 6-11:** DSC of PSU samples with varying triptycene content according to the molar ratios “n-m” defined in Fig. 6-10.

PSU possess high defect sensitivity, just like PC, and therefore must be prepared very carefully for tensile testing (thick dogbones are probably required). Triptycenes should influence the mechanical behavior in PSU in a very similar way as PC.

### 6.8.2 Polyurethanes (PU)

PUs can be very difficult systems to synthesize in a controlled and reliable manner. However, many types have been found to exhibit intriguing mechanical behavior. Depending on the chemical structure used, they have applications as rubbery materials, artificial “spider-silk” fibers, and transparent bullet-proof layers. Many types of PUs are implemented commercially, and thus, improvements to these materials could garner

significant attention in a number of markets. There also exist segmented PUs, in which the incorporation of triptycene into different segments would also be an interesting study.

### *6.8.3 Highly Oriented Liquid Crystal (LC) Fibers*

In the area of polymers used in ballistic armor, highly oriented fibers from LC, rigid-rod systems are the most prevalent. These materials are described in detail in Chapter 1 along with the many failed attempts to incorporate pendant units, which usually disrupt the alignment of chains. However, pendant units with IMFV may produce different results. A highly ductile Kevlar® would be an extraordinary polymer. It would be interesting to observe how the minimization of IMFV affects the mechanical properties.

One important note is that these systems are usually lyotropic LC and require quite strong solvents, like hot concentrated sulfuric acid, and dry jet-wet spinning to obtain highly aligned fibers.

### *6.8.4 Non-Condensation Reaction Polymers*

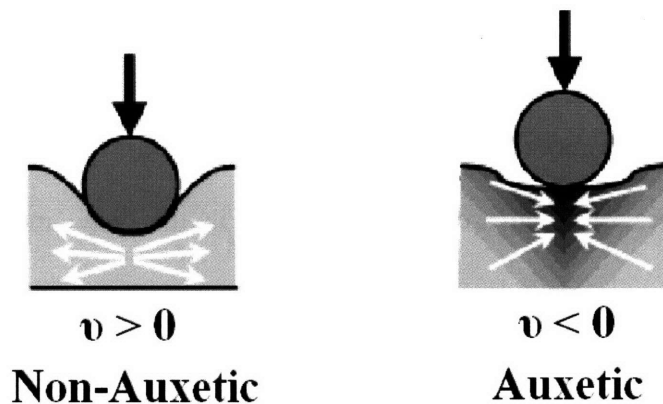
Triptycene (or any other iptycene) hydroquinone monomer lends itself naturally to condensation reactions. Therefore any polymers synthesized in this way provide suitable hosts for iptycene incorporations. However, there are many polymers with significant commercial applications that are not synthesized in this way, including polystyrene, polyethylene, and poly(methylmethacrylate). Poly(methylmethacrylate) or PMMA is of particular importance as it is used often in conjunction with PC in transparent bullet-proof laminates. PMMA is a brittle polymer. If there was a way to incorporate triptycene (or any unit with IMFV) into the synthesis, this would provide an attractive

host for two reasons. First, a ductile PMMA would garner considerable commercial interest. And second, PMMA also exhibits rate-dependent mechanical behavior as well as a distinct  $\beta$ -transition. But in contrast to PC and PSU, this  $\beta$ -transition is attributed to side chain motions as opposed to main chain motions. Therefore, it would be interesting to see how iptycenes affect the  $\beta$ -transition in systems like this.

## 6.9 Other Applications

### 6.9.1 Auxetic Behavior

In section 6.3.2, one particular incorporation was presented that may lead to auxetic behavior, or negative Poisson's ratio (NPR). NPR materials have a number of intriguing applications, and Evans [159] summarizes many of them in his review on the subject. One application relevant to the funding source for this thesis work is protective materials. Auxetic behavior could be promising in impact scenarios because of the flow of material inward towards the deformation zone during impact. A cartoon illustrating this behavior is shown in Fig. 6-12.



**Figure 6-12:** Illustration of contrasting responses of a positive versus negative Poisson's Ratio ( $\nu$ ) material during impact, adapted from Evans [159].

There exist many geometric ways to generate a theoretically auxetic material [159-161]. In practice, almost all actual materials that have been shown to demonstrate auxetic behavior are cellular foams [160, 162, 163] or clever structural morphologies involving micropores [164-166]. There even exist some auxetic materials in nature [159, 167], but these are too brittle to be useful for any sort of application. The molecularly auxetic material still remains elusive. There have been some attempts [168-170] with LC systems, but none have produced commercially viable molecularly auxetic materials as of yet. If the minimization of IMFV could be reversed during deformation (as in the example given in section 6.3.2), it might be possible to produce auxetic behavior. A successful product would represent the first true molecularly auxetic material.

#### *6.9.2 Phase Mixing / Dispersion of Additives*

Often times in blends, high aspect ratio additives will tend to phase separate. The minimization of IMFV has already been seen to represent a strong enough driving force to overcome alignment based on aspect ratios. Thus, it may be possible to utilize this mechanism to offset phase separation. In systems where units with IMFV are covalently incorporated (and thus the homogeneity is controlled), additives attracted to fill the IMFV would necessarily have to be homogeneously dispersed as well. In a case of polymer blends where the repulsive forces are known (enthalpy of mixing), any promotion towards mixing would be able to provide a numerical value for the actual energy related to the minimization of IMFV.

### 6.9.3 *Drug Delivery and Medical Applications*

Triptycene quinones have been investigated in antitumor applications purely because of the quinone's tendency to be effective in battling the spread of cancer [171-175]. This indicates that there are no strong biological concerns as to negative side-effects of triptycene in the body. However, there has been no use of the concept of IMFV with triptycene (or any other iptycenes) to aid in any sort of medical application. It might be possible to use the minimization of IMFV for drug delivery, the directive ordering of biological entities or the attraction of biological entities. Additionally, medical applications could utilize molecular scaffolds, particularly auxetic scaffolds for stents.

## 6.10 Other Characterization Techniques

Additional characterization techniques beyond what were utilized in this thesis could offer many insights. One observation was that the iptycene-containing polyester films exhibited almost complete recovery when heated above  $T_g$ . Therefore, stress relaxation tests of strained samples may provide interesting information about threading and interlocking. Biaxial tension tests (or uniaxial tension tests in the perpendicular direction of oriented samples) might also be useful in examining the effects of directionality and anisotropy on threading and interlocking. Finally, examining both true stress-strain and engineering stress-strain curves when possible would provide more a comprehensive outlook on the mechanical properties enhancements.



# Bibliography

- [1] P.J. Flory. *Principles of Polymer Chemistry*, Cornell University Press, Ithaca, **1953**.
- [2] P.J. Flory. *Chemical Reviews*, **1944**, 35, 51.
- [3] P.J. Flory. *Journal of Chemical Physics*, **1950**, 18, 108.
- [4] F.T. Wall. *Journal of Chemical Physics*, **1942**, 10, 485.
- [5] F.T. Wall. *Journal of Chemical Physics*, **1943**, 11, 527.
- [6] K.H. Meyer and A.J.A. van der Wyk. *Helvetica Chimica Acta*, **1946**, 29, 1842.
- [7] L.A. Wood and F.L. Roth. *Journal of Applied Physics*, **1944**, 15, 781.
- [8] F.L. Roth and L.A. Wood. *Journal of Applied Physics*, **1944**, 15, 749.
- [9] [www.matweb.com](http://www.matweb.com).
- [10] Y. Rao, A.J. Waddon and R.J. Farris. *Polymer*, **2001**, 42, 5925.
- [11] T. Kitagawa, K. Yabuki and R.J. Young. *Polymer*, "An investigation into the relationship between processing, structure and properties for high-modulus PBO fibres. Part 1. Raman band shifts and broadening in tension and compression", **2001**, 42, 2101.

- [12] Y.H. So. *Progress in Polymer Science*, "Rigid-rod polymers with enhanced lateral interactions", **2000**, *25*, 137.
- [13] M. Lammers, E.A. Klop, M.G. Northolt and D.J. Sikkema. *Polymer*, "Mechanical properties and structural transitions in the new rigid-rod polymer fibre PIPD ('M5') during the manufacturing process", **1998**, *39*, 5999.
- [14] A.J. Pennings, J.M.A.A. van der Mark and A.M. Kiel. *Kolloid Z.Z. Polymere*, **1970**, *237*, 336.
- [15] D.J. Sikkema, M.G. Northolt and B. Pourdeyhimi. *MRS Bulletin*, "Assessment of new high-performance fibers for advanced applications", **2003**, *28*, 579.
- [16] B. Kalb and A.J. Pennings. *Polymer Bulletin*, **1979**, *1*, 871.
- [17] Y. Takahashi. *Macromolecules*, **2003**, *36*, 8652.
- [18] J.R. Brown and N.A.S. John. *Trends in Polymer Science*, **1996**, *4*, 416.
- [19] L.H. Sperling. *Introduction to Physical Polymer Science*, 3rd ed, Wiley, New York, **2001**.
- [20] M. Dotrong, M.H. Dotrong and R.C. Evers. *Polymeric Materials Science and Engineering*, **1991**, *65*, 38.
- [21] M. Dotrong, M.H. Dotrong, H.H. Song, U. Santhosh, C.Y.C. Lee and R.C. Evers. *Polymer*, "Rigid-rod benzobisthiazole polymer with reactive 2,6-dimethylphenoxy pendent groups", **1998**, *39*, 5799.
- [22] U. Santhosh, M. Dotrong, H.H. Song and C.Y.-C. Lee. *Polymeric Materials Science and Engineering*, **1991**, *65*, 40.
- [23] R.H. Baughman, A.A. Zakhidov and W.A. de Heer. *Science*, "Carbon nanotubes - the route toward applications", **2002**, *297*, 787.
- [24] P.M. Ajayan, O. Stephan, C. Colliex and D. Trauth. *Science*, "Aligned Carbon Nanotube Arrays Formed by Cutting a Polymer Resin-Nanotube Composite", **1994**, *265*, 1212.
- [25] S. Kumar, T.D. Dang, F.E. Arnold, A.R. Bhattacharyya, B.G. Min, X.F. Zhang, R.A. Vaia, C. Park, W.W. Adams, R.H. Hauge, R.E. Smalley, S. Ramesh and P.A. Willis. *Macromolecules*, "Synthesis, structure, and properties of PBO/SWNT composites", **2002**, *35*, 9039.

- [26] A. Usuki, Y. Kojima, M. Kawasumi, A. Okada, Y. Fukushima, T. Kurauchi and O. Kamigaito. *Journal of Materials Research*, "Synthesis of Nylon 6-Clay Hybrid", **1993**, *8*, 1179.
- [27] Y. Kojima, A. Usuki, M. Kawasumi, A. Okada, Y. Fukushima, T. Kurauchi and O. Kamigaito. *Journal of Materials Research*, "Mechanical-Properties of Nylon 6-Clay Hybrid", **1993**, *8*, 1185.
- [28] D.W. Grijpma, H. Altpeter, M.J. Bevis and J. Feijen. *Polymer International*, "Improvement of the mechanical properties of poly(D,L-lactide) by orientation", **2002**, *51*, 845.
- [29] D. Blond, V. Barron, M. Ruether, K.P. Ryan, V. Nicolosi, W.J. Blau and J.N. Coleman. *Advanced Functional Materials*, "Enhancement of modulus, strength, and toughness in poly(methyl methacrylate)-based composites by the incorporation of poly(methyl methacrylate)-functionalized nanotubes", **2006**, *16*, 1608.
- [30] S. Fakirov, M. Evstatiev and J.M. Schultz. *Journal of Applied Polymer Science*, "Polyamides and Polyesters with Improved Mechanical-Properties", **1991**, *42*, 575.
- [31] D.W. Grijpma, R.D.A. Vanhofslot, H. Super, A.J. Nijenhuis and A.J. Pennings. *Polymer Engineering and Science*, "Rubber Toughening of Poly(Lactide) by Blending and Block Copolymerization", **1994**, *34*, 1674.
- [32] J.-H. Jang, C.K. Ullal, T. Choi, M.C. Lemieux, V.V. Tsukruk and E.L. Thomas. *Advanced Materials*, "3D Polymer Microframes that Exploit Length-Scale Dependent Mechanical Behavior", **2006**, *18*, 2123.
- [33] R.F. Boyer. *Polymer Engineering and Science*, "Dependence of Mechanical Properties on Molecular Motion of Polymers", **1968**, *8*, 161.
- [34] A. Avgeropoulos, B.J. Dair, N. Hadjichristidis and E.L. Thomas. *Macromolecules*, "Tricontinuous double gyroid cubic phase in triblock copolymers of the ABA type", **1997**, *30*, 5634.
- [35] Y. Okumura and K. Ito. *Advanced Materials*, "The polyrotaxane gel: A topological gel by figure-of-eight cross-links", **2001**, *13*, 485.
- [36] C.G. Gong and H.W. Gibson. *Journal of the American Chemical Society*, "Self-threading-base approach for branched and/or cross-linked poly(methacrylate rotaxane)s", **1997**, *119*, 5862.
- [37] P.-G. de Gennes. *Physica A: Statistical Mechanics and its Applications*, "Sliding gels", **1999**, *271*, 231.

- [38] G. Fleury, G. Schlatter, C. Brochon and G. Hadziioannou. *Polymer*, "From high molecular weight precursor polyrotaxanes to supramolecular sliding networks. The 'sliding gels'", **2005**, *46*, 8494.
- [39] G. Fleury, G. Schlatter, C. Brochon and G. Hadziioannou. *Advanced Materials*, "Unveiling the sliding motion in topological networks: Influence of the swelling solvent on the relaxation dynamics", **2006**, *18*, 2847.
- [40] S. Granick and M. Rubinstein. *Nature Materials*, "Polymers - A multitude of macromolecules", **2004**, *3*, 586.
- [41] J.F. Espeso, J.G. De la Campa, A.E. Lozano and J. de Abajo. *Journal of Polymer Science Part a-Polymer Chemistry*, "Synthesis and characterization of new soluble aromatic polyamides based on 4-(1-adamantyl)-1, 3-bis(4-aminophenoxy) benzene", **2000**, *38*, 1014.
- [42] H.Y. Jeong, Y.K. Lee, A. Talaie, K.M. Kim, Y.D. Kwon, Y.R. Jang, K.H. Yoo, D.J. Choo and J. Jang. *Thin Solid Films*, "Synthesis and characterization of the first adamantane-based poly(p-phenylenevinylene) derivative: an intelligent plastic for smart electronic displays", **2002**, *417*, 171.
- [43] A. Romo-Uribe, P.T. Mather, T.S. Haddad and J.D. Lichtenhan. *Journal of Polymer Science Part B-Polymer Physics*, "Viscoelastic and morphological behavior of hybrid styryl-based polyhedral oligomeric silsesquioxane (POSS) copolymers", **1998**, *36*, 1857.
- [44] E.T. Kopesky, T.S. Haddad, R.E. Cohen and G.H. McKinley. *Macromolecules*, "Thermomechanical properties of poly(methyl methacrylate)s containing tethered and untethered polyhedral oligomeric silsesquioxanes", **2004**, *37*, 8992.
- [45] W.H. Zhang, B.X. Fu, Y. Seo, E. Schrag, B. Hsiao, P.T. Mather, N.L. Yang, D.Y. Xu, H. Ade, M. Rafailovich and J. Sokolov. *Macromolecules*, "Effect of methyl methacrylate/polyhedral oligomeric silsesquioxane random copolymers in compatibilization of polystyrene and poly(methyl methacrylate) blends", **2002**, *35*, 8029.
- [46] B.X. Fu, W.H. Zhang, B.S. Hsiao, M. Rafailovich, J. Sokolov, G. Johansson, B.B. Sauer, S. Phillips and R. Balnski. *High Performance Polymers*, "Synthesis and characterization of segmented polyurethanes containing polyhedral oligomeric silsesquioxanes nanostructured molecules", **2000**, *12*, 565.
- [47] J.S. Yang and T.M. Swager. *Journal of the American Chemical Society*, "Fluorescent porous polymer films as TNT chemosensors: Electronic and structural effects", **1998**, *120*, 11864.

- [48] J.S. Yang and T.M. Swager. *Journal of the American Chemical Society*, "Porous shape persistent fluorescent polymer films: An approach to TNT sensory materials", **1998**, *120*, 5321.
- [49] V.E. Williams and T.M. Swager. *Macromolecules*, "Iptycene-containing poly(aryleneethynylene)s", **2000**, *33*, 4069.
- [50] T.M. Long and T.M. Swager. *Journal of the American Chemical Society*, "Using "internal free volume" to increase chromophore alignment", **2002**, *124*, 3826.
- [51] J.P. Amara and T.M. Swager. *Macromolecules*, "Incorporation of internal free volume: Synthesis and characterization of iptycene-elaborated poly(butadiene)s", **2004**, *37*, 3068.
- [52] C.A. Breen, S. Rifai, V. Bulovic and T.M. Swager. *Nano Letters*, "Blue electroluminescence from oxadiazole grafted poly(phenylene-ethynylene)s", **2005**, *5*, 1597.
- [53] T.M. Long and T.M. Swager. *Advanced Materials*, "Minimization of free volume: Alignment of triptycenes in liquid crystals and stretched polymers", **2001**, *13*, 601.
- [54] Z.G. Zhu and T.M. Swager. *Journal of the American Chemical Society*, "Conjugated polymer liquid crystal solutions: Control of conformation and alignment", **2002**, *124*, 9670.
- [55] E. Hoffmeister, J.E. Kropp, T.L. McDowell, R.H. Michel and W.L. Rippire. *Journal of Polymer Science Part A-1*, "Triptycene Polymers", **1969**, *7*, 55.
- [56] T.R. Kelly, J.P. Sestelo and I. Tellitu. *Journal of Organic Chemistry*, "New molecular devices: In search of a molecular ratchet", **1998**, *63*, 3655.
- [57] T.R. Kelly, M.C. Bowyer, K.V. Bhaskar, D. Bebbington, A. Garcia, F.R. Lang, M.H. Kim and M.P. Jette. *Journal of the American Chemical Society*, "A Molecular Brake", **1994**, *116*, 3657.
- [58] A.M. Stevens and C.J. Richards. *Tetrahedron Letters*, "A metallocene molecular gear", **1997**, *38*, 7805.
- [59] H. Iwamura and K. Mislow. *Accounts of Chemical Research*, "Stereochemical Consequences of Dynamic Gearing", **1988**, *21*, 175.
- [60] M. Hashimoto, H. Takagi and K. Yamamura. *Tetrahedron Letters*, "Three dimensional supramolecules of triptycene-quinone and its 6,7-dimethyl derivative formed by weak intermolecular pi-pi interactions and C-H center dot center dot center dot O hydrogen bonds", **1999**, *40*, 6037.

- [61] M. Hashimoto, K. Yamamura and J. Yamane. *Tetrahedron*, "Characteristic ribbon-like supramolecular structure and intermolecular D-A interactions in the crystals of triptycenequinones, triptycene-TCNQs and their clathrates as studied by X-ray investigations", **2001**, *57*, 10253.
- [62] S. Norvez. *Journal of Organic Chemistry*, "Liquid-Crystalline Triptycene Derivatives", **1993**, *58*, 2414.
- [63] K. Yamamura, T. Kawashima, K. Eda, F. Tajima and M. Hashimoto. *Journal of Molecular Structure*, "Solid solution of triptycenequinone and triptycenehydroquinone as a non-stoichiometric quinhydrone. Bathochromic changes in color caused by local intermolecular interaction between p-benzoquinone and hydroquinone moieties", **2005**, *737*, 1.
- [64] G. Maier. *Progress in Polymer Science*, "Low dielectric constant polymers for microelectronics", **2001**, *26*, 3.
- [65] M. Morgen, E.T. Ryan, J.H. Zhao, C. Hu, T.H. Cho and P.S. Ho. *Annual Review of Materials Science*, "Low dielectric constant materials for ULSI interconnects", **2000**, *30*, 645.
- [66] R.H. Havemann and J.A. Hutchby. *Proceedings of the Ieee*, "High-performance interconnects: An integration overview", **2001**, *89*, 586.
- [67] M. McCoy. *Chemical & Engineering News*, "Deciding on a dielectric", **2001**, *79*, 43.
- [68] S.J. Martin, J.P. Godschalx, M.E. Mills, E.O. Shaffer and P.H. Townsend. *Advanced Materials*, "Development of a low-dielectric-constant polymer for the fabrication of integrated circuit interconnect", **2000**, *12*, 1769.
- [69] H. Treichel. *Journal of Electronic Materials*, "Low dielectric constant materials", **2001**, *30*, 290.
- [70] D. Mecerreyes, E. Huang, T. Magbitang, W. Volksen, C.J. Hawker, V.Y. Lee, R.D. Miller and J.L. Hedrick. *High Performance Polymers*, "Application of hyperbranched block copolymers as templates for the generation of nanoporous organosilicates", **2001**, *13*, S11.
- [71] S. Mikoshiba and S. Hayase. *Journal of Materials Chemistry*, "Preparation of low density poly(methylsilsesquioxane)s for LSI interlayer dielectrics with low dielectric constant. Fabrication of angstrom ngstrom size pores prepared by baking trifluoropropylsilyl copolymers", **1999**, *9*, 591.

- [72] C. Jin, S. Lin and J.T. Wetzel. *Journal of Electronic Materials*, "Evaluation of ultra-low-k dielectric materials for advanced interconnects", **2001**, *30*, 284.
- [73] M. O'Neill, A. Lukas, R. Vrits, J. Vincent and e. al. *Semiconductor International*, "Low-k materials by design", **2002**, *25*, 93.
- [74] J.H. Golden, C.J. Hawker and P.S. Ho. *Semiconductor International*, "Designing porous low-k dielectrics", **2001**, *24*, 79.
- [75] M.E. Thomas. *Solid State Technology*, "Spin-on stacked films for low-k(eff) dielectrics", **2001**, *44*, 105.
- [76] H. Treichel and C. Goonetilleke. *Advanced Engineering Materials*, "Integration challenges for low dielectric constant materials", **2001**, *3*, 461.
- [77] T.M. Long and T.M. Swager. *Journal of the American Chemical Society*, "Molecular design of free volume as a route to low-kappa dielectric materials", **2003**, *125*, 14113.
- [78] K. Matsumoto, Y. Shibasaki, S. Ando and M. Ueda. *Polymer*, "Synthesis of novel poly (1,3-adamantyl)bis(2-naphthol) with low dielectric constant", **2006**, *47*, 3043.
- [79] Q. Zhou and T.M. Swager. *Journal of the American Chemical Society*, "Methodology for Enhancing the Sensitivity of Fluorescent Chemosensors - Energy Migration in Conjugated Polymers", **1995**, *117*, 7017.
- [80] Q. Zhou and T.M. Swager. *Journal of the American Chemical Society*, "Fluorescent chemosensors based on energy migration in conjugated polymers: The molecular wire approach to increased sensitivity", **1995**, *117*, 12593.
- [81] V. Williams, J.S. Yang and T.M. Swager. *Abstracts of Papers of the American Chemical Society*, "Design of porous shape persistent fluorescent polymer films for the detection of TNT", **1998**, *216*, U354.
- [82] Y.J. Miao, J.S. Yang and T.M. Swager. *Abstracts of Papers of the American Chemical Society*, "Fluorescence sensory polymers containing rigid non-planar aromatic scaffolds", **1998**, *216*, U171.
- [83] R.A. Maureen. *C&EN News*, **1997**, 14.
- [84] A.J. Paraskos. *Unusual Molecular Architectures in Liquid Crystal and Polymer Chemistry*, Thesis (Ph.D.) -- Massachusetts Institute of Technology, Dept. of Chemistry, **2004** (Chapter 6).

- [85] N.T. Tsui, L. Torun, A.J. Paraskos, T.M. Swager and E.L. Thomas. *Macromolecules*, "Minimization of Internal Molecular Free Volume: A Mechanism for the Simultaneous Enhancement of Polymer Stiffness, Strength and Ductility." **2006**, *39*, 3350.
- [86] N.T. Tsui, L. Torun, B.D. Pate, A.J. Paraskos, T.M. Swager and E.L. Thomas. *Advanced Functional Materials*, "Molecular Barbed Wire: Threading and Interlocking for the Mechanical Reinforcement of Polymers", **2007**, in press.
- [87] R. Denkwicz and N. Rice. *Transparent Energy Absorbing Materials for Ballistic Protection, Progress Report No. 1*, Triton Systems, Inc., Job #3107 Subcontract No. 5710001731 (under Prime Contract #DAAD19-02-D0002-14), **2004**.
- [88] R. Denkwicz and N. Rice. *Transparent Energy Absorbing Materials for Ballistic Protection, Progress Report No. 2*, Triton Systems, Inc., Job #3107 Subcontract No. 5710001731 (under Prime Contract #DAAD19-02-D0002-14), **2005**.
- [89] R. Denkwicz and N. Rice. *Transparent Energy Absorbing Materials for Ballistic Protection, Progress Report No. 3*, Triton Systems, Inc., Job #3107 Subcontract No. 5710001731 (under Prime Contract #DAAD19-02-D0002-14), **2005**.
- [90] R. Denkwicz and N. Rice. *Transparent Energy Absorbing Materials for Ballistic Protection*, Triton Systems, Inc., Job #3107 Subcontract No. 5710001731 (under Prime Contract #DAAD19-02-D0002-14), **2005**.
- [91] E. Davies and S. Hunter. *Journal of the Mechanics and Physics of Solids*, **1963**, *11*.
- [92] G.T. Gray, W.R. Blumenthal, C.P. Trujillo and R.W. Carpenter. *Journal De Physique Iv*, "Influence of temperature and strain rate on the mechanical behavior of Adiprene L-100", **1997**, *7*, 523.
- [93] W. Chen, B. Zhang and M.J. Forrester. *Experimental Mechanics*, "A split Hopkinson bar technique for low-impedance materials", **1999**, *39*, 81.
- [94] A.D. Mulliken. *Low to High Strain Rate Deformation of Amorphous Polymers: Experiments and Modeling*, Thesis (M.S.) -- Massachusetts Institute of Technology, Dept. of Mechanical Engineering, **2004** (Chapter 2).
- [95] C.Y. Liu, J.S. He, E. van Ruymbeke, R. Keunings and C. Bailly. *Polymer*, "Evaluation of different methods for the determination of the plateau modulus and the entanglement molecular weight", **2006**, *47*, 4461.
- [96] R.N. Haward and G. Thackray. *Proceedings of the Royal Society of London Series A*, **1968**, *302*, 453.



- [97] J.G. Rider and E. Hargreaves. *Journal of Polymer Science A-2*, **1969**, 7, 829.
- [98] A.S. Argon. *Philosophical Magazine*, "Theory for Low-Temperature Plastic-Deformation of Glassy Polymers", **1973**, 28, 839.
- [99] D.J. Brown and A.H. Windle. *Journal of Materials Science*, "Stress-Orientation-Strain Relationships in Non-Crystalline Polymers .1. Strategy for a Model", **1984**, 19, 1997.
- [100] I.M. Ward. *Polymer Engineering and Science*, "The Role of Molecular Networks and Thermally Activated Processes in the Deformation-Behavior of Polymers", **1984**, 24, 724.
- [101] M.C. Boyce and E.M. Arruda. *Polymer Engineering and Science*, "An Experimental and Analytical Investigation of the Large Strain Compressive and Tensile Response of Glassy-Polymers", **1990**, 30, 1288.
- [102] M. Ravnitzky. *AIAA Aerodynamic Decelerator Systems Technology Conference, 10th, Cocoa Beach, FL*, "Innovative Parachute Materials", **1989**, *Technical Papers A89-35201 14-03*, 125.
- [103] A.D. Mulliken and M.C. Boyce. *International Journal of Solids and Structures*, "Mechanics of the rate-dependent elastic-plastic deformation of glassy polymers from low to high strain rates", **2006**, 43, 1331.
- [104] C.R. Siviour, S.M. Walley, W.G. Proud and J.E. Field. *Polymer*, "The high strain rate compressive behaviour of polycarbonate and polyvinylidene difluoride", **2005**, 46, 12546.
- [105] J. Richeton, S. Ahzi, K.S. Vecchio, F.C. Jiang and R.R. Adharapurapu. *International Journal of Solids and Structures*, "Influence of temperature and strain rate on the mechanical behavior of three amorphous polymers: Characterization and modeling of the compressive yield stress", **2006**, 43, 2318.
- [106] B.K. Satapathy, R. Weidisch, P. Potschke and A. Janke. *Composites Science and Technology*, "Tough-to-brittle transition in multiwalled carbon nanotube (MWNT)/polycarbonate nanocomposites", **2007**, 67, 867.
- [107] P. Potschke, A.R. Bhattacharyya, A. Janke and H. Goering. *Advances in Polycarbonates*, ACS Symposium Series 898, **2005**, 148.
- [108] A. Karbach, D. Drechsler, C.L. Schultz, U. Wollborn, M. Moethrath, M. Erkelenz, J.Y.J. Chung and J.P. Mason. *Advances in Polycarbonates*, ACS Symposium Series 898, **2005**, 96.

- [109] A. Karbach, D. Drechsler, C.L. Schultz, U. Wollborn, M. Moethrath, M. Erkelenz, J.Y.J. Chung and J.P. Mason. *Advances in Polycarbonates*, ACS Symposium Series 898, **2005**, 112.
- [110] A.D. Mulliken and M.C. Boyce. *Journal of Engineering Materials and Technology-Transactions of the Asme*, "Polycarbonate and a polycarbonate-POSS nanocomposite at high rates of deformation", **2006**, *128*, 543.
- [111] A.D. Mulliken, S.Y. Soong, M.C. Boyce and R.E. Cohen. *Journal De Physique IV*, "High-rate thermomechanical behavior of poly(vinyl chloride) and plasticized poly(vinyl chloride)", **2006**, *134*, 217.
- [112] S.Y. Soong, R.E. Cohen, M.C. Boyce and A.D. Mulliken. *Macromolecules*, "Rate-dependent deformation behavior of POSS-filled and plasticized poly(vinyl chloride)", **2006**, *39*, 2900.
- [113] J.A. King. "*Synthesis of Polycarbonates*", chapter 2 in Handbook of Polycarbonate Science and Technology, Marcel Dekker, Inc., New York, **2000**.
- [114] H. Schnell, L. Bottenbruch and H. Krimm. U.S. Patent 3,028,365 assigned to Farbenfabriken Bayer AG. **1962**.
- [115] D.W. Fox. U.S. Patent 3,144,432 assigned to the General Electric Company. **1964**.
- [116] H.-J. Buysch and H. Krimm. DE-A 2447348, **1974**, Bayer AG.
- [117] J. E. Hallgren. DE-A 2738437, **1976**, General Electric Company.
- [118] A. J. Chalk. DE-A 2738487, **1976**, General Electric Company.
- [119] K. Okuyama, J. Sugiyama, R. Nagahata, M. Asai, M. Ueda and K. Takeuchi. *Macromolecules*, "Direct synthesis of polycarbonate from carbon monoxide and bisphenol a catalyzed by Pd-carbene complex", **2003**, *36*, 6953.
- [120] E.P. Boden, D.J. Brunelle and T.G. Shannon. *Abstracts of Papers of the American Chemical Society*, "Efficient Preparation of Cyclic Oligomeric Bisphenol-a Carbonates - Mechanism for Selective Formation of Cyclic Oligomers", **1989**, *198*, 332.
- [121] D.J. Brunelle, T.L. Evans, T.G. Shannon, E.P. Boden, K.R. Stewart, L.P. Fontana and D.K. Bonauto. *Abstracts of Papers of the American Chemical Society*, "Cyclic Oligomeric Carbonates - New Route to Super High-Molecular-Weight Polycarbonate - an Overview", **1989**, *198*, 331.

- [122] K. Okuyama, J. Sugiyama, R. Nagahata, M. Asai, M. Ueda and K. Takeuchi. *Journal of Molecular Catalysis a-Chemical*, "Oxidative carbonylation of phenol to diphenyl carbonate catalyzed by Pd-carbene complexes", **2003**, *203*, 21.
- [123] H. Schnell. *Angewandte Chemie*, **1956**, *68*, 633.
- [124] H. Schnell. *Industrial & Engineering Chemistry*, **1959**, *51*, 157.
- [125] W.F. Christopher and D.W. Fox. *Polycarbonates*, Reinhold Publishing Corporation, New York, **1962**.
- [126] J.E. Robertson and T.C. Ward. *Journal of Polymer Science Part B-Polymer Physics*, "Development of a methodology to predict material properties from environmental exposure. II. Structural features", **2002**, *40*, 802.
- [127] K. Cheah and W.D. Cook. *Polymer Engineering and Science*, "Structure-property relationships of blends of polycarbonate", **2003**, *43*, 1727.
- [128] J.M. Jonza and R.S. Porter. *Journal of Polymer Science Part B-Polymer Physics*, "High-Melting Bisphenol-a Polycarbonate from Annealing of Vapor-Induced Crystals", **1986**, *24*, 2459.
- [129] G.V. Difilippo, M.E. Gonzalez, M.T. Gasiba and A.V. Muller. *Journal of Applied Polymer Science*, "Crystalline Memory on Polycarbonate", **1987**, *34*, 1959.
- [130] L.J. Fetters, D.J. Lohse, D. Richter, T.A. Witten and A. Zirkel. *Macromolecules*, "Connection between Polymer Molecular-Weight, Density, Chain Dimensions, and Melt Viscoelastic Properties", **1994**, *27*, 4639.
- [131] R. Wimberger-Friedl and H.F.M. Schoo. *Macromolecules*, "On the Secondary Relaxation of Substituted Bis-A Polycarbonates", **1996**, *29*, 8871.
- [132] A.F. Yee and S.A. Smith. *Macromolecules*, "Molecular Structure Effects on the Dynamic Mechanical Spectra of Polycarbonates", **1981**, *14*, 54.
- [133] J.Y. Jho and A.F. Yee. *Macromolecules*, "Secondary Relaxation Motion in Bisphenol A Polycarbonate", **1991**, *24*, 1905.
- [134] C. Xiao and A.F. Yee. *Macromolecules*, "Scale of Cooperative Gamma-Relaxation of Bisphenol A Polycarbonate", **1992**, *25*, 6800.
- [135] M.T. Hansen, A.S. Kulik, K.O. Prins and H.W. Spiess. *Polymer*, "Effect of High Hydrostatic-Pressure on the Phenylene Motion in Polycarbonate as Revealed by H-2 Spin-Lattice Relaxation", **1992**, *33*, 2231.

- [136] J.H. Walton, M.J. Lizak, M.S. Conradi, T. Gullion and J. Schaefer. *Macromolecules*, "Hydrostatic-Pressure Dependence of Molecular Motions in Polycarbonates", **1990**, *23*, 416.
- [137] C.J.T. Landry and P.M. Henrichs. *Macromolecules*, "The Influence of Blending on the Local Motions of Polymers - Studies Involving Polycarbonate, Poly(Methyl Methacrylate), and a Polyester", **1989**, *22*, 2157.
- [138] J. Schaefer, E.O. Stejskal, D. Perchak, J. Skolnick and R. Yaris. *Macromolecules*, "Molecular Mechanism of the Ring-Flip Process in Polycarbonate", **1985**, *18*, 368.
- [139] J.Y.J. Chung and W.G. Paul. *SPE ANTEC Proceedings*, "Dynamic Mechanical Analysis and Toughening Mechanisms of Polycarbonate and 4,4'-Dihydroxydiphenyl Copolycarbonate", **2002**, *2*, 780.
- [140] B.U. Kang, J.A. Lee and J.Y. Jho. *Journal of Industrial and Engineering Chemistry*, "Synthesis and dynamic mechanical behavior of some poly(carbonate-co-sulfone)s", **1999**, *5*, 77.
- [141] G.R. Mitchell and A.H. Windle. *Colloid & Polymer Science*, "The effect of annealing on the local structure of glassy polycarbonate", **1985**, *263*, 280.
- [142] J.M. Hutchinson, S. Smith, B. Horne and G.M. Gourlay. *Macromolecules*, "Physical Aging of Polycarbonate: Enthalpy Relaxation, Creep Response, and Yielding Behavior", **1999**, *32*, 5046.
- [143] O.A. Hasan and M.C. Boyce. *Polymer*, "Energy storage during inelastic deformation of glassy polymers", **1993**, *34*, 5085.
- [144] D.G. LeGrand. *Journal of Applied Polymer Science*, "Crazing, yielding, and fracture of polymers. 1. Ductile brittle transition in polycarbonate." **1969**, *13*, 2129.
- [145] R.J. Morgan and J.E. O'Neal. *Journal of Polymer Science, Polymer Physics Edition*, **1976**, *14*, 1053.
- [146] O.A. Hasan, M.C. Boyce, X.S. Li and S. Berko. *Journal of Polymer Science Part B-Polymer Physics*, "An Investigation of the Yield and Post-Yield Behavior and Corresponding Structure of Poly(Methyl Methacrylate)", **1993**, *31*, 185.
- [147] C.P. Yang and S.H. Hsiao. *Journal of Applied Polymer Science*, "Flameproofed Polyesters Prepared by Direct Polycondensation of Aromatic Dicarboxylic-Acids and Brominated Bisphenols with Tosyl Chloride and N,N'-Dimethylformamide in Pyridine", **1988**, *36*, 1221.

- [148] C.P. Yang and S.H. Hsiao. *Journal of Polymer Science Part a-Polymer Chemistry*, "Preparation and Properties of Brominated Poly(Arylcarboxylate)S Via Interfacial Polycondensation", **1990**, *28*, 871.
- [149] M. Nagata, N. Tsutsumi and T. Kiyotsukuri. *Journal of Polymer Science Part a-Polymer Chemistry*, "Synthesis and Properties of Polyamides Derived from Systematically Halogenated Terephthalic Acids with Fluorine, Chlorine, or Bromine Atoms", **1988**, *26*, 235.
- [150] C.S. Wang, J.Y. Shieh and Y.M. Sun. *European Polymer Journal*, "Phosphorus containing PET and PEN by direct esterification", **1999**, *35*, 1465.
- [151] C.S. Wang and J.Y. Shieh. *Journal of Polymer Research-Taiwan*, "Synthesis and flame retardancy of phosphorus containing polycarbonate", **1999**, *6*, 149.
- [152] D. Derouet, F. Morvan and J.C. Brosse. *Journal of Applied Polymer Science*, "Chemical modification of epoxy resins by dialkyl(or aryl) phosphates: Evaluation of fire behavior and thermal stability", **1996**, *62*, 1855.
- [153] S. Maiti, S. Banerjee and S.K. Palit. *Progress in Polymer Science*, "Phosphorus-Containing Polymers", **1993**, *18*, 227.
- [154] C.S. Wang and J.Y. Shieh. *Polymer*, "Synthesis and properties of epoxy resins containing 2-(6-oxid-6H-dibenz c,e 1,2 oxaphosphorin-6-yl)1,4-benzenediol", **1998**, *39*, 5819.
- [155] M. Banks, J.R. Ebdon and M. Johnson. *Polymer*, "The Flame-Retardant Effect of Diethyl Vinyl Phosphonate in Copolymers with Styrene, Methyl-Methacrylate, Acrylonitrile and Acrylamide", **1994**, *35*, 3470.
- [156] S. Banerjee, S.K. Palit and S. Maiti. *Journal of Polymer Science Part a-Polymer Chemistry*, "Phosphorus-Containing Polymers .3. Polyimidophosphonates", **1994**, *32*, 219.
- [157] E.D. Weil, R.H. Hansen and N. Patel. *Acs Symposium Series*, "Prospective Approaches to More Efficient Flame-Retardant Systems", **1990**, *425*, 97.
- [158] G. Wittig. *Organic Syntheses*, "Triptycene", **1963**, *4*, 964.
- [159] K.E. Evans and A. Alderson. *Advanced Materials*, "Auxetic materials: Functional materials and structures from lateral thinking!" **2000**, *12*, 617.
- [160] N. Gaspar, X.J. Ren, C.W. Smith, J.N. Grima and K.E. Evans. *Acta Materialia*, "Novel honeycombs with auxetic behaviour", **2005**, *53*, 2439.

- [161] J.N. Grima and K.E. Evans. *Journal of Materials Science*, "Auxetic behavior from rotating triangles", **2006**, *41*, 3193.
- [162] J.N. Grima, R. Gatt, N. Ravirala, A. Alderson and K.E. Evans. *Materials Science and Engineering a-Structural Materials Properties Microstructure and Processing*, "Negative Poisson's ratios in cellular foam materials", **2006**, *423*, 214.
- [163] F. Scarpa, J. Giacomini, Y. Zhang and P. Pastorino. *Cellular Polymers*, "Mechanical performance of auxetic polyurethane foam for antivibration glove applications", **2005**, *24*, 253.
- [164] N. Ravirala, K.L. Alderson, P.J. Davies, V.R. Simkins and A. Alderson. *Textile Research Journal*, "Negative Poisson's ratio polyester fibers", **2006**, *76*, 540.
- [165] V.R. Simkins, A. Alderson, P.J. Davies and K.L. Alderson. *Journal of Materials Science*, "Single fibre pullout tests on auxetic polymeric fibres", **2005**, *40*, 4355.
- [166] R.S. Webber, K.L. Alderson and K.E. Evans. *Polymer Engineering and Science*, "Novel variations in the microstructure of the auxetic microporous ultra-high molecular weight polyethylene. Part 1: Processing and microstructure", **2000**, *40*, 1894.
- [167] J.N. Grima, R. Jackson, A. Alderson and K.E. Evans. *Advanced Materials*, "Do zeolites have negative Poisson's ratios?" **2000**, *12*, 1912.
- [168] Y.L. Liu, L. Zhang, J. Shi and S.K. Cao. *Reactive & Functional Polymers*, "Synthesis and characterization of liquid crystalline copolyesters containing horizontal and lateral rods in main chain (II)", **2005**, *64*, 35.
- [169] C.B. He, P.W. Liu, P.J. McMullan and A.C. Griffin. *Physica Status Solidi B-Basic Solid State Physics*, "Toward molecular auxetics: Main chain liquid crystalline polymers consisting of laterally attached para-quaterphenyls", **2005**, *242*, 576.
- [170] C.B. He, P.W. Liu, A.C. Griffin, C.W. Smith and K.E. Evans. *Macromolecular Chemistry and Physics*, "Morphology and deformation behaviour of a liquid crystalline polymer containing laterally attached pentaphenyl rods", **2005**, *206*, 233.
- [171] E.M. Perchellet, M.J. Magill, X.D. Huang, C.E. Brantis, D.H. Hua and J.P. Perchellet. *Anti-Cancer Drugs*, "Triptycenes: a novel synthetic class of bifunctional anticancer drugs that inhibit nucleoside transport, induce DNA cleavage and decrease the viability of leukemic cells in the nanomolar range in vitro", **1999**, *10*, 749.

- [172] Y. Wang, E.M. Perchellet, M.M. Ward, K.Y. Lou, H.P. Zha, S.K. Battina, B. Wiredu, D.H. Hua and J.P.H. Perchellet. *International Journal of Oncology*, "Antitumor triptycene analogs induce a rapid collapse of mitochondrial transmembrane potential in HL-60 cells and isolated mitochondria", **2006**, *28*, 161.
- [173] E.M. Perchellet, Y. Wang, R.L. Weber, K.Y. Lou, D.H. Hua and J.P.H. Perchellet. *Anti-Cancer Drugs*, "Antitumor triptycene bisquinones induce a caspase-independent release of mitochondrial cytochrome c and a caspase-2-mediated activation of initiator caspase-8 and-9 in HL-60 cells by a mechanism which does not involve Fas signaling", **2004**, *15*, 929.
- [174] Y. Wang, E.M. Perchellet, M. Tamura, D.H. Hua and J.P. Perchellet. *Cancer Letters*, "Induction of poly(ADP-ribose) polymerase-1 cleavage by antitumor triptycene bisquinones in wild-type and daunorubicin-resistant HL-60 cell lines", **2002**, *188*, 73.
- [175] B.N. Wang, M.F. Wu, E.M. Perchellet, C.J. McIlvain, B.J. Sperfslage, X.D. Huang, M. Tamura, H.A. Stephany, D.H. Hua and J.P. Perchellet. *International Journal of Oncology*, "A synthetic triptycene bisquinone, which blocks nucleoside transport and induces DNA fragmentation, retains its cytotoxic efficacy in daunorubicin-resistant HL-60 cell lines", **2001**, *19*, 1169.